Journal Pre-proof

Progress in 3D bioprinting technology for tissue/organ regenerative engineering

Ishita Matai, Gurvinder Kaur, Amir Seyedsalehi, Aneesah McClinton, Cato T. Laurencin

Please cite this article as: Matai I, Kaur G, Seyedsalehi A, McClinton A, Laurencin CT, Progress in 3D bioprinting technology for tissue/organ regenerative engineering, *Biomaterials* (2019), doi: https://doi.org/10.1016/j.biomaterials.2019.119536.

This is a PDF file of an article that has undergone enhancements after acceptance, such as the addition of a cover page and metadata, and formatting for readability, but it is not yet the definitive version of record. This version will undergo additional copyediting, typesetting and review before it is published in its final form, but we are providing this version to give early visibility of the article. Please note that, during the production process, errors may be discovered which could affect the content, and all legal disclaimers that apply to the journal pertain.

Progress in 3D Bioprinting Technology for Tissue/Organ Regenerative Engineering

Contributing authors: Ishita Matai[1], Gurvinder Kaur[1], Amir Seyedsalehi[2,3,4,6],

Aneesah McClinton[2,4], Cato T. Laurencin[2,3,4,5,6,7*]

Affiliations:

[1] Central Scientific Instruments Organization (CSIR-CSIO), Chandigarh, 160030, India

[2] Connecticut Convergence Institute for Translation in Regenerative Engineering, UConn Health,

Farmington, CT, USA

[3] Department of Orthopedic Surgery, UConn Health, Farmington, USA

[4] Raymond and Beverly Sackler Center for Biomedical, Biological, Physical and Engineering Sciences,

UConn Health, Farmington, USA

[5] Department of Materials Science and Engineering, University of Connecticut, Storrs, USA

[6] Department of Biomedical Engineering, University of Connecticut, Storrs, USA

[7] Department of Chemical and Biomolecular Engineering, University of Connecticut, Storrs, USA

*Correspondence to: Dr. Cato T. Laurencin, M.D., Ph.D., Connecticut Convergence Institute for

Translation in Regenerative Engineering, laurencin@uchc.edu

ABSTRACT

Escalating cases of organ shortage and donor scarcity worldwide are alarming reminders of the need for alternatives to allograft tissues. Within the last three decades, research efforts in the field of regenerative medicine and tissue engineering continue to address the unmet need for artificial tissues and organs for transplant. Work in the field has evolved to create what we consider a new field, Regenerative Engineering, defined as the Convergence of advanced materials science, stem cell science, physics, developmental biology and clinical translation towards the regeneration of complex tissues and organ systems. Included in the regenerative engineering paradigm is advanced manufacturing. Three-dimensional (3D) bioprinting is a promising and innovative biofabrication strategy to precisely position biologics, including living cells and extracellular matrix (ECM) components, in the prescribed 3D hierarchal organization to create artificial multi-cellular tissues/organs. In this review, we outline recent progress in several bioprinting technologies used to engineer scaffolds with requisite mechanical, structural, and biological complexity. We examine the process parameters affecting bioprinting and bioink-biomaterials and review notable studies on bioprinted skin, cardiac, bone, cartilage, liver, lung, neural, and pancreatic tissue. We also focus on other 3D bioprinting application areas including cancer research, drug testing, high-throughput screening (HTS), and organ-on-a-chip models. We also highlight the current challenges associated with the clinical translation of 3D bioprinting and conclude with the future perspective of bioprinting technology.

Keywords: *Tissue engineering, regenerative engineering, artificial tissues, three-dimensional, bioprinting, bioinks*

1. Introduction

The human body has limited capabilities for regeneration. Current treatment options to replace damaged tissue and organs rely on obtaining tissue from the same individual or transplantation from cadavers. There are limitations to these treatments that include donor site morbidity and donor scarcity. These circumstances further support the need for biological substitutes and the fields of tissue engineering and regenerative medicine have worked towards this end. Work in the field has evolved to create what we consider a new field, Regenerative Engineering, defined as the Convergence of advanced materials science, stem cell science, physics, developmental biology and clinical translation towards the regeneration of complex tissues and organ systems [1]. Included in the regenerative engineering paradigm is advanced manufacturing.

Three-dimensional (3D) bioprinting, is a state-of-the-art technology to fabricate biological constructs with hierarchical architecture similar to their native counterparts. Developing living functional tissues by artificial means can address an unmet need in tissue replacement and organ transplantation [2,3]. With this perspective, bioprinting is gaining overwhelming acceptance from doctors and researchers across the globe as a viable option to improve the lives of disease-stricken patients.

In essence, bioprinting is an extended application of rapid prototyping or an additive manufacturing technique to print bio-functional materials in a layer-by-layer (LbL) manner on substrates when embedded in cytocompatible biomaterials [4]. The process refers to printing and patterning cells, or other biological entities, directly on a substrate or tissue culture dish through an automated dispensing system. This fascinating development ensures that individual cells and multiple cell types are held together when dispensed in biocompatible materials to form desired 3D functional structures [5–7]. Biomaterials consisting of cells, base structure material, and other requisite components are referred to as 'bioinks' [8]. Cell-based bioinks are then fabricated into desired shapes and sizes with geometrical complexities to create multifaceted 3D mimetic tissue constructs. This serves as a promising gateway for organ and tissue printing to create new and functional 3D tissues from a source of cells [9,10].

3D printing facilitates the application of scaffold-based or scaffold-free tissue and organ constructs, mini-tissues, and organ-on-a-chip model systems to generate functional human organs–such as heart, kidneys, skin, and liver–on a large-scale in the upcoming future [11–17]. Using a 3D bioprinter allows for the proper distribution and positioning of biomaterials, signaling factors, and heterogeneous cells in high densities to form tissue-engineering constructs (TECs). The quality of the final bioprinted scaffold is influenced by its biocompatibility, biodegradability, cellular response, and the tissue-microenvironment where it is exposed [18]. Moreover, 3D bioprinted constructs with interconnected pores and large surface areas support cell attachment, growth, intercellular communication and exchange of gas and nutrients, a notable advantage over traditional–solvent casting, phase separation and melt molding techniques [19].

To recapitulate aspects of the complex 3D micro-tissue environment, bioprinting can generate identical biomimetic 3D scaffolds with uniform cell distribution to form reproducible 3D cell culture. Such biomimetic 3D printed models can substitute the conventional 2D cell culture where cells are grown as monolayers on hard polystyrene coated plates, which therefore primarily lack the dynamic and complex cell-cell and cell-matrix interactions [20–22]. Bioprinted cell-laden 3D scaffolds provide spatial depth and better cell-cell communication for improved in vivo physiology. This can also contribute to, or even eliminate, the need for animal tests that cannot accurately predict the human toxicological and pathophysiological responses [23]. Creating *in vitro* conditions that can closely mimic the *in vivo* milieu will not only be cost-effective but will also allow batch to batch consistency and improved control over individual variables. This would, in turn, be fundamental to understanding and contributing to delivery applications, drug discovery, and testing of new materials [24].

Despite being a relatively young while innovative tissue engineering technology, 3D bioprinting has several challenges. These include: (1) identification of biodegradable and biomimetic printable materials that enable prompt cell attachment and proliferation, (2) the need for vascularization at the single-cell level, (3) complex patterning of heterocellular tissues and (4) maintaining cell viability and long-term functionality post-printing until remodeling and regeneration is complete [2,6,7,25].

At the outset, this review will focus on prime bioprinting strategies currently used for 3D tissue/organ engineering with an emphasis on the impact of 3D printer process parameters on the bioprinted constructs. We present a comprehensive overview of several natural, synthetic, and composite bioinks applied to print 3D tissue models, and provide insight into cells as the critical component of bioinks and peptide-based bioinks. We outline the recent and on-going research in 3D bioprinting of skin, cardiac, bone, cartilage, liver, lung, neural, and pancreatic tissues followed by the progress made in their clinical translation. We will also discuss the current state of 3D bioprinting applications in the context of organ-on-a-chip models, cancer research, and high-throughput screening. Finally, we will highlight particular challenges and limitations associated with the translation of cell-laden 3D models from lab research to clinical utilization, and discuss the perspective solutions to secure the seminal benefits of bioprinting technology to create on-demand tissues/organs for human needs.

2. Strategies for bioprinting

The success of tissue engineering chiefly depends on the ability to formulate complex, cell-laden 3D structures that intimately resemble the original living tissues. Therefore, the strategies put to use to design and create the architecture and topography of biomaterial scaffolds are a vital aspect of functional tissue engineering. Functional scaffolds can be prepared by following either top-down or bottom-up approaches [26]. There are different bioprinting strategies depending on their fundamental working principles for fabricating functional tissue constructs, namely inkjet-based bioprinting, laser-assisted bioprinting (LAB), pressure-assisted (extrusion) based bioprinting, acoustic bioprinting, stereolithography (SLA)-based bioprinting, and magnetic bioprinting [18,27]. These bioprinting strategies can be used alone or in combination to achieve the desired additive manufacturing objective and tissue fabrication. These strategies are schematically described in **Fig. 1** [28].

2.1 Inkjet-based bioprinting

Inkjet-based printing is the most widely understood printing technology derived from the conventional 2D desktop inkjet printers. In this non-contact bioprinting process, the image reconstruction is based on creating and precisely positioning picoliter volume (1-100 pL) droplets of "bioink" on a substrate under computer control [29]. Each droplet of bioink holds 10^4-30^4 cells [30]. The drops of ink used in bioprinting are formed by two strategies: (1)

continuous inkjet printing (CIJ) and (2) drop-on-demand printing (DOD). Briefly, CIJ printing relies on the inherent tendency of liquid stream to flow and undergo morphological transformation leading to continuous-discrete drops of ink (by Rayleigh-plateau instability). The drops are electrically conductive and are easily steered to their respective locations under the influence of electric or magnetic fields. The ink drop diameter ranges from 10-150 µm. On the contrary, DOD printing as the name suggests generates drops of bioink over the substrate when required. Comparatively, CIJ based bioprinters generate drops at a much faster rate than DOD systems. However, the requirement for conductive fluid inks and risk for contamination during fluid recycling hinders their use for biomedical applications. Instead, DOD based bioprinters are well suited for material deposition and patterning for their precision and minimal waste of bioink [31].
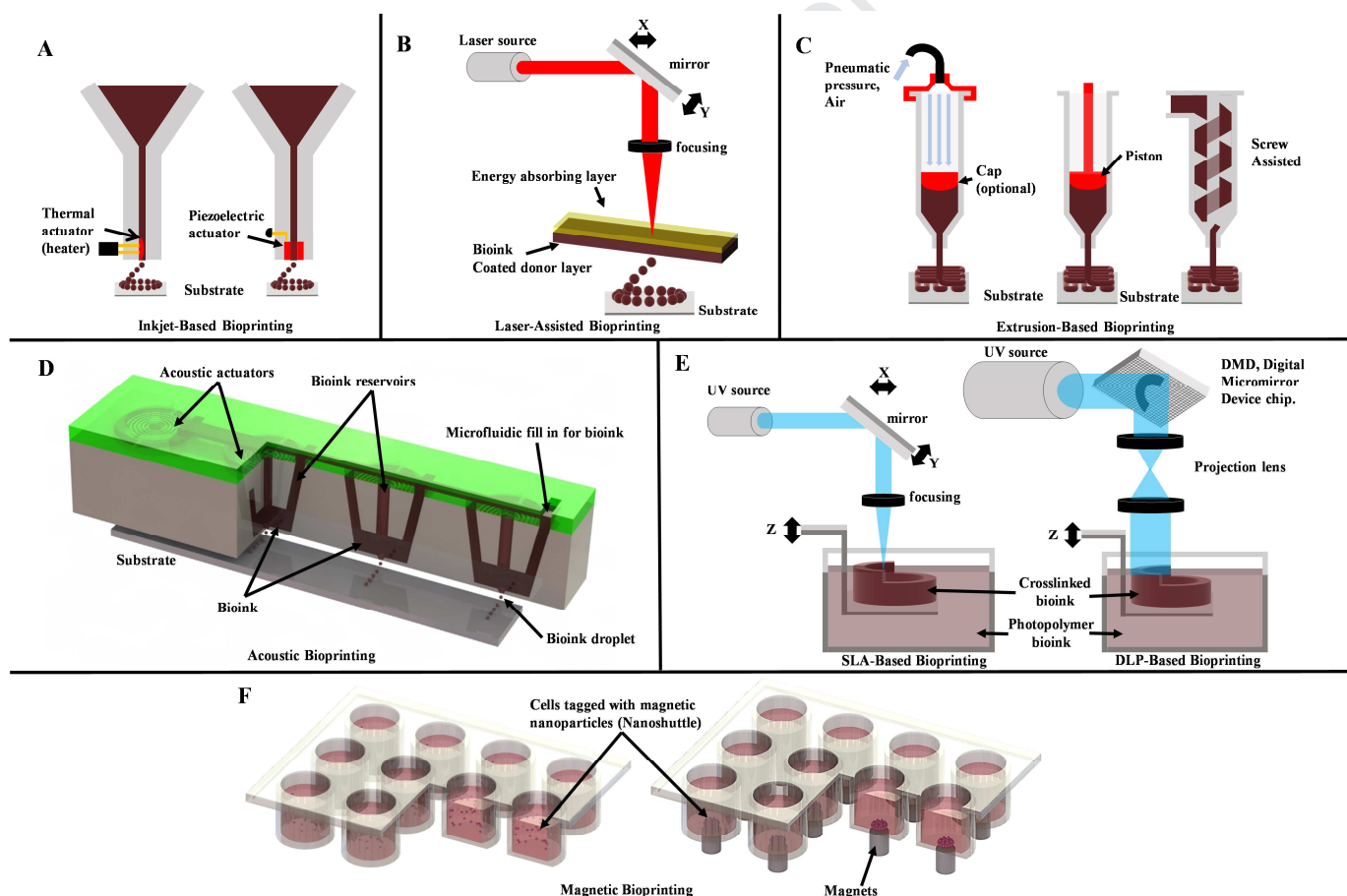
Fig. 1. Schematic figures showing the Bioprinting modalities. (A) Inkjet Bioprinting systems including Thermal and Piezoelectric Drop-On-Demand (DOD) based mechanisms. (B) Laser-Assisted Bioprinting system; Laser-Induced Forward Transfer mechanism. (C) Extrusion-based Bioprinting systems including Pneumatic pressure,

4

Piston and Screw assisted mechanisms. (D) Acoustic Bioprinting system; a type of DOD mechanism. (E) Stereolithography Bioprinting systems including SLA and DLP (Digital Light Processing) Laser-based mechanisms. (F) Magnetic Bioprinting system; cells are shown within the culture media.

The DOD can be created by thermal, piezoelectric, or acoustic approaches [27]. The commonly used inkjet bioprinters utilize heat or mechanical compression to create and eject drops. The ejected drops mostly have a diameter of <30 µm which offers high resolution. A thermal inkjet bioprinter consists of an ink chamber with a nozzle and a heating element (a thin film resistor) [32]. To generate a drop, a short electric pulse is applied to the resistor, generates heat, and forms a small vapor pocket or bubble. The bubble inflates or collapses when the heat is removed. These expanding and collapsing forces drive the ink drops of various volumes out of the nozzle orifice [33–36]. Thus, thermal inkjet bioprinters are also referred to as "bubble jet bioprinters."

In piezoelectric inkjet, the pressure pulse is generated by mechanical actuation of piezoelectric crystals that are placed on the back of an ink chamber that causes them to vibrate. The inner vibrations pressure the bioink droplet out of the nozzle. The thermal inkjet technology is simple, efficient, economical, and hence preferred. However, frequent clogging of nozzles by bioink gelation and production of unequal sized drops disturbs the smooth printing process [37]. Another challenge involves the thermal and shear stresses involved in creating bioink drops that may affect cell viability. According to several reports, during the printing process, cells are not greatly affected by an increase in the local temperature up to 300 ℃ due to short exposure of 2 μs [38–41]. While, the vibration frequencies and power levels in piezoelectric based bioprinting can disrupt cell membranes and the structure of biomolecules, such as the unfolding of proteins [42], Saunders et al. reported appreciable cell viability (> 90%) of human fibroblasts post-printing using a piezoelectric inkjet printer [43–45]. Overall, thermal inkjet bioprinters are widely used for printing biological entities [42].

2.2 Laser-assisted bioprinting

This bioprinting strategy stems from the laser-induced forward transfer (LIFT) effect to print different living cells and biomaterials with precision and micrometer resolution [46]. Originally developed for the direct writing of metals, LIFT has been successfully applied to deposit biological materials such as cells, nucleic acids (DNA), and peptides using a laser

pulse repetition rate of 5 kHz [47–50]. In 2004, Barron and colleagues developed a biological laser printer (BioLP) to transfer biological patterns to substrates with spatial accuracy of > 5 µm [51]. LIFT based bioprinters or LAB mainly consist of (a) an energized pulsed laser (mostly infrared laser), (b) target or ribbon which serves as donor film of biological material, and (c) a receiving substrate to collect the printed material. The ribbon assembly includes a laser-transparent substrate (e.g. quartz or glass) coated with a thin layer of laser-absorbing metal (e.g. gold (Au) or titanium (Ti)). Bioinks comprising of cells or molecules (organic component) in liquid or gel solution (e.g. culture media, collagen) are then deposited over the metal-film support. The incident laser light vaporizes the metal film causing ejection of bioink droplets, which are subsequently received on the facing substrate [52–54].

During this process, the laser-cell interactions and cell-substrate interactions can alter cellular integrity [53,55]. However, LAB being an orifice-free technology can work with bioinks with varied viscosities ranging from 1-300 mPa.s and cell concentration $\sim 10^8$ cells mL^{-1} [2]. Hence, LAB is highly versatile to fabricate heterogeneous tissue constructs with high cell densities, high resolution (10-100 µm), and various sizes to closely mimic their native physiological counterparts. Other advantages include automation, reproducibility, and high-throughput that makes LAB an attractive approach for 3D tissue fabrication. An important consideration for LAB is the selection of biomaterial. The selected biomaterials should exhibit fast gelation kinetics (i.e. rapid cross-linking) and ensure compatibility of working wavelengths to preserve the resolution and arrangement of cells and biomaterials in 3D printed constructs, which is a challenging aspect of the printing process. Moreover, gravitational-settling of cells in solution and long-fabrication times are other major concerns.

2.3 Extrusion-based bioprinting

Pressure-assisted or extrusion-based bioprinting is the most popular approach in research and commercial areas to create 3D cell-laden constructs. Thermal inkjet bioprinters can only dispense low viscous bioinks with <10 mPa.s air bubbles [56]. Highly viscous bioinks cannot be ejected out of its nozzle orifice. In extrusion bioprinting, bioinks are placed in disposable medical-grade plastic syringes and then dispensed pneumatically or mechanically (piston or rotating screw) onto sterile substrates. The set up with piston-driven deposition provides extended control overflow of bioink while screw-driven systems enable good spatial control and are valuable for depositing highly viscous bioinks. The pneumatic driven system is

advantageous in depositing bioinks of various types and viscosities by modulating pressure and valve gating time [57]. Upon applying pressure, highly viscous bioinks flow out as seamless cylindrical filaments (diameter ~150-350 µm) [5,58]. The printed filaments are then cross-linked by light (mostly UV), enzymes, chemicals, or heat to form mechanically durable structures.

To dispense thermo-sensitive and light-sensitive polymers, the temperature of the ink container and receiving platform are primarily maintained to control bioink viscosity and induce *in situ* gelation [59]. Other parameters such as air pressure, extrusion speed, collecting platform position, and type can also be adjusted which directly affects the printing fidelity and resolution. However, high pressure and rapid speed can induce shear stress, which in turn reduces cell viability, an undesirable outcome. Other concerns include frequent nozzle clogging and inferior resolution (200-1000 µm) [5,60]. Thus, the printing parameters must be carefully optimized to ensure stable printed structures, without affecting cell viability, to reap the benefits and ease of extrusion printing.

To fabricate custom 3D structures, the desired shape is first created using CAD/CAM (computer-aided design/manufacturing) in STL (standard template library) file format and then printed LbL to a particular thickness [20]. Recent extrusion bioprinters are equipped with multiple printer heads that allow simultaneous deposition of different bioinks with minimal cross-contamination [61]. Furthermore, they permit better control over porosity, shape, and cell-distribution in the printed construct. A myriad of cell types and designs have been printed as tissue substitutes [62,63]. Other biomolecules including DNA, RNA, and peptide fibrils have also been 3D printed with this technology [50,64]. Extrusion bioprinting is highly versatile and therefore most suited to fabricate scaffolds or prosthetic implants for tissue engineering.

2.4 Acoustic bioprinting

Single-cell manipulation and building 3D structures using surface acoustic wave technology have added a new dimension to bioprinting [65]. Acoustic or sound waves can move cells in different directions to fabricate intricate 3D patterns. Acoustic bioprinters work on the principle of generating and depositing cell encapsulated picoliter droplets from an open-pool

of bioink in the presence of a gentle acoustic field. Being a nozzle-free technology, it eludes clogging issues and protects cells from detrimental shear stresses, heat, and pressure frequently encountered with DOD printers [66]. Over a decade ago, investigators designed an acoustic bioprinter to encapsulate and print multiple cell types (stem cells, fibroblasts, hepatocytes, cardiomyocytes, etc.) in biological fluids at high throughput levels while preserving cell viability (> 85%). It comprised of a single or an array of 2D microfluidic channels to hold bioinks in position. The acoustic ejector was made of a piezoelectric substrate (lithium niobate/tantalate, murata and quartz) with interdigitated Au rings on top to build surface sound waves on demand. These circular sound waves formed an acoustic focal point at air-fluid interface. When the acoustic vibration forces exceeded the surface tension of bioink, acoustic droplets generate. The diameter of the droplets varies as a function of acoustic frequency. The picoliter droplet ejection rate ranges from $1\text{-}10^4$ droplets per second [67,68].

Recently, researchers demonstrated the use of 3D acoustic tweezers utilizing standing surface acoustic wave (SSAW) technology to pick up, translate, and deliver single cells or cell assemblies to make 2D or 3D patterns. This technique prints cells in a precise, non-invasive, label-free, and contact-free way [65]. However, the potential of acoustic bioprinting to combine multiplexed cell types and other growth factors to form biomimetic cell-laden scaffolds requires further exploration.

2.5 Stereolithography bioprinting

Stereolithography (SLA) bioprinting is another technical approach to fabricate 3D patterned scaffolds with micro-and nano-architecture [69,70]. 3D scaffold structures created using common printing techniques usually lack the properties to allow users to control the porosity, resolution, and mechanical properties. SLA bioprinting is a typical light-assisted direct printing method to cure light-sensitive bioinks in a LbL process to additionally build-up materials. It is a projection-printing system which employs a light projector to cross-link photo-curable bioinks plane-by-plane [71,72]. The printing time for each layer is independent of the layer complexity and size. The total printing time can be estimated from the thickness of the structure. 3D cell encapsulated structures with resolution as low as 100 µm and very high cell viability (>90%) have been printed in less than 30 minutes using SLA [73]. Visible-light cross-linkable bioinks of polyethylene glycol diacrylate (PEG-DA) and gelatin

methacrylate (GelMA) hydrogels, combined with fibroblast (NIH 3T3) cells, were SLA printed with a low-cost setup, 50 μm resolution, and 85% cell viability [74]. In a recent study, SLA bioprinting was combined with electrospinning for neural tissue engineering. Aligned electrospun fibers of polycaprolactone (PCL)/ gelatin composite, combined within SLA 3D printed microporous scaffolds of PEG-DA with 66% porosity, were determined to improve neural cell behavior and mechanical properties [75].

2.6 Magnetic bioprinting

Assembly of 3D multitype co-cultures in the laboratory has become possible with magnetic 3D bioprinting (M3DB) based on the principle of magnetic levitation [76]. This technique provides various advantages of fine spatial control, endogenous synthesis of ECM without needing any artificial protein substrate, and the capability to print multiple tissue-like structures rapidly [77,78].

Primarily, it is a contactless technique employing two distinct strategies for manipulation and assembly of cells into shaped structures [79]. First, in the label-free diamagnetophoretic printing the cell-medium is mixed with a paramagnetic buffer and then exposed to an external magnetic field to form cell aggregates [80]. In the second approach, cells are incubated with nanoparticle assembly consisting of poly-L-lysine, magnetic iron oxide (Fe_3O_4, magnetite), and gold nanoparticles (NanoShuttle-PL) that form a gel via electrostatic interactions. When the cells take up the gel they become magnetic, which allows for their manipulation, enabling the cells to levitate off the plate surface and into the media where they form cell aggregates [78]. The magnetized cell aggregates are then guided into 3D patterns using mild magnetic forces generated by a prefabricated magnetic template. Spatial patterning of the cell aggregates can be altered by varying the shape of the magnetic template used [81].

Tissues of fat, lung, aortic valve, blood vessels and tumors of glioblastoma and breast have been fabricated by similar methods; all of which showed *in vivo*-like protein expression and ECM [82]. With this foundation of M3DB, Tseng et al. validated spheroid contraction as a biologically relevant cytotoxic endpoint using 3T3 murine embryonic fibroblasts in response to five toxic compounds. This study revealed that the assay developed, employing M3DB

spheroids to determine cytotoxicity in a 3D microenvironment, could overcome limitations of handling, speed, throughput, and imaging of other 3D cell culture platforms [82].

Further, they proposed a 3D *in vitro* model for the evaluation of uterine contractility physiology using human uterine myometrial cells. Patient-derived myometrium cells were magnetically printed into hollow rings for throughput uterine contractility analysis over time and as a function of various clinically relevant agents. These printed uterine rings, derived from different cell origins and patients, differed in their contractility patterns and response to the uterine contractility inhibitors, nifedipine, and indomethacin. This study could address the need for high-throughput evaluation of multiple agents and conditions in uterine contractility for clinical research [83].

3D pancreatic cancer organoids in standard flat-bottom well plates were developed by Hou et al. employing M3DB and cell-repellent forces. Inhibitory effect of ~3,300 clinically approved drugs was tested against pancreatic cancer patient-derived cells (including cancer-associated fibroblasts, CAFs) [84]. Further, Baillargeon et al. used similar technology to extend the conventional 96- and 384- well microtiter plate densities to 1536- well plate for executing automated large-scale screening. The strategy was found to be efficient for fully automated large-scale spheroid and organoid production to support high throughput screening [85].

3. Process parameters affecting 3D bioprinting

Extensive literature is available focusing on 3D bioprinting for tissue engineering and bioengineering applications. However, the process parameters involved in extrusion-based bioprinting translating 2D or 3D designs of tissues or organs into synthetic structures under computer control are seldomly addressed. Proper knowledge and understanding of such process variables can prompt the fabrication of user-defined 3D hierarchical structures that accurately reflect the native tissues. The diameter of the deposited/printed strand (strut) predominantly influences the overall porosity, mechanical strength, and layer height of the scaffold. Several factors affect printing fidelity, including solution viscosity, applied pressure, printing speed, and printing distance are critical working parameters of a 3D bioprinter. These parameters are interrelated and require proper optimization to ensure a reproducible bioprinting process. [86].

10

The viscosity of the solution or bioink is of utmost importance to produce 3D printed cell-laden constructs in cases of inkjet and extrusion-based bioprinting [87]. In such cases, an ideal printable biomaterial should have sufficient viscosity to enable smooth nozzle extrusion and rapid solidification post-printing, either through gelation or shear thinning properties. Frequent clogging of the nozzle occurs with highly viscous inks while deformation and collapse of structures occur with low viscous materials [88]. On the other hand, viscosity is not a limitation for laser-assisted bioprinting technology since there is no ejection from the nozzle in these methods [89]. Therefore, bioink viscosity requires modification depending on the type of bioprinter used [87]. Numerous bioprinters have different working ranges of viscosity. The common inkjet or droplet-based bioprinters have a viscosity value close to 10 mPa.s, LAB bioink viscosity ranges from 1-300 mPa.s, and extrusion-based bioprinter viscosity ranges from 30-6 x 10^7 mPa.s [9,87,90–93]. In addition, increasing the concentration of bioinks directly affects cell viability. Cell migration and proliferation are inhibited due to the entangling of polymer chains with an increase in bioink concentration, which reduces the cell viability [94]. Printability, shape fidelity, structural resolution, and cell survival of the 3D printed construct are greatly affected by the bioink composition which dominates cross-linking during pre and post gelation processes [92,95,96]. In the subsequent section, we present a brief overview of the different bioinks that influence scaffold properties.

3.1 Bioinks

The solution or hydrogel form of biomaterials loaded with desired cell types is referred to as bioinks. Bioinks are crucial for bioprinting to develop functional tissue or organ constructs [92,95]. The terms bioinks and biomaterial bioinks are often used interchangeably. However, the cellular component is defined as a bioink if it is constructed in 3D on or within hydrogels. On the contrary, the term biomaterial bioink is used for the hydrogel precursors or aqueous polymer formulation that can contain biological factors and be used for subsequent cell seeding or *in vivo* studies [97]. Bioinks are further divided into four different classes on the basis of their roles. (1) Structural−bioinks support cell adhesion, proliferation, differentiation, imitate extracellular matrix (ECM) during cell multiplication, and maintain the mechanical integrity of the construct. (2) Fugitive−bioinks or sacrificial bioinks are temporary materials that can be rapidly removed to form internal voids or channels in a 3D printed construct. (3) Support−bioinks are non-biologic materials with good mechanical strength to resist loads and

provide mechanical support for softer materials or complex structures during the printing process. (4) Functional-bioinks provide mechanical, biochemical, and electrical signals to influence cellular behavior post-printing [98]; sacrificial and support bioinks are technically biomaterial inks rather than bioinks. The functionality of final printed tissues and organs depends on the rheological, mechanical, and biological properties of the bioink [96].

The polymers used in bioinks can be natural, synthetic, or a combination of both. They promote beneficial cellular interactions, increased cell proliferation, motility, and differentiation [95,96]. Some of the natural polymers widely used as a base for bioinks include alginate [99], collagen [100], silk [101], dextran [102], gelatin [103], fibrin [104], agarose-chitosan [100], agarose [105], gellan gum [106], hyaluronic acid (HA) [107], de-cellularized matrix [108], matrigel [91], and hydroxyapatite (Hap) [109]. Synthetic polymers include polyethylene glycol (PEG) [110], methacrylated hyaluronic acid (HAMA)- methacrylated poly[N-(2-hydroxypropyl)methacrylamide mono/dilactate (Phpma-lac)/PEG [111], polyvinylpyrrolidone (PVP) [112], poly(ε-caprolactone) (PCL) [104], pluronic [113], poly(glycidol)-HA (PG-HA) [114], and polyhydroxybutyrate (PHB) [115]. Tables 1−3 review the use of several natural, synthetic, and composite materials used as base biomaterials with distinct cell types to formulate bioinks, respectively.

The most predominant approach in using additive manufacturing technologies in tissue engineering is cell-seeding of the porous scaffold after printing them, using biomaterial inks rather than cell contained bioinks. This approach has a crucial limitation as it usually hinders even distribution of cell density in a way that cells will be more populated on the edges of the construct; this heterogeneous cell density can lead to unsuitable oxygen gradients from edge to core of the construct which can affect the cell growth and proliferation negatively [116]. Bioprinting or printing cell contained bioinks can bypass such a limitation as the cells will be homogeneously distributed within the bioinks and consequently within the printed construct. In this approach, the characteristics of the biomaterials that are used as the base for the bioinks can largely affect the cell encapsulation process and cell viability. One such characteristic is the encapsulating hydrogel's moduli; generally low moduli hydrogels (<1 kPa) behave better in terms of cell attachment, viability, expansion, and proliferation [117,118].

As mentioned above, cells are the primary and important component of bioinks and need to be considered first before choosing the base biomaterials. The suitable cell density and cell type

or combination of cells for bioinks should be determined based on the tissue of the interest; for example, for bone tissue engineering 5 to 10 million cells per milliliter of bioink can be optimal [116].

3.1.1 Cell density

One important factor to be considered regarding the cell component of bioinks is cell density. It is important to have enough live cells after the printing process to yield the suitable cell density, as the process will apply some forces to the cells within the bioinks that can lead to some extent of cell necrosis. This issue even exacerbates in cases of using high polymer content hydrogels as a base for the bioink due to the high forces and stress on encapsulated cells from the concentrated polymer content. Cell density is crucial for finding the best printing strategy as different bioprinting techniques have different cell viability outputs; inkjet-based, laser-assisted and stereolithography techniques have cell viability outputs of more than 85% while the extrusion-based bioprinting yield only 40% to 80% cell viability [38,55].

Bioprinting of large-scale tissues or organs is even more challenging in terms of cell viability as it will be challenging to maintain enough cell viability within the first printed layers of the construct when the printing time is more than a few hours. Moreover, the cell density that can be used with each technique is different, the inkjet-based technique can provide low cell density ($<10^6$ cells/mL), laser-assisted and stereolithography can work with medium cell density up to 10^8 cell/mL, while extrusion-based technique yields high cell density and even cell spheroids [2]. From the printing process point of view, cell density also affects the viscosity of the bioinks, the higher the cell density the higher the average viscosity, and this can affect the final construct's fidelity and the functionality of the printed tissue or organ [38,91]. These points need to be considered when adding a cell population to a hydrogel to make a bioink.

3.1.2 Cell type

The cells that are used within the bioinks can be either functional primary cells or stem cells that can be chosen based on the tissue or organ of interest [104,119–124]. Primary cells can be a good choice in cases of bioprinting of single tissues especially in the case of extrusion-based bioprinting since stem cells are more prone to environmental stimulation. When stem cells are forced to pass through narrow needle channels their membrane integrity,

13

differentiation capacity, and proliferation rate may be negatively affected [125,126]. Conversely, for complex tissues or organs, stem cells are a better choice since different cells need to be embedded in various biomaterial inks, which increases the complexity of the printing process and the potential for errors.

Although multiple cell bioprinting, or generally multiple bioink printing, is practical using multi-head bioprinters such as the commercially available 3-D Bioplotter (EnvisionTEC, Germany), there are limitations on the number of bioinks used on a single printer. For instance, the maximum cartridges (heads) that can be used with the Bioplotter on a single print is five. This problem can be addressed if the cartridges are not mounted on the robotic head and are not used in a cyclical manner. In this case, cartridges containing bioink that has already been used and no longer needed can be replaced with new cartridges and new bioink while the robotic head is using the other cartridges and bioinks. Generally, in cases involving complex tissue or organ bioprinting, it seems more reasonable to use stem cells as they can differentiate into a variety of tissues by using growth factors or inducerons [127]. This feature of stem cells makes them a good cell source for the bioinks especially if they are harvested directly from patients, which reduces the chance of an immune response and rejection [16]. The primary challenge of this approach is to precisely incorporate growth signals with the bioinks to elicit control of the cells' differentiation.

Table 1: Natural materials used as base biomaterials to formulate bioinks.

Table 2: Synthetic materials used as base biomaterials to formulate bioinks.

Table 3: Composite materials used as base biomaterials to formulate bioinks.

ALGINATE						
S.no.	**Cell type**	**Bioprinting method**	**Printing process parameters**	**Printed tissue**	**Outcomes**	**Ref.**
1.	HepG2	Layered direct cell-writing (type of extrusion-based)	Na-alg- 3 % (w/v), CaCl$_2$ – 5 % (w/v), strut diameter-125 µm, flow rate- 0.25 µl/h, channel depth- 20.5 µm, width- 817 µm down to 88 µm	Liver	• Increased metabolic drug conversion • Enhanced cell viability and controlled cellular level differentiation	[99]
2.	NIH 3T3	Extrusion-based	Na-alg 2 % (w/v), CaCl$_2$ – 400 mM, agarose- 2 % (w/v), gelatin- 10 % (w/v), flow rate- 10 µl/min	-	• Same cell viability observed between day 1 and day 7 • Jet of alginate beads can be controlled by optimizing printing parameters	[128]
3.	NIH 3T3	Laser-assisted	Na-alg- 1 %, 2 %, 3 % (w/v), CaCl$_2$- 2 % (w/v) ArF excimer wavelength-193 nm, strut diameter- 150 µm, frequency- 30 Hz, cell density- 5 x 10^6 cells/ml	-	• After 24 h, with increased alginate concentration, Ca^{2+}, gelation or laser exposure cell viability decreased	[129]
4.	CPCs	Extrusion-based	Na-alg- 3-6 % (w/v), CaCl$_2$- 2-5 % (w/v), 5 %, strut diameter- 445 µm, Na-alg and CaCl$_2$ flow rate- 6.6 and 4.15 ml/min, respectively	Vascular	• Alginate concentration affected diffusion rate of Ca^{2+} ions and thickness of hollow filament • Better differentiation and cell viability observed in 7 days was ~ 95 %	[130]
5.	L929	Extrusion-based	Na-alg- 2 % (w/v), CaCl$_2$- 4 % (w/v), Na-alg & CaCl$_2$ flow rate- 1 ml/min and 2 ml/min respectively, cell density- 1 x 10^6 cells/ml	Vascular	• High alginate concentration with smaller distance between adjacent hollow filaments generated high strength construct • Cell viability observed on day 1 and 7 was > 90 % and > 70 % , respectively	[37]
6.	HUVSMCs	Extrusion-based	Na-alg- 3-5 % (w/v), CaCl$_2$- 4 % (w/v), flow rate- 16 ml/min, printing pressure- 21 kPa, cell density- 10 x 10^6 cells/ml	Vascular	• Conduits with higher alginate concentration had lower cell viability, less porosity, lower permeability capacity and slower degradation process • ECM formation; high proliferation up to 7 days	[131]
7.	M231	Laser-assisted	Na-alg- 2 % (w/v), NaCl- 0.9 % (w/v), ArF excimer wavelength- 193 nm, deposition rate- 600 µm/s	-	• Beads with large range of sizes can be produced by laser direct-write technique • Cell viability decreased from 89.6 % to 84.3 % after 5 days	[132]
8.	Ea.hy926 and B16	Laser-assisted	Na-alg- 1 % (w/v), source wavelength- 1064 nm, frequency- 5 kHz, scanning speeds- 200, 400, 800 and 1600 mm/s	-	• Higher the viscosity or lesser the energy deposit, smaller will be the droplet size • The best cell printing resolution was achieved with a scanning speed of 200 mm/s	[91]
9.	RAMEC	MHDS	Na-alg- 1.5 % (w/v), strut diameter- 150-400 µm , printing pressure- 5 to 40 psi, cell density- 1 x 10^6 cells/ml, solution viscosity- 490 cP	-	• Increased printing pressure and small strut diameter decreased the cell viability • The cell viability was reduced to < 50 % when shear stress > 150 kPa with 250 µm strut diameter	[133]
10.	ASVFC	Extrusion-based	Na-alg- 1.5 % (w/v), flow rate- 5 mm/sec, cell density- 3 x 10^6 cells/ml, impeller speed- 5-10 rpm		• Controlled cell density in spheroids could control the cell delivery dose • Cell viability observed after 9 days was > 90%	[134]
11.	RHECs	MHDS	Na-alg- 1.5 % (w/v) , CaCl$_2$ – 0.5 % (w/v), strut diameter- 250 µm, printing pressure- 8-32 psi, resolution- 10 µm, deposition velocity- 100 µm/sec		• Due to porosity alginate scaffolds had lower elastic modulus compared to alginate disks • Elastic modulus decreased by 35 % after 3 weeks • For shear stress range of 100 kPa to 1150 kPa, cell viability ranged from 76 to 83 %	[12]
12.	NIH 3T3	Inkjet	Na-alg- 2 % (w/v), strut diameter-120 µm, voltage rise or fall time- 3 µs, dwell or echo time- 16-30 µs, excitation frequency- 50 Hz, waveform voltage- 45 V	-	• Increase in bioink cell concentration increased the droplet size and velocity resulting in the suppressed formation of satellite drop • Increase in bioink cell concentration increased the breakup time and decreased the ligament length	[135]

15

13.	NIH 3T3	Inkjet	Na-alg – 1 % (w/v), CaCl$_2$ - 2 % (w/v), cell density- 3 x 10^6 cells/ml, strut diameter- 120 µm, deposited layer thickness- 70 µm, excitation frequency- 50 Hz	Vascular	• Cell viability observed was > 80% after 72 h	[25]
14.	hASCs	Extrusion-based	Na-alg- 2 %, 5 %, 8 %, 10 %, 15 %, 20 % (w/w), NaCl- 0.9 % (w/w), porcine gelatin- 2 % (w/w), flow rate- 10 µl/s	-	• Oxidized alginate had high printing resolution and cell viability • Cell viability observed was < 90 % and > 90 % in alginate solutions with high and medium viscosity, respectively	[136]
COLLAGEN						
15.	hMSCs	Extrusion-based	Col I- 3 mg/ml, agarose- 3 % (w/v), strut diameter- 1.5-2.5 mm, agarose-collagen- 1:1, agarose-chitosan- 1:1	Bone	• Anisotropic soft collagen rich substrates supported osteogenesis whereas adipogenesis was mostly achieved in isotropic stiff agarose-rich matrices • Cell viability observed after 21 days was > 95%	[100]
16.	HFF-1 and HaCaT	Robotic dispensing	Col I- 3 mg/ml, dispensing cells volume- 15 nL, pulse duration- ~100-800 µs, actuation frequency- 1 kHz, cell density- 0.5-5 x 10^6 cells/ml	Skin	• The cell viability for HFF-1 observed was ~ 98 % at large droplet spacing of 400-750 mm and very low cell density of 0.5-0.75 x 10^6 cells/ml • The cell viability for HaCaT observed was ~ 98 % at small droplet spacing of 200-400 mm and very high cell density of 2-5 x 10^6 cells/ml	[137]
17.	NIH 3T3 and HaCaT	Laser-assisted	Col I- 3 mg/ml, laser wavelength- 1064 nm, pulse duration- ~10 ns, pulse frequency- 20 Hz	Skin	• The printed cells evolved intercellular communication and adhesion via gap junctions and adherens • The printed tissue model in the study was analogous to the native skin archetype.	[138]
18.	SMCs	Droplet ejector	Col I- 250 µL, agarose- 10 % (v/v), valve opening duration- 60 µs, nitrogen gas pressure- 34.4 kPa	-	• Uniform cell seeding and cell viability over long term culture • Cell viability observed was > 90% after 14 days	[139]
19.	MC3T3-E1 and hASCs	Extrusion-based	Col- 2 % (w/w) with pH- 7.5, cell density- 1 x 10^6 cells/pellet, pneumatic pressure- 150-220 kPa	Liver and bone	• Considerable cell proliferation/migration activity and osteogenic differentiation as compared to alginate based bioink • Cell viability observed after 1 day was ~ 88 %; higher hepatogenic differentiation and osteogenic activity was also observed	[140]
20.	NIH 3T3 and HaCaT	Laser-assisted	Col I- 37 µl, pH- 7.1 ± 0.3, cell density- 1.5 x 10^6 cells/pellet	Skin	• The printed skin constructs were connected fully to the surrounding tissue after 11 days of implantation on skin wounds in mice • Cell differentiation and proliferation found similar to native tissue	[121]
SILK						
21.	hTMSCs	MHDS	Silk fibroin- 5 % (w/v), cell density- 2-5 x 10^6 cells/ml, frequency- 1 Hz, agitation temperature- 40 ˚C, shear rate- 0.1- 1000/s, strain value- 5 %	-	• Hydrogel crosslinking with tyrosinase supported adipogenic and chondrogenic differentiation whereas crosslinking with sonication supported osteogenic differentiation	[141]
22.	BALB/3T3	Robotic dispensing	Silk protein- 3 % (w/v), strut diameter- 0.3 mm, cell density- 7.5 x 10^4 cells/cm^2, pre-gelling temperature- 37 ˚C and humidity- 95 %, valve opening time- 700-900 µs, flow pressure- 1-1.1 bar	-	• Recombinant spider silk proteins can be used as bioinks without need of any additive such as crosslinker • Cell viability observed was ~ 70 % after 2 days	[101]
DEXTRAN						
23.	Equine chondrocytes	Pneumatic Dispensing	Dex-HEMA- 10 % (w/v), frequency- 1 kHz, force measurement accuracy- 0.0025 %, resolution- 0.0025 mm, stress sweep pressure- 0.1-200 Pa	-	• Printed construct had well defined strand spacing and high porosity • Polysaccharide semi-IPN hydrogels showed excellent cytocompatibility	[102]
GELATIN						
24.	HNDFs and HUVECs	MHDS	Gelatin- 10 % (w/v), GelMA- 15 % (w/v), cell density- 2 x 10^6 cells/mL, frequency- 1 kHz, oscillatory strain- 0.01, temp. sweeps- -5 ˚C to 40 ˚C, printing speed- 1-10 mm/s, pressure- 20-	Vascular	• PDMS can print high-aspect ratio borders around the fabricated engineered tissue constructs • Cell viability observed was ~ 70 % and > 80 % on days 0 and 7, respectively	[103]

16

			60 psi			
25.	BMSCs, ACPCs and chondrocytes	Extrusion-based	Gelatin- 10 % (w/v), cell density- 1.5 x 10^7 cells/ml , strain range- 10-15 %, pressure- 0.180 MPa, translation speed- 20 mm/s	Cartilage	• ACPCs showed highest transcript expression of PRG4 and the lowest expression of col type X • Cell viability observed was ~ 75 % and ~ 90 % on days 1 and 14, respectively	[142]
26.	VIC and SMCs	Extrusion-based	Gelatin- 0.06 g/ml, cell density- 2 x 10^6 cells/ml, resolution- 100 µm, exposure time- 30 ms, path width- 0.8 mm, path height- 0.7 mm, path speed- 0.5 mm/s	Aortic valve	• Cell viability observed for VIC was ~ 91 % and ~ 86 % on days 1 and 7, respectively • Cell viability observed for SMCs was ~ 90 % and ~ 84 % on days 1 and 7, respectively	[119]
27.	C2C12	Cell assembler	Gelatin- 20 % (w/v), alginate- 7.5 % (w/v), cell density- 6 x 10^6 cells/ml, strut diameter- 150 µm, interlayer distance- 0.15 mm, filament gap- 1 mm, scanning speed- 7 mm/s , jet speed- 0.01 mm/s	-	• After 2 h post-printing cell viability obtained was ~ 54.72 % which increased after 24 h • Two types of samples were printed: acellular constructs and soft tissue models with cells • With an increase in culture time, acellular construct maintained their structural integrity without any collapse whereas structural integrity of soft tissue models decreased • Angled layers configuration (like 60˚) enhanced the strength of construct compared to 0˚/90˚ configuration	[122]
28.	MSCs	Extrusion-based	Gelatin- 10 % (w/v), agarose- 2 % (w/v), alginate- 3.5 % (w/v), cell density- 5 x 10^3 cells/cm², compressive strain- 10 %, ramp displacement- 0.001 mm/s , relaxation period- 30 min	Cartilage	• Alginate and agarose hydrogels supported hyaline-like cartilage formation whereas GelMA and BioINK™ (PEGMA based hydrogel) supported more fibrocartilage-like tissue	[143]
29.	SaOS-2	Extrusion-based	Gelatin- 50 mg/ml, Na-alg- 50 mg/ml, polyP.Ca²⁺ complex- 100 µM, cell density- 5 x 10^5 cells/ml, pressure- 0.9 bar, speed- 26 mm/s, scaffold diameter- 13 mm and height- 1.5 mm	-	• Addition of agarose and polyP.Ca²⁺on alginate/gelatin/SaOS-2 cell scaffold showed marked increase in cell proliferation • Hardness of alginate/gelatin hydrogel increased in presence of polyP.Ca²⁺ • The reduced Young's modulus for alginate/gelatin hydrogel increased from 13-14 kPa to about 22 kPa due to addition of 100 µM polyP.Ca²⁺	[144]
30.	NIH 3T3 and HepG2	Extrusion-based	Gelatin- 10 % (w/v), capillary inner diameter- 500 µm and height- 85 mm, flow rate- 2 mm/s , UV light- 6.9 mW/cm²	Vascular	• The elastic modulus of the hydrogels increased proportionally with an increase in polymer concentration and UV light exposure time • Cell viability observed was > 80 % after 8 days.	[145]
FIBRIN						
31.	Rabbit articular chondrocytes	Inkjet	Fibrinogen- 10 mg/ml, collagen I- 1.5 mg/ml, electrospinning speed 3 ml/h and duration- 30 min at 20 kV	Cartilage	• Inkjet printing, when used in combination with electrospinning, produced scaffolds with enhanced mechanical properties and higher cell viability than inkjet printing alone • Cell viability observed was > 80 % after 7 days	[104]
32.	-	Custom-made inkjet bioprinter	Na-alg- 0.8 % (w/v), CaCl₂- 2 % (w/v)	-	• Fibrin gel formed was soft and fragile which created difficulty in maintaining the fabricated 3D structure	[146]
33.	hASCs and ECFCs	Laser-assisted	Fibrinogen- 13.3 mg/ml, HA-Fibrinogen- 1:2 (v/v), cell density- 1 x 10^5 cells/cm², shear viscosity- 120 mPa	Vascular	• Cell viability obtained just after printing was ~ 99 % and ~ 97 % for hASCs and ECFCs, respectively • No significant difference was observed between the proliferation of hASCs and ECFCs after 11 days	[147]
AGAROSE						
34.	L929 and MG-63	Extrusion-based (submerged bioprinting)	Agarose- 3 % (w/v), Na-alg- 3 %, CaCl₂- 50 mg/ml, strut diameter- 570 µm, cell density- 2 x 10^6 cells/ml, orifice diameter- 5 mm	-	• Cell viability observed was 96, 99 and 97 %, on days 1, 4 and 7, respectively • Cells survived the submerged bioprinting minimally for 21 days	[105]
35.	MG-63 and MSCs	Extrusion-based	Agarose- 3 % (w/w), dispensing accuracy- 46 µm, axis resolution- 15 µm, dispensing volume- 15 nl, resolution-	-	• MG-63 and MSCs cell-agarose gels showed excellent compressive strength of 10 and 15 kPa, respectively	[120]

17

No.	Cells	Method	Parameters	Tissue	Remarks	Ref.
			575 µm			
36.	SMCs	Droplet generation by valve opening and nitrogen pressure	Col I- 250 µL, agarose- 10 % (v/v), valve opening duration- 60 µs, nitrogen gas pressure- 34.4 kPa	-	• Cell viability was > 90% after 14 days	[139]
37.	NIH 3T3	Bioprinting with a valve ejector	Agarose- 1 % (w/w), 2 % (w/w), speed- 20 mm/s, pulse width- 200 µs, valve pressure- 5 psi, ejection frequency- 10 Hz, agarose-bacteria mixture concentration- 9.5 x 10^7, 1.9 x 10^8, 3.8 x 10^8 CFUs/ml	-	• Mechanical properties, pore interconnectivity and porosity of scaffolds can be controlled by incorporating microorganisms in hydrogels	[148]
			GELLAN GUM			
38.	MSCs	Extrusion-based	GelMA- 10 % (w/v), gellan gum- 1 % (w/v), strut diameter- 0.61 mm, cell density- 1 x 10^5 - 3 x 10^5 cells/well, inoculum cell density- 2 x 10^5 cells/ml, UV exposure- 15 min	Bone/cartilage	• Addition of gellan gum improved the printing ability and enhanced the solution viscosity of bioink • Osteogenic differentiation and cell viability supported by microcarriers • Cell viability was > 90 % after 3 days	[106]
39.	MC3T3	Extrusion-based	GelMA- 10 % (w/v), gellan gum- 0.75 % (w/v), strut diameter- 0.21 mm, solution viscosity- 1, flow index- 0.33, strain- 10-15 %	-	• Addition of high concentration of gellan gum to hydrogels led to decrease in swelling and increase in compressive moduli • Cell viability did not get affected by addition of gellan gum	[15]
40.	Primary neural cells	Extrusion-based hand held printing	Gellan gum- 1 % (w/v), paraformaldehyde- 3.7 %, strut diameter- 0.2 mm, cell density- 2 x 10^6 cells/ml, crosslinker dispensing rate- 0.1 ml/min	Brain	• Peptide modification of gellan gum hydrogel had positive effect on primary cell proliferation and network formation • Cell viability observed was > 70 % after 5 days	[149]
41.	Equine chondrocytes and MSCs	Extrusion-based	Na-alg- 10 % (w/v), GelMA- 10 % (w/v), gellan gum- 1.1 % (w/v), cell density- 5 x 10^3 cells/cm^2, strand spacing- 0.8 -1.8 mm	-	• High viscosity alginate was stable enough to carry the overlying structures without crosslinking • Cell viability observed was ~ 75-86 % after 1-3 days	[123]
			HYALURONIC ACID			
42.	Int-407, HepG2 C3A and NIH 3T3	Extrusion-based	AuNPs- 24 nm, cell density- 25 x 10^6 cells/ml, syringe tip- 250 µm, disc diameter- 3-5 mm, construct diameter- 0.8-1.0 cm, construct height- 1-2 cm	-	• Fibroblasts had remodeled the temporary AuNP-semi-synthetic ECM after 4 weeks in culture and secreted an endogenous collagen-rich ECM • Cell viability observed was > 95 % on days 3 and 7, respectively	[107]
43.	Chondrocytes and osteoblasts	Extrusion-based	HA- 2 % (w/v), cell seeding density- 2 x 10^4 cells/ml, optical density- 450 nm, steel ball diameter- 0.3 mm and mass- 0.9 g	Osteochondral	• Col-1 based matrixes supported bone tissue engineering whereas cartilage tissue engineering was better supported by HA-based matrixes	[150]
44.	Bovine chondrocytes	Extrusion-based	HA- 1 % (w/v), amino-terminated pNIPAAM- 3.5 g, flow rate- 0.8 ml/min, cell density- 2 x 10^4 cells, pH-8, strain- 1 %, shearing rate- 100/s for 1 s	-	• Scaffolds with high-resolution were printed by addition of HA-pNIPAAM to HAMA • HA-pNIPAAM provided immediate post-printing structural fidelity and fast gelation • But, cell death occurred when cells were embedded in HAMA-HA-pNIPAAM bioink; cell viability increased after removal of HA-pNIPAAM	[151]
45.	Int-407, HepG2 C3A, and NIH 3T3	Dual syringe deposition tool	HA- 1 g, HAMA- 1.5 % (w/v), HAMA : GEMA- 4:1 (w/w), cell density- 25 x 10^6 cells/ml, shear modulus- < 50 Pa, shear sweep test- 0.6-20 Pa, frequency- 1 Hz	-	• The hydrogels of HAMA and GEMA were biocompatible in vivo and cytocompatible *in vitro* and supported cell attachment and proliferation • Cells maintained their viability under high-stress conditions (5–20 g of rotational force)	[152]
46.	Chondrocytes	Pneumatic dispensing	Gelatin- 10 % (w/v), HA- 2.4 % (w/v), MA- 0.6 g/g of gelatin, cell density- 5 x 10^6 cells/ml, strain- 10 to 15 %, deposition speed- 176 mm/min, spindle speed- 1.5, strand distance- 1.5 mm	Cartilage	• When combined with GelMA, HA act as viscosity enhancing agent for human cartilage engineering • Cell viability was ~ 82 % and 73 % after 3 days on GelMA-HA and GelMA scaffolds, respectively	[153]

18

47.	HAVIC	Multi-material bioprinter	Me-HA 2, 4 and 6 % (w/v) and Me-Gel 6,10 and 12 % (w/v), cell density- 5 x 10^6 cells/ml, hydrogel diameter- 8 mm and thickness- 2 mm, cross-head speed- 0.075 mm/s, shear stress- 1 to 1000 Pa	Heart valve	• Increased Me-Gel concentration in hybrid hydrogel led to decreased hydrogel stiffness and increased cell adhesion density • Cell viability observed was > 90% after 7 days	[154]
DE-CELLULARIZED MATRIX						
48.	hASCs	Dispensing system	Acetic acid- 0.5 M, pepsin- 10 mg/100 mg DAT, strut diameter- 250 µm, cell density- 2 x 10^6 to 5 x 10^6 cells/ml, pneumatic pressure- 20 kPa	Adipose	• DAT bioink had better induction of hASCs towards adipogenic lineages without any deleterious effect on hASCs	[108]
49.	hTMSCs, hASCs and rat myoblasts	Plunger-based dispensing system	Acetic acid- 0.5 M, pepsin- 10 mg/ 100 mg dECM, cell density- 5 x 10^5 cells/ml, shear rate- 2/s, strain- 2 %, dynamic frequency sweep- 1-1000 rad/s, temperature ramp- 4-37 °C, pneumatic pressure- 400-650 kPa	Heart/adipose/ cartilage	• Cellular construct fabricated using dECM ink demonstrated tissue specific gene expression and organized spatial pattern	[155]
50.	Primary human stellate cells, primary human hepatocytes, and primary human kupffer cells	Extrusion-based	HA- 1 % (w/v), gelatin- 2 % (w/v), force- 0.4 N, shear stress sweep- 0.6 to 10 Pa, frequency- 1 Hz	Liver	• Maintenance of physiological temperature, printing time under 1 h, and incorporation of liver-specific cell culture media into bioink resulted in increased cell viability	[156]
MATRIGEL						
51.	HUVECs and B16	Laser-assisted	Matrigel- 4 mg/ml, cell density- 50 x 10^6 cells/ml, pulse duration- 30 ns, frequency- 5 kHz, scanning speed- 200, 400, 800 and 1600 mm/s, distance between ribbon and substrate- 200 µm	-	• Higher the viscosity or lesser the energy deposit, smaller will be the droplet diameter • The best cell printing resolution was achieved with a scanning speed of 200 mm/s	[91]
52.	EPCs	Pneumatic dispensing system	Matrigel- 200 µl, VEGF- 10 µg/ml, cell density- 2 x 10^6 cells/cm^2, ramp force- 0.1 to 1 N	Vascular	• Increased scaffold vascularization was observed in vivo due to lengthened presence of VEGF • Formation of vessel-like structures was decreased and degradation was increased	[157]
53.	EA.hy926 and A549	Inkjet	Strut diameter- 0.3 mm, cell density- 4.5 x 10^6 cells/ml, printing resolution- < 5 µm, printable volume- 5 to 10 nl	Lung	• Printed endothelial cells were less permeable whereas there was no difference between the printed epithelial and manually seeded cells • Cell viability was > 86% and > 95% after 3 days for endothelial and epithelial cells, respectively	[158]
54.	Goat multipotent stromal cells	Pneumatic dispensing	Matrigel- 100 µl, Na-alg- 3 % (w/v), HA- 82 %, cell density- 1 x 10^7 cells/ml	Bone	• BMP-2 significantly increased bone formation and led to osteogenic differentiation independent of its release profile • Fast release group: empty GMPs (PBS laden) and 25 ng/ml BMP-2 in the alginate, Slow release group: 25 ng/ml BMP-2 loaded on 2 mg GMPs. • Osteocalcin expression was lower in fast release group than the slow release group	[159]
HYDROXYAPATITE						
55.	EA.hy926	Laser-assisted	Cell density- 10^6 cells/ml, pulse duration- 30 ns, frequency- 1-100 kHz, mean power- 7 W, (x,y) axis resolution- 1 µm, z axis resolution- 5 µm, scanning speed- 2000 mm/s	-	• HT-BioLP requires low glycerol concentration as compared to conventional laser bioprinting which reduces experimental time and deleterious effects of placing cells in glycerol • HT-BioLP successfully created well-defined nano-sized HAp patterns	[109]
56.	hMSCs	Inkjet	HAp- 2 % (w/v), cell density- 6 x 10^6 cells/ml, UV exposure intensity- 4 to 8 mW/cm^2, plastic mold internal diameter- 4 mm, acetic acid- 0.05 M, pepsin- 100 µg/ml, printed layer thickness- 18 µm	Bone	• Col and ALP expression were highest in HAp used group • Presence of HAp in scaffold stimulated the hMSCs osteogenic differentiation, osteogenic ECM production with minimum cell toxicity • Cell viability was ~ 86 % after 21 days	[160]

57.	hMSCs	3D printing with a heatable nozzle	HAp- 8, 16 %, Na-alg- 4 % (w/v), gelatin- 20 % (w/v), mold diameter- 5 mm and height- 2 mm, CaCl$_2$- 2 % (w/v), shear rate- 0.0001/s to 100/s, temperature ramp- 50 °C to 10 °C	Bone	• Inclusion of HAp enabled the visualization of hydrogel with µCT and increased the gel point with minimal loss in filament homogeneity • Cell viability was ~ 85 % after 3 days	[161]
58.	HOP cells	Laser-assisted	Cell density- 50 x 10^6 cells/ml, pulse duration- 30 ns, bioink film thickness- 20-30 µm, frequency- 5 kHz, spot size- 40 µm, distance between ribbon and substrate- 400 µm	Bone	• Nano-HAp and HOPs were printed in 2D and 3D without affecting their physiochemical properties • Cell viability was retained for 15 days	[162]
			GROWTH FACTOR			
59.	C2C12	Inkjet	Orifice diameter- 30 µm, center to center drop spacing- 75 µm, printed gradient length- 1.5 mm and width- 1 mm, deposited drops spacing- 80 µm, pH- 7.4	-	• *In vitro* osteoblast formation could be spatially controlled by printing growth factor (BMP-2) within derma matrix scaffolds	[163]
60.	C2C12	Inkjet	BMP-2- 10 µg/ml, printed gradient length- 1.5 mm, center to center drop spacing- 67 µm, spot size- 70 µm, pH- 7.4	-	• ALP expression was not observed in cells present in FGF-2 printed part whereas it is observed in cells lying in BMP-2 printed part	[164]

PEG						
S.no.	**Cell type**	**Bioprinting method**	**Printing process parameters**	**Printed tissue**	**Outcomes**	**Ref.**
1.	MSCs	Extrusion-based	Na-alg- 4 % (w/v), gelatin- 20 % (w/v), shear stress ramp- 0.01-100 Pa, shear rate- 0.01-2000/s, dispensing tip length-	-	• Shear level up to 1639/s did not affect the cell viability • The flow rate between samples increased	[110]

Table 1: Natural materials used as base biomaterials to formulate bioinks.

			12.22 mm and inner diameter- 0.2-0.33 mm		significantly and the residence time of the bioink within the needle was very short due to increased pressure	
2.	hMSCs	Modified inkjet	Cell density- 5 x 10^3 cells/cm^2, mold inner diameter- 4 mm, acetic acid- 0.05 M, pepsin- 100 µg/ml, printing resolution- 300 dPi, printed layer- 18 µm	Bone	• As compared to bioactive glass, HAp was found more effective towards osteogenic differentiation and osteogenic ECM production with minimum cell toxicity • Cell viability observed was > 85 % after 21 days	[160]
3.	NIH 3T3	Extrusion-based	GelMA- 15 % (w/v), PEGDA- 20 % (w/v), RAPID- 5 % (w/v), cell density- 10 x 10^3 cells/µl, flow rate- 60-75 µl/min, plate diameter- 8 mm, strain sweep- 0.001 to 100	-	• Three types of bioinks: PEGDA, GelMA, RAPID were used in the study • RAPID inks showed 4 % or less damaged cells whereas PEGDA and GelMA had < 10 % cell damage	[165]
4.	HUVECs	Extrusion-based	PEGX- 5000 g/mol, strut diameter- 200 µm, sweep time-120 min., printable volume- 200 µl, strain- 0-20 %, pressure- 1- 2.5 bar, printing speed- 5 mm/s	-	• Various new 3D-printable bioinks could be developed using other PEGX which may permit additional crosslinking chemistries	[166]
5.	hMSCs	Extrusion-based	Col- 2 mg/ml, PEG – 20 % (w/w), Na-alg- 2.5 % (w/w), acetic acid- 0.6 %, cell density- 3 x 10^6 cells/ml, resolution- 500 µm	-	• Tough hydrogel with high elasticity can be created using PEG • PEG hydrogels had lower fracture energies than the corresponding PEG–alginate hydrogels • Cell viability observed was > 75% after 7 days	[167]
6.	Int-407, HepG2 C3A, and NIH 3T3	Extrusion-based	PEG- 1.7 g, cell density- 5 x 10^4 cells/100 µl, steel disc- 40 mm, shear stress sweep- 0.6 to 20 Pa, frequency- 1 Hz	Vascular	• Two four-armed PEG derivatives were synthesized for the fabrication of extrudable ECM hydrogels which were easy to prepare and biocompatible for printing tubular tissue construct	[168]
7.	hMSCs	Extrusion-based	PEG-norbornene- 5, 10, and 20 kDa, colloidal probe diameter- 5 µm, spring constants- 0.6 N m^{-1}, printing speed- 10 mm s^{-1} or 0.27 ml min^{-1}, nozzle tip sizes- 840 and 600 µm, infill printing density- 60 %, cell density- 5 x 10^6 cells per ml, strain- 1 %	-	• hMSCs were attached and spread on RGD presenting microgels, whereas aggregated into cell clusters and did not interact with microgels lacking RGD • cell viability was ~88 % at 1 hour, ~80 % at day 1 and ~90 % at day 5 and 10	[169]
PVP						
8.	HFF-1	Inkjet	PVP- 2.5 % (w/v), cell density- 0.5-2.5 x 10^6 cells/ml, shear rate- 0.1 to 1000/s, strut diameter- 100 µm, printing pressure- 0.25 bar	-	• PVP molecules inclusion affects the Z value which influenced the printability of bioinks • PVP based bioinks improved the homogeneity and viability of printed cells	[112]
PCL						
9.	Rabbit chondrocytes	Inkjet	PCL- 10 % (w/v), construct thickness- 0.4 mm, cell density- 3-4 x 10^6 cells/ml, stretch rate- 0.2 mm/s	Cartilage	• Cartilage construct with enhanced mechanical properties could be fabricated using electrospinning and inkjet printing in combination rather than inkjet printing alone • Cell viability observed was > 80 % after 7 days	[104]
10.	C20A4	Pneumatic dispenser	PCL Mw- 70 000–90 000 Da, cell density- 5 x 10^6 cells/ml, pressure- 0.5 Pa, strut diameter- 210 µm, deposition speed- 176 mm/min, spindle speed- 1.5, force rate- 0.2 N/min	-	• Addition of PCL support increased Young's modulus significantly • Cell viability also increased after printing due to PCL in construct rather than alone alginate-based scaffolds • Cell viability observed was 90 % and 70 % on days 1 and 3, respectively	[63]
11.	Human nasal septal chondrocytes	MHDS	Na-alg- 2, 6 % (w/v), TGFβ - 10 ng/ml, strut diameter- 250 µm, pressure- 650 kPa, deposition speed- 400 mm/min	Cartilage	• PCL-alginate gels showed higher ECM formation due to the presence of TGFβ • Increased Col-II and cartilage tissue formation were observed in PCL–alginate gel withTGFβ	[170]
12.	Chondrocytes and osteoblasts	Extrusion-based	HA- 2 %, alginate- 2 %, cell density- 5 x 10^4 cells/well, , cell culture dish- 35 mm, steel ball diameter- 0.3 mm and mass- 0.9 mg	Osteochondral tissue	• The higher amount of osteogenic marker and chondrocytes marker were seen with Col-1 and HA hydrogels, respectively	[150]
PLURONIC						
13.	Primary culture bovine	Extrusion-	Pluronic F127- 20.05 g, HA- 1 g, cell density- 2 x 10^7 cells/ml, strain- 0.5 %,	-	• Mechanical properties and bioactivity of pluronic hydrogels could be enhanced by inclusion of	[113]

21

| chondrocytes | based | frequency- 5 rad/s, heating rate- 0.5 °C/min, feed rate- 100 mm/min | | methacrylated biopolymer and degradable MMP sequence or cell recognition sites such as RGD, respectively
• For pure pluronic and modified pluronic bioinks, cell viability observed was 62 and 86 %, respectively | |

Table 2: Synthetic materials used as base biomaterials to formulate bioinks.

S.no.	Cell type	Bioprinting method	Printing process parameters	Printed tissue	Outcomes	Ref.
AGAROSE/CHITOSAN						
1.	MSCs	Extrusion-based	Agarose-chitosan- 1:1, hydrogel drop diameter- 1.5-2.5 mm, NaCl- 0.9 g, cell density- 1×10^5 cells/ml	Bone	• Cells differentiated into adipogenic tissue in agarose matrix and into osteogenic tissue in collagen matrix • Cell viability was > 95 % after 21 days	[100]
HAMA-Phpma-lac/PEG						
2.	Primary culture equine chondrocytes	Extrusion-based	HAMA- 0-1 % (w/w), cell density- 5×10^3 cells/cm^2, strut diameter- 0.56 mm, mold diameter- 6 mm, mold height- 2 mm, force- 0.001 N, force ramp- 0.1 N/min	Cartilage	• Stiffness of 3D construct increased with increase in HAMA concentration • Higher HAMA concentration led to undesirable fibrocartilage formation	[111]
PG-HA						
3.	Human and equine MSCs	Extrusion-based	HA- 5 g, cell density- $3-5 \times 10^4$ cells/ml, sample elution rate- 0.7 ml/min, cylindrical mold diameter- 6 mm and height- 2 or 1 mm, displacement rate- 0.001 mm/s, strain- 0-10 %	Articular cartilage	• HA amount should be lower as the higher amount of HA leads to decrease in chondrogenic potential • PG-HA bioink showed better cell differentiation and viability as compared to PG alone bioink	[114]
ALGINATE/GELATIN						
4.	AECs and WJMSCs	Extrusion-based	Na-alg- 2 % (w/v), gelatin – 15 % (w/v), CaCl$_2$- 2 % (w/v), printing resolution- 151 ± 13.04 μm, temperature- 4 °C, Cell density- 1×10^5 cells/ well, stage moving velocity- 7 mm/s, shear rate- 0.01-300/s, temperature ramp- 40 °C to 0 °C, cooling rate- 2 °C/min, frequency- 1 Hz, strain rate- 5 mm/min	Skin	• AECs could differentiate into epithelial cells whereas, WJMSCs showed a superior angiogenic potential and fibroblastic phenotype • Cell viability was > 95 % up to 6 days after printing	[171]
FIBRINOGEN/GELATIN						
5.	HDF-n	Extrusion-based rotary bioprinting	Gelatin- 7.5% (w/v), fibrinogen- 10 mg/ml, flow rate- 1-7 ml/min, cell density- 1 or 3×10^6 cells/ml, shear rate- 0.1/s to 100/s, frequency- 0.1 Hz	Vascular	• Heat treated gelatin (90 °C for 1 h) with 3.75 % (w/v) or higher was suitable to have an extrudable bioink that could maintain shape during printing • Cell viability was ~84 % (5 % (w/v) and 1 h heat-treated gelatin) and ~61 % (10% (w/v) and 1 h heat-treated gelatin)	[172]
PLA/PEG/nHAp/DEXAMETHASONE						
6.	MC3T3-E1	Extrusion-based	PLA- 90, 91, 92, 93, 94 % (w/w), PEG- 4, 6, 8 % (w/w), nHAp- 1, 2, 3 % (w/w), dexamethasone- 1, 2, 3 % (w/w), strut diameter- 0.5 mm, scanning speed- 30 mm/s, cell density- 5×10^4 and 3×10^4 cells/ml	Bone	• PEG with 8% (w/w) concentration led to the fastest degradation due to solubility of PEG into surrounding media • The increase in nHAp content resulted in enhanced tensile strength upto 36.49 MPa • Addition of dexamethasone slowed down the degradation rate • Cell viability was ~77 % at 72 h in scaffold with PLA, PEG, nHAp and Dex with 92 %, 6 %, 2 % and 3 % (w/w), respectively	[173]
ALGINATE/CNC						
7.	NIH 3T3 and human hepatoma cells	Extrusion-based	Na-alg- 4 and 6 % (w/v), CNC- 2, 4, 6 and 8 % (w/v), CaCl$_2$- 1 % (w/v), extruding pressure- 5-25 psi, printing speed- 25 mm/s, cell density- 10^6 cells/ml, shear rate- 0.1-500/s, frequency- 1 Hz	Liver	• Hybrid pre-gel solutions were solid-like and provided good shape fidelity after extrusion as compared to pure alginate • Amongst various compositions, the 20/40 bioink (Na-alg, CNC and water content were 2, 4 and 96 % (w/v), respectively) exhibited highest printing accuracy • Cell viabilities of fibroblast and hepatoma cells on day 0 were ~70 % and ~67 %, respectively which decreased to ~58 % and ~49 %, respectively after 3 days	[174]
8.	Human nasoseptal	Extrusion-	Na-alg- 0.625 %, 1.25 %, 2.5 %, 5 %, 7.5 % and 10 % (w/v), CNC- 3 % (w/v),	-	• Nanocellulose-alginate bioink combinations showed reversible stress softening behavior with	[175]

23

	chondrocytes	based	NCB- 3 wt %, CNF- 6 wt %, cell density- 2 x 10^6 cells/ml, stress- 0.5 Pa, shear rate- 0.1-100/s		• high degree of shear thinning • Cell viability for NCB-AG, CNC-AG and CNF-AG were ~84 %, ~80 % and ~72 %, respectively immediate after the printing	
HAMC						
9.	MSCs	Extrusion-based	HAMC blends- 0.25/0.5, 0.5/1, 1/2, 1/3, 2/5, 2/6, 2/7 and 2/9 wt %, deposition speed- 3 mm/s, printing air pressure- < 200 kPa, strain- 1 %, frequency- 1 Hz	-	• The HAMC blend with composition HA- 1 wt % and MC- 3 wt % showed the best printing accuracy • HAMC blends have gelling typically upon reaching 37 ˚C and showed viscous behavior at 4 °C and have faster gelation times at higher temperatures • Cell viability was > 75 % and remained viable for 1 week post printing	[176]
SF-PEG4A						
10.	NIH/3T3 and keratinocyte	Digital light processing 3D printing (modified form of SLA)	SF-PEG4A- 4 % (w/v), SF- 0, 0.25, 0.5,1 and 2%, light irradiation time- 120 s, cell density- 1.5 x 10^6 cells/ml, strain- 0-10 %	Skin	• SF polyethylene glycol hydrogels showed higher cell proliferation and cell spreading • Keratin layer was formed thicker with SF-PEG4A hydrogels as compared to PEG4A hydrogels • SF-PEG4A hydrogels showed improved mechanical properties with increasing SF content due to contribution of crystalline SF structures • SF-PEG4A hydrogel with 1 wt % SF have 15.5 kPa compressive modulus as compared with 4.5 kPa in the pure PEG4A hydrogel	[177]
HYDROXYAPATITE/GELATIN						
11.	MC3T3-E1	Extrusion-based	Gelatin- 2.4 g, HAp- 3.6 g, printing air pressure- 0.35 MPa, printing speed- 8 mm/s, nozzle diameter- 0.42 mm, cell density- 1 x 10^5 cells/well, strain- 50 %	Bone	• LbL coating of chitosan and sodium hyaluronate on porous scaffolds reduced the swelling ratio of scaffolds in size with increase in compressive strength by ~ 70% • Rhodamine-B (model drug) released little slower whereas bovine serum albumin (model drug) showed faster released rate with LbL coated scaffold as compared to that without coating • Cell adhesion was higher in coated scaffolds as compared to blank scaffolds	[178]
LPN-GelMA						
12.	HBMSCs	Extrusion-based	GelMA- 5, 7.5 and 10 % (w/v), LPN-0.5, 0.75, 1, 2 % (w/v), cell density- 5 x 10^6 cells/ml, strain- 10-15 %, shear rate- 8/s, frequency- 1 Hz	Bone	• Inclusion of LPN (0.5 and 1 wt %) significantly improved the printability of bioinks resulting in high quality 3D printed scaffolds, • Cell viability was ~ 86 % over 21 days of culture in LPN-GelMA, whereas there was a significant decrease in cell viability in GelMA alone from ~ 96 % at day 7 to ~ 56 % at day 21	[179]

Table 3: Composite materials used as base biomaterials to formulate bioinks.

HepG2- liver hepatocellular cells, Na-alg- sodium alginate, CaCl$_2$- calcium chloride, NIH 3T3- mouse embryo fibroblast cell line, ArF- argon fluoride, CPCs- Cartilage progenitor cells, L929- mouse fibroblast cell line, HUVSMCs- human umbilical vein smooth muscle cells, ECM- extra-cellular matrix, M231- human breast cancer cells, NaCl- sodium chloride, EA.hy926- human endothelial cell line, B16- rabbit carcinoma cell line, RAMEC- rat adrenal medulla endothelial cells, MHDS- multi-head deposition system, ASVFCs- adipose stromal vascular fraction cells, RHECs- Rat heart endothelial cells, hASCs- human adipose derived stem cells, hMSCs- human mesenchymal stem cells, Col- collagen, HFF-1- human foreskin fibroblasts, HaCaT- aneuploid immortal keratinocyte cell line from adult human skin, SMCs- smooth muscle cells, MC3T3-E1- preosteoblast cells, hTMSCs- human nasal inferior turbinate tissue-derived mesenchymal stromal cells, BALB/3T3- mouse fibroblasts, Dex-HEMA- hydroxyethyl-methacrylate-derivatized Dextran, semi-IPN- semi-interpenetrating network, HNDFs- human neonatal dermal fibroblasts, HUVECs- human umbilical vein endothelial cell line, GelMA- gelatin methacrylate, PDMS- poly(dimethyl siloxane), BMSCs- bone marrow derived mesenchymal stromal cells, ACPCs- articular cartilage-resident chondroprogenitor cells, PRG4- proteoglycan 4, VIC- aortic valve leaflet interstitial cells, C2C12- mouse myoblasts, PEGMA- poly(ethylene glycol) methacrylate, SaOS-2- human osteogenic sarcoma cells, polyP.Ca^{2+}- calcium salt of polyphosphate, UV- ultraviolet, ECFCs- endothelial

24

colony-forming cells, HA- hyaluronic acid, MG-63- human osteosarcoma cells, PCL- polycaprolactone, PLGA - poly(lactic-co-glycolic acid), Int-407- human intestinal epithelial cells, AuNPs- gold nanoparticles, pNIPAAM- poly(N-isopropylacrylamide), HAMA- methacrylated hyaluronic acid, GEMA- methacrylated ethanolamide derivative of gelatin, HAVIC- human aortic valvular interstitial cells, Me-Gel- methacrylated gelatin, Me-HA- methacrylated hyaluronic acid, DAT- decellularized adipose tissue, dECM- decellularized extracellular matrix, EPCs- Endothelial progenitor cells, VEGF- vascular endothelial growth factor, A549- alveolar epithelial type II cells, BMP-2- bone morphogenetic protein 2, GMPs- gelatin microparticles, PBS- phosphate buffered saline, HT-BioLP- high-throughput BioLP, Hap- hydroxyapatite, ALP- alkaline phosphatase, μ-CT- micro-computed tomography, HOPs- human osteoprogenitors, C2C12- myogenic precursor cells, FGF-2- fibroblast growth factor-2, PEG- polyethylene glycol, PEGDA- poly(ethylene glycol) diacrylate, RAPID- recombinant-protein alginate platform for injectable dual-crosslinked, HAMA-Phpma-lac/PEG - methacrylated hyaluronic acid-methacrylated poly[*N*-(2-hydroxypropyl)methacrylamide mono/dilactate/ polyethylene glycol, PVP- polyvinylpyrrolidone, C20A4- human chondrocyte cells, TGF*β*- transforming growth factor- *β*, MMP- matrix metallopeptidases, RGD- arginine-glycine-aspartic acid, PG- poly(glycidol), AECs- human amniotic epithelial cells, WJMSCs- Wharton's jelly derived mesenchymal stem cells, HDF-n- neonatal human dermal fibroblasts, CNC- cellulose nanocrystals, CNF- cellulose nanofibrils, NCB- bacterial nanocellulose HAMC- hyaluronic acid/ methylcellulose, SF-PEG4A- silk fibroin incorporated 4-arm polyethylene glycol acrylate, LPN- laponite, HBMSCs- human bone marrow stromal cells

3.2 Peptide bioinks

Self-assembling peptide hydrogels (SAPHs) are gaining increasing interest as advanced printable bioinks. Their seminal features include high water content, great biocompatibility, capacity to print 3D cell-laden constructs with improved structural integrity and tunable mechanical stability, whilst providing an ECM-like microenvironment [180,181]. This class of 8-32 amino acid long oligopeptides, with hydrophilic and hydrophobic side chains) can undergo self-assembly predominantly via non-covalent interactions such as Van der Waals forces, hydrogen bonding, and hydrophobic interactions to form secondary structures such as α-helix and β-sheets [182]. External stimuli such as temperature, electrolytes, and pH further trigger the secondary structures to form nanostructures with distinct morphologies such as micelles, nanofibers, and nanotubes [183]. Such nanostructures augment the shape fidelity and mechanical rigidity of the 3D bioprinted construct.

Chemical modifications and conjugation of the amino acid side chains in peptides can induce additional functionalities such as bioactivity, self-healing, shear-thinning, and shape memory to the bioinks [184]. Ultra-short peptides (≤ 4 amino acids) are preferred in bioinks for their facile synthesis, stimuli-responsive gelation behavior under physiological conditions and cost-effectiveness [185,186]. Loo et al. reported first peptide bioinks with lysine-containing hexapeptides (Ac-ILVAGK-NH$_2$) that could self-assemble into nanofibrous 3D stable hydrogels. These peptide hydrogels printed via an extrusion-method presented stiffness of

~40 kPa could support the 3D culture of human stem cells and differentiation of primary cells [186].

Synthetic self-assembling tetramer peptide (CH-01 and CH-02) biomaterials have been used for skeletal muscle tissue engineering. These peptide biomaterials could promote the growth and alignment of mouse myoblast cells (C2C12) while preserving their viability. Also, the 3D cultured cells in peptide-based scaffold printed via extrusion could replace the degrading hydrogel by secreting their ECM-like matrix. When compared to the alginate-gelatin hydrogel as control, the proliferation of C2C12 cells was well-aligned in the peptide hydrogels [187].

Recently, Cofiño et al. added methylcellulose (MC, reinforcer and thickening material) to self-assembling peptide RAD16-I (16-amino acid peptide, 'PuraMatrix') solution for biocompatibility and to enhance printability. Among various concentrations tested, MC with 4 % (w/v) blended with 3 % (w/v) peptide solution resulted in scaffolds with high shape fidelity and a strand diameter of ~ 400 μm. Results from the study showed that rat MSCs were able to differentiate into adipogenic lineage reflecting the potential of this peptide bioink for soft tissue engineering systems [182].

Most recently, Gatenholm invented a method to print a novel bioink of RGD-conjugated alginate together with human fibroblasts for human skin 3D bioprinting, particularly dermis. A coaxial needle was used to cross-link the bioink during the printing operation. This methodology conferred the printed construct with high amounts collagen I, a high degree of stretching of fibroblasts, high cell viability, and proliferation. This bioink construct offers a way to test cosmetics, skincare products, and skin grafts for skin repair [188].

4. Bioprinting for tissue regeneration

Various tissue constructs mimic native tissues and organs such as skin, cardiac, bone, cartilage, liver, lung, neural, and pancreas, and they have been successfully bioprinted using several 3D printing approaches. In this section, we present an overview and progress in the printing of the various tissue and organ constructs.

4.1 Skin

26

It is now possible to mimic and fabricate the largest and complex multi-layered organ of the body i.e., skin with 3D bioprinting technology. 3D printed skin possesses enormous potential as grafts for wound healing, burned skin replacement, and *in vitro* human skin models for product and drug testing [189,190]. Lee et al. reported the first printing of keratinocytes and fibroblasts together in a stratified arrangement with a solid freeform fabrication (modified version of extrusion-based bioprinting) technique forming dermal/epidermal-like distinctive layers in a 3D scaffold. Collagen-based hydrogel bioink was printed in LbL fashion, i.e. collagen-fibroblast-collagen-keratinocyte-collagen. Cell proliferation with high viability was observed on both planar and non-planar surfaces. However, cell proliferation was affected by the printing resolution [191].

LIFT bioprinting was employed by Koch et al. to print cells derived from skin cell lines (fibroblasts: NIH 3T3/ keratinocytes: HaCaT) and human mesenchymal stem cells (hMSC) with ~98% and ~90% cell survival, respectively. No significant difference in proliferation, survival, apoptosis, and DNA damage of printed and control cells was observed, demonstrating that there is no negative effect on these qualities via the 3D bioprinting process. These results also showed that stem cells are more prone to decreased cell survival rates due to the printing process as compared with cell lines [192]. To understand the tissue formation process in native conditions, Koch et al. demonstrated LbL bioprinting of NIH 3T3 and HaCaT cells in the collagen matrix using LAB. Different histological and immunohistological methods revealed that the cells could proliferate in complete areas of the construct while maintaining their vitality and printing pattern [138].

Furthermore, Michael et al. used LAB to print layers of collagen pre-loaded with NIH 3T3 and HaCaT on a matriderm sheet. The resulting skin construct was implanted within the dorsal skinfold of mice for *in vivo* testing. After 11 days of implantation, the skin construct was completely connected to the tissue surrounding the skin wound [121]. The *in vivo* function of this construct was a key step in skin bioprinting, yet one major limitation was the absence of complete skin vascularization and keratinocyte differentiation due to the short duration of the experiment.

To overcome poor printability and long cross-linking duration of collagen biomaterials, Ng et al. reported the use of polyelectrolyte gelatin-chitosan (PGC) hydrogel for 3D bioprinting of skin. The inherent antimicrobial and hemostatic properties of chitosan make it compatible for

27

wound healing applications. HFF-1 cells were successfully encapsulated in PGC hydrogel using extrusion-based bioprinting to fabricate a similar architecture of the outer epidermal layer and part of the dermal region. The printed PGC hydrogel resulted in good shape fidelity and was biocompatible for various bioprinting applications [193].

Cubo et al. demonstrated the successful generation of human bilayered skin constructs via free-form fabrication bioprinting. Bioink comprised of human plasma, fibroblasts (hFBs) and keratinocytes (hKCs) cells obtained from skin biopsies. As skin substitutes, fibrin scaffolds were fabricated with two layers. The lower layer (representing dermis) was hFBs laden plasma-derived fibrin matrix and the upper layer (representing epidermis) was of hKCs seeded on top of fibrin scaffold. The resulting skin construct (100 cm^2) could be printed in less than 35 minutes. The histological and immunohistochemical analysis was performed *in vivo* by grafting on to the back of immunodeficient athymic mice (skin-humanized mice). The bioprinted skin was structurally, functionally and morphologically similar to normal human skin. The viability of cells remained unaffected during printing [189].

Kim et al. developed a new strategy for constructing 3D human skin models with a functional transwell by combining the extrusion and inkjet modules simultaneously. The extrusion module fabricated the transwell system and human primary dermal fibroblasts (HDFs) populated dermis successively. Whereas the inkjet module was used to obtain a uniform distribution of human epidermal keratinocytes (HEKs) on the dermis. The constructed and compatible skin model comprised of stable fibroblast-stretched dermis and stratified epidermal layers after 14 days. This bioprinting strategy was found to be cost- and time-effective, and innovative in terms of combining two different bioprinting methods [194].

To suppress improper skin regeneration, Xiong et al. fabricated gelatin-sulfonated silk composite scaffolds with fibroblast growth factor 2 (3DG-SF-SO$_3$-FGF) using self-made extrusion-based pneumatic bioprinting. The resultant scaffold showed increased blood vessel and granular tissue formation with ~75% cell proliferation when placed on the dorsal surface of Sprague Dawley rats. The full-thickness skin defects were repaired after 14 and 28 days post-implantation [195].

Shi et al. reported >90% cell viability of human melanocytes (HEM), HaCaT, and HDF upon the inclusion of gelatin methacrylamide and collagen doped with tyrosinase (GelMA/Col-Ty)

into the scaffold by extrusion bioprinting. The resultant 3D living skin constructs from the GelMA/Col-Ty bioink was found stable. Tyrosinase used in the process elevated the proliferation of HEM, exhibited no effect on HaCaT, and inhibited growth and migration of HDF cells [196].

The general trend demonstrates that laser-assisted bioprinting technique has been used more often in skin bioprinting than in the fabrication of other tissue types. Although more recent work in the field of skin bioprinting has utilized nozzle based bioprinters. This finding can be explained by the nature and structure of skin itself, it is less complicated than other tissues. This feature makes it a suitable choice for printing, especially since a few years ago, it was difficult to print multi-material constructs precisely with nozzle based bioprinters. This feature of skin has made it a perfect choice for *in situ* bioprinting and clinical application for accelerated wound healing.

Recently, Albanna et al. demonstrated proof-of-concept validation of a clinical skin bioprinter integrated with an imaging technology to print autologous skin cells on-site to treat full-thickness wounds **(Fig. 2)**. Dermal fibroblasts and epidermal keratinocyte cells were contained in a fibrin/collagen hydrogel carrier to ensure their viability, rapid hydrogel cross-linking, and precise deposition to form multicellular, multi-layered skin constructs. The wound scanning and imaging systems employed could convert wound size, depth, and topology in a two-layered format: lower fibroblast layer and upper keratinocyte layer. In a murine full-thickness wound model, this *in situ* bioprinting system showed accelerated wound closure (< 15% of original wound size at 2 weeks) with entire wound closed after 3 weeks post-surgery, compared to 5 weeks for both matrix (fibrin and collagen alone) and untreated controls. The presence of human fibroblasts, keratinocytes, and endogenous cells was observed within the wound 3 and 6 weeks post-printing. Well-defined epidermis and organized dermis indicating re-epithelialization in bioprinted wounds and complete wound healing were observed by the end of week 6. The authors also compared this bioprinting technology with the clinically-used cell spraying technique. There were no significant differences in wound closure, contraction, and re-epithelialization. Nevertheless, the early formation of defined epidermis and mature dermis layers with bioprinting was a striking difference. A probable explanation could be due to the spatial orientation of skin cells matching the wound architecture while bioprinting [197].
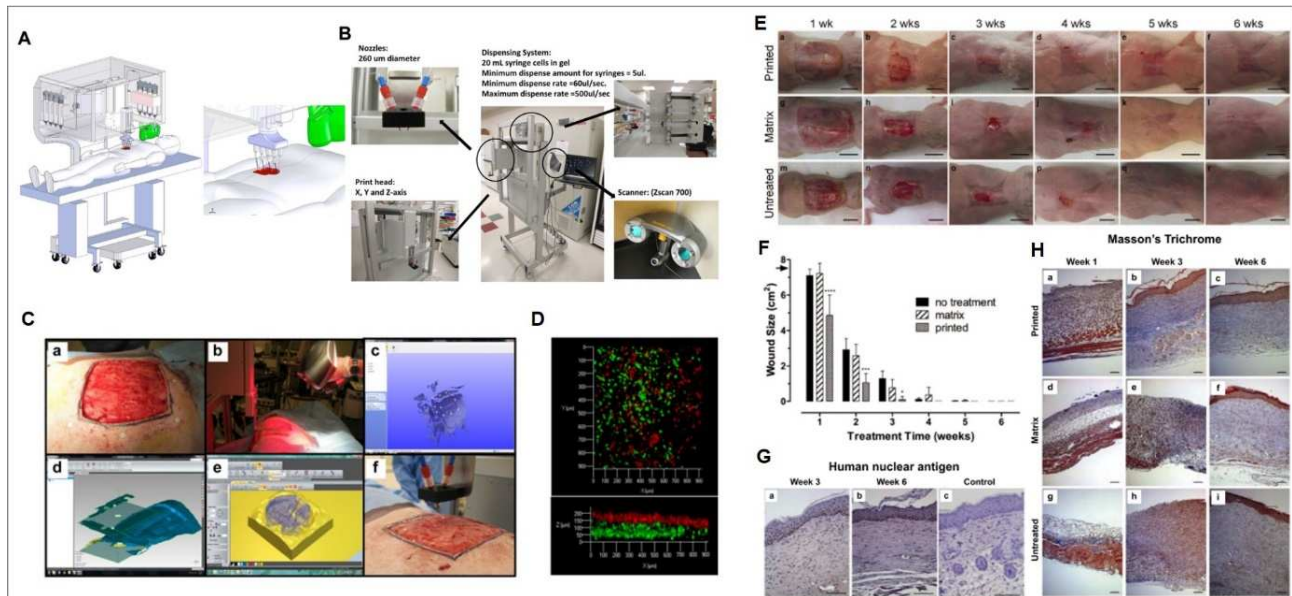
Fig. 2. *In situ* skin bioprinting prototype and gross examination of printed skin in murine full-thickness excision wound repair. **(A)** Schematic of scale, design, and components of the mobile skin bioprinter. **(B)** The main components of bioprinter include 260 µm diameter nozzles, dispensing system connected to XYZ movement system and a 3D wound scanner. **(C)** Steps involved in skin bioprinted process. (a) Markers are placed around the wound area as reference points, (b) scanning of wound surface with a hand-held ZScanner™ Z700 scanner, (c) retrieved geometrical information is inputted in an STL file format to orient scanned images in standard coordinate system. (d) Generation of fill volume and path points for nozzle-head to travel to print the fill volume based on scanned data, (e,f) output code is then provided to the custom bioprinter control interface for generation of nozzle path needed to print fill volume. **(D)** Precise and controlled deposition of fibroblasts (green) and keratinocytes (red) in a layered format. **(E)** Epithelium forming over the wound in cell-printed athymic nude mice in week 1, developing skin covering wound by week 2, complete wound coverage by week 3 and maturing epithelium (with minimal contraction) between weeks 4 to 6. In contrast, matrix-treated and untreated groups show minimal epithelialization until week 4, resulting in a significant proportion of the open wound area. Significant contraction between weeks 4 to 6 following wound closure. Scale bar:1 cm. **(F)** Variation in wound sizes in over 6 weeks. Printed skin closed the wound in 3 weeks compared to 5 weeks for controls. Statistical analysis was done using one-way ANOVA. ****$p < 0.0001$, n=12; ***$p < 0.01$, n=8; *$p < 0.05$, n=8. Data presented as mean ± standard deviation (SD). **(G)** Human nuclear antigen show presence of human cells within epidermis and dermis of printed skin at center of wound at week 3, and 6 post-printing. Human cells were found absent in matrix printed control wounds after 6 weeks. Scale bar:100 µm. **(H)** Masson's Trichrome staining of skin. (a-c) Increased cellularity in printed skin (in week 1), presence of defined epidermis or matured dermis with aligned blue stained collagen fibers (from weeks 3 to 6). (d-f) Matrix-printed wounds lacked cellularity, and well-defined epidermis or mature dermis after 1 week of printing. Thereafter,

epidermis formation started with prominence of blue stained collagen fibers was seen after week 3 and 6. (g-i) Untreated wounds also lacked cellularity but appeared similar to matrix-printed wounds at weeks 3 and 6. Scale bar:100 µm. Adapted with permission from Ref. [197] CC by license.

4.2 Cardiac

Bioengineering cardiac tissue via bioprinting technology is gaining increasing importance owing to the rising numbers of heart attack, heart failure, toxicology research, drug testing and screening, and personalized medicine [198,199]. Along these lines, Xu et al. reported the fabrication of a functional "half-heart" using modified inkjet printers (**Fig. 3A**). The 3D cardiac constructs within the "half-heart" model have a one cm inner diameter with two connected ventricles and rectangular sheet measuring 3×0.8×0.5 cm, it was successfully printed using a LbL approach**.** Cardiac cells (primary feline adult cardiomyocytes and HL-1 cardiac muscle cells) were printed in layers of alginate/gelatin gels cross-linked on-demand with calcium chloride ($CaCl_2$). The printed cardiac construct had a lower elastic modulus as compared to manually prepared scaffolds. The whole construct contracted rhythmically along with encapsulated individual adult feline cardiomyocytes under electrical stimulation [200]. This innovative method provided the researchers with a cost-effective tool for fabrication of hierarchical and functional cardiac tissues.

Subsequently, regenerated cardiac patches, obtained via the LIFT approach, showed increased blood vessel formation and notable functional improvement of infarcted hearts after implantation into rats suffering from myocardial infarction. This cardiac patch was prepared after seeding human umbilical vein endothelial cells (HUVEC) and human mesenchymal stem cells (hMSC) in a defined pattern on polyester urethane urea (PEUU) for cardiac regeneration [201]. The *in vivo* functionality of this bioprinted patch was a key step in the field.

Gaetani et al fabricated bioprinted constructs that demonstrated significant gene expression of early cardiac transcription factors (Nkx2.5, Gata-4, and Mef-2c), cell viability, and retention of cardiogenic potential. This bioprinted tissue was used in combination with human cardiac-derived cardiomyocyte progenitor cells (hCMPCs) entrapped in alginate gel to develop a 3D construct using an inkjet bioprinter. Cell viability observed on days 1 and 7 was ~92% and ~89%, respectively [202]. They showed that hCMPCs can be bioprinted and cultured without

31

any negative alterations to the growth or commitment of the cells. This work presented the first step toward *in vitro* creation of a well-differentiated cardiac construct.

Owing to the potential of stem cell therapy to treat ischemic heart diseases, Jang et al. printed MSC (pre-vascularized stem cells) patch, using an extrusion-based bioprinter, to induce vascularization, tissue remodeling, and prolonged cell survival following transplantation for cardiac repair. Also, the pre-vascularized stem cell patch exhibited enhanced therapeutic and promoting effects of cardiomyogenesis and neovascularization at the injured myocardium [198]. This technique provided the spatial patterning of cells in a way that is in favor of rapid vascularization. This platform is a new approach for stem cell delivery with high retention capability and regenerating ischemic tissue areas.

The fabrication of functional heart tissue *in vitro* by employing a microfluidic-based printing head (MPH) was recently reported. Maiullari et al. fabricated *in vitro* and *in vivo* models of vascularized cardiac tissue by a new approach that integrated induced pluripotent stem cell-derived CM (iPSC-CM) and HUVEC to develop a multi-cellular construct by extrusion bioprinting. This is the first study that showed vasculature development in transplanted tissue by printed endothelial cells. The resultant cardiac tissue was better suited for integration with the host's vasculature owing to its composition of iPSC-CM with a high orientation index and HUVEC originated blood vessel-like shapes. They also demonstrated the potential for bioprinted multi-cellular constructs to mature in vascularized functional tissues *in vivo,* which can be employed in various translational applications [203].

Very recent printing of 3D cellularized human hearts has proven to be a major breakthrough in transplant science. Dvir and the team have demonstrated bioprinting of fully personalized contracting cardiac patches using patient's cells, which minimizes the chance of an immune response **(Fig. 3B)**. In the study, the personalized hydrogel was derived from processing of extracellular matrix (ECM) obtained via biopsy of fatty tissue (omentum) from patients. They combined this personalized hydrogel with patient's own cells (iPSC-derived CMs) as bioink. Vascularized, thick, and perfusable cardiac patches were printed using an extrusion-based bioprinter. These vascularized cardiac patches could fully match the anatomical, cellular, biochemical, and immunological properties of the patient. The engineered cells in printed cardiac patch were elongated and aligned, with massive striation, which indicated their contractile ability. Thereafter, they showed free-form printing of volumetric and anatomically

complex−cellularized human hearts (height: 20 mm; diameter: 14 mm) with major blood vessels. Support medium with two customized bioinks-with CMs and endothelial cells were employed for the printing process. When examined, CMs were found homogeneously distributed in the 3D printed heart [204]. However, the printed blood vessel network is still limited and requires further investigation.
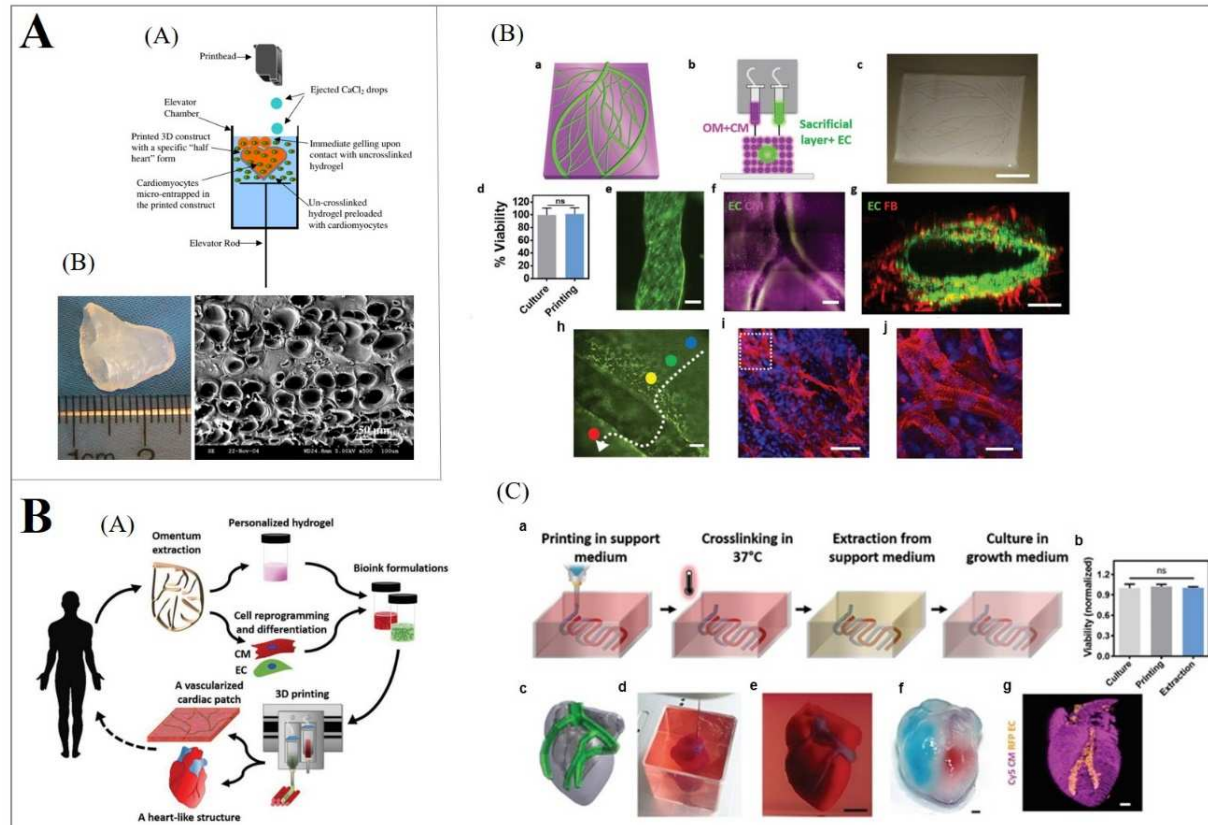
Fig. 3A. Fabrication of 3D printed 'half-heart' structure. (A) Schematic of the printing process. The printing chamber is filled with the alginate-gelatin mixture containing isolated feline cardiomyocytes. CaCl$_2$ solution is ejected on demand from the ink-cartridge in droplet form to cross-link alginate at target sites in LbL to form a 3D 'half-heart' structure. (B) Photograph of the printed cardiac construct with connected ventricles and scanning electron microscopy (SEM) image of its cross-section. Scale bar= 50 µm. Adapted with permission from Ref.[200] CC by license. **B.** 3D printing of personalized thick and perfusable cardiac patch and heart constructs. (A) Concept schematic. Omentum tissue extraction from patient, and its processing into a personalized thermoresponsive hydrogel. Re-programming of cells to become pluripotent and differentiation into cardiomyocytes and endothelial cells. Bioink for generating cardiac patch and heart constructs comprise of this differentiated cell-laden hydrogel solution. Finally, the engineered cardiac tissue can be transplanted back to the patient to repair/replace damaged tissue with low rejection risks. (B) 3D printing of personalized cardiac patch. 3D model of patch (a) printed using distinct cellular bioinks (b) to form a vascularized cardiac patch (c). Cell viability in patch after printing (d). A printed blood vessel, layered with GFP-expressing ECs (e), printed iPSCs cardiac patch with blood vessels (CD31: green) in-between cardiac tissue (actinin: pink) (f). Cross-section of

33

lumen depicting interactions between GFP-ECs and RFP-fibroblasts (g). Lumen of blood-vessel in-between the cardiac cells (h). Sarcomeric actinin (red) and nuclei (blue) staining of sections from explanted patch between the two layers of rat omentum. White dashed line highlights the patch border (i). Magnified view of marked area in (i) is shown in (j). Scale bars: (c)= 1 cm, (e, g)= 100 µm, (f)= 500 µm, (i)= 50 µm, (j)= 25 µm. (C) Printing thick vascularized tissues in supporting medium. Scheme of the 3D printing concept is shown in (a). The personalized hydrogel is free-form printing in support medium followed by its cross-linking, safe-extraction by an enzymatic or chemical degradation process of the support material and transfer into growth medium for culturing. Cell viability before and after printing and after extraction (b). Printing of small-scaled, cellularized human heart (c-g). CAD model of a human heart (c), printed within the support bath (d,e). After extraction, the left-and right ventricles are injected with red and blue dyes, respectively, to represent hollow chambers and septum in-between them (f). 3D confocal image of the printed heart (CMs in pink, ECs in orange) (g). Scale bars: (f,g)= 1 mm, (e)= 0.5 cm. GFP/RFP= green/red fluorescent protein. ECs= endothelial cells. iPSCs= induced pluripotent stem cells. CMs= cardiomyocytes. Adapted with permission from Ref. [204] CC by license.

4.3 Bone

Bone bioprinting has become a viable alternative for replacement of lost or damaged bone tissue, rather than traditional methods involving autografts and allografts [205]. It negates the problems of graft unavailability, donor site morbidity, immunogenicity, and risk for disease transmission associated with conventional bone grafting [206].

For instance, Lee et al. studied the *in vitro* cell differentiation of pre-osteoblasts (MC3T3-E1) and *in vivo* bone regeneration in rat cranial defects after implantation of 3D scaffolds incorporating poly (DL-lactic-co-glycolic acid) (PLGA) microspheres loaded with bone morphogenetic protein-2 (BMP-2) growth factor. BMP-2 loaded scaffolds, printed by micro SLA technology, revealed high expression of alkaline phosphatase (ALP) and osteocalcin with improved cell differentiation ability [207]. This work was a noble approach in incorporating bioactive agents such as BMP-2 into a 3D printed scaffold.

Mechanically robust 3D tricalcium phosphate (TCP) scaffolds were later developed by Tarafder et al. by employing microwave sintering followed by laser/metal printing. Both *in vitro* and *in vivo* studies conducted using human osteoblast cells and femoral defects in Sprague Dawley rats showed that controlled pore size (by microwave sintering 3D printing) resulted in high compressive strength, increased cell density, excellent biocompatibility, and

osteogenesis as compared to conventional sintering [208]. The same group extended their work and reported that TCP scaffolds when doped with strontium (Sr^{2+}) and magnesium (Mg^{2+}) showed an increase in osteoid like bone formation, mineralization, multiscale porosity, and osteocalcin and type I collagen levels in rat blood serum as compared to pure TCP scaffolds [209]. They also doped TCP scaffolds with silica (SiO_2) and zinc oxide (ZnO) to promote osteoinduction and angiogenesis [210].

To augment osteogenic activity in bone scaffolds, Jensen et al. used 3D printing for LbL deposition of PCL to develop scaffolds with nano-structured pores (NSP). A combination of rapid prototyping fused deposition model (FDM) technology, a type of extrusion-based 3D printing, and lyophilization was used to add multilevel porous morphology. *In vivo* osteogenic potential of NSP-PCL scaffold was tested for calvarial defects in pigs. Good osteoconductivity and osteointegration of the FDM-PCL scaffold after implantation were observed [211]. Furthermore, Temple et al. investigated PCL scaffolds with varying porosity in the shape of human mandibular and maxillary bones using a custom-build extrusion-based 3D printing. The resultant scaffold was tested *in vitro* and *in vivo* to induce human adipose-derived stem cells (hASCs) for vascularized bone formation [212].

Inzana et al. used phosphoric acid (H_3PO_4) based binder solution in combination with type I collagen to fabricate collagen-calcium phosphate (col-CaP) scaffolds via inkjet printing. These scaffolds were found to be promising, biocompatible, and mechanically stable synthetic bone graft substitutes [213]. Another study reported varying bone augmentation in rabbits with monetite onlays (bioresorbable bioceramics) designed with variable porosity (according to the metabolic activity of bone) via 3D powder printing or laser-assisted sintering [214].

Byambaa et al. demonstrated the formation of 3D bone-like tissue constructs (with separate osteogenic and vasculogenic niches) using extrusion-based bioprinting to repair large bone defects **(Fig. 4)**. Two types of GelMa hydrogels bioinks were employed for printing. A central vascular fiber construct was printed using fast degradable GelMA bioink (5% VEGF-conjugated GelMA with low methacryloyl substitution (GelMA$_{LOW}$-VEGF) containing HUVECs and hMSCs). Silicate nanoplatelets loaded GelMA bioink (10% GelMA$_{HIGH}$+VEGF in gradient concentrations) were printed around the central fiber to induce osteogenesis. HUVECs and hMSCs, when co-cultured in bioprinted fibers, retained

35

viability and could undergo cell proliferation and vasculogenesis. In medium perfused bone construct −enhanced mineralized bone-like ECM, osteoblastic maturation (strong OCN expression), RUNX2 (transcription factor of bone formation), and CD31 (angiogenic-gene) expression showed formation and maturation of bone tissue construct facilitated by a central angiogenic vessel after 21 days of culture [215]. This bone bioprinting approach can pave the road to fabricate cell-laden structures that are able to accelerate large bone defect healing.

Recently, Alba et al. developed a new method for periosteum tissue engineering by printing periosteal derived cells (PDCs) in a precise pattern onto collagen scaffolds. The bioink was prepared by mixing PDCs with alginate and then printed on type I (COL 1) and type II (COL 2) collagen scaffolds, separately. Structural integrity was found to be higher in COL 1 and COL 2 scaffolds than in bioink alone. Osteocalcin and ALP gene expression were more significant in the COL1 group indicating osteogenic differentiation of PDCs [216].

To develop modified bioinks with optimal biological and physicochemical properties, Ojansivu and colleagues used wood-based nanocellulose (CNF) and bioactive glass (BaG) to strengthen gelatin-alginate bioinks for 3D bioprinting of bone cells using a commercially available extrusion-based bioprinter, Bioplotter. The flow behavior of hydrogels was modified by CNF, which improved its printability. The viability of osteoblast-like cells (Saos-2) confirmed the good cytocompatibility of the modified hydrogels. Saos-2 cells remained viable in BaG-free gels but their viability and proliferation decreased in the presence of BaG along with an increase in viscosity [217]. This study was a key step in the field of bone 3D bioprinting as it developed a multi-component bioink for bone regenerative engineering. Moreover, this study emphasized the importance of viscosity for extrusion-based bioprinting as it can influence short- and long-term viability and proliferation of cells.

In this section, we included some 3D printing for bone regenerative engineering works in addition to bone bioprinting research since additive manufacturing techniques have been used extensively for bone tissue engineering due to the nature of bone itself, which is a load-bearing tissue with lots of calcified and mineral areas along with cells. These features of bone support the motivation to use harder polymers such as thermoplastics and ceramics as biomaterial inks for 3D printing research in the field of bone tissue engineering.
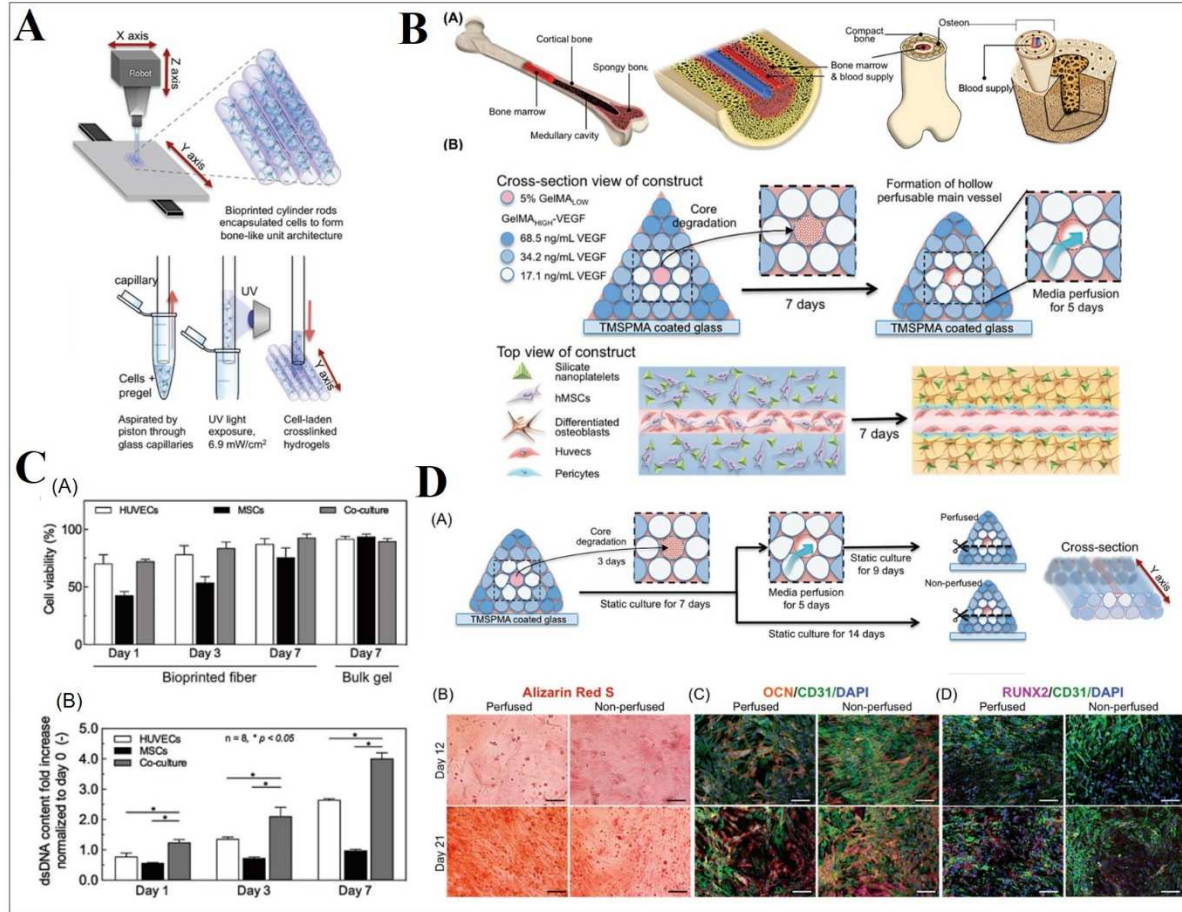
Fig. 4. Fabrication of a 3D bone-mimetic construct with osteogenic and vasculogenic niches. **(A)** Schematic of an automated bioprinter demonstrating procedure while printing the complex bone architecture (panel (A) in B) as cell-laden cylinders using the strategy shown in **B**. (B) A perfusable vascular lumen lined with HUVECs could be fabricated within a pyramidal bioprinted construct by arranging individual rods of VEGF-functionalized GelMA bioinks with different mechanical strengths. The hMSCs-laden three outer layers of cylinders were loaded with silicate nanoplatelets to induce osteogenic differentiation of hMSCs into bone tissue. The VEGF (17.1, 34.2, and 68.5 ng mL^{-1}) was covalently conjugated into the three outer layers of the cylindrical hydrogels. **(C)** Cell growth analysis of hMSCs and HUVECs in co-culture conditions. Cellular viability (A) and proliferation (B) estimated as dsDNA contents by PicoGreen staining of mono- and co-cultured cells at days 1, 3 and 7. Data represented as mean ± standard deviation ($n = 8$; *$p < 0.05$). **(D)** Osteogenic and vasculogenic examination of bioprinted bone construct. Schematic depiction of cross-sectioned samples for ARS and immunostaining is shown in (A). Representative microscopic images of ARS stained (B) and fluorescence microscopy of double-immunostained with OCN/CD31/DAPI and RUNX2/CD31/DAPI perfused and non-perfused samples (C, D) on days 12 and 21 of culture. Scale bar: 50 µm. Osteogenic markers:

4.4 Cartilage

Joint injuries leading to osteoarthritis, traumatic rupture of cartilage, and limited effectiveness of conventional surgical procedures are a concerning reality. Cartilage tissue defects are difficult to repair. Its limited self- repairing capacity is due to an insufficient supply of healthy chondrocytes to the defective sites [218]. Therefore, the potential of bioprinting to produce complex 3D scaffolds similar in architecture to native tissues makes it well suited for cartilage tissue engineering.

Currently, the scaffolds for *in vivo* implantation of cartilage tissue have dimensions suitable for small joints but not for large human hip and knee joints. The efforts for a scale-up of bioengineered grafts to match the native architecture is challenging due to the potential for compromised diffusion of nutrients and metabolic products, which are necessary for cell survival.

With these concerns in mind, using an extrusion-based bioprinter, Lee et al. employed LbL printing to fabricate a composite of PCL and HA to generate tissue formation and vascularization of anatomically shaped human tibial condyles. The resultant PCL-HA scaffold measured 20 x 15 x 15 mm^3, was double in size to the scaffold reported earlier, and had the potential for joint regeneration and arthritis treatment [219].

Furthermore, they regenerated the entire articular surface of the synovial joint of a rabbit without cell transplantation. Composite polymers (PCL-HA) were used to fabricate bioscaffolds with surface adsorbed transforming growth factor β3 (TGFβ3) and TGFβ3-free collagen solution to replace humeral condyles of skeletally mature rabbits, using the same extrusion-based bioprinter. TGFβ3- infused bioscaffolds demonstrated full-tissue coverage, more uniform chondrocyte distribution, greater matrix density, and articular cartilage thickness than TGFβ3-free group **(Fig. 5)**. TGFβ3 served as a chemotactic cue to recruit

130% more cells in the regenerated cartilage than did spontaneous cell migration without TGFβ3 [220].

Additionally, the development of functional articular cartilage capable of bearing heavy loads is still challenging. A hybrid system was developed using electrospinning and inkjet printing techniques to produce scaffolds with enhanced mechanical and biological properties for load-bearing cartilage tissue regeneration. PCL was fabricated alternatively LbL with rabbit elastic chondrocytes in the fibrin-collagen hydrogel. The 3D hybrid construct displayed >80% chondrocyte viability and was more mechanically robust than alginate or fibrin-collagen gels, respectively [104]. This technique has the potential to be refined for fabrication of functional complex cartilage tissue using oriented fibers to direct the incorporated chondrocytes and their growth.

O'Connell et al. developed a novel device named "Biopen"- a handheld biofabrication tool that allowed the use of 3D printing and manual control while depositing scaffold during the surgical process with or without live cells [221]. Biopen is basically an extrusion-based bioprinter. The group further tested Biopen to develop core/shell GelMa/HAMa bioscaffolds that have mechanical strength of 200 KPa and high cell viability for chondral repair [222]. This work showed the great potential of multi-ink bioprinting, especially co-axial bioprinting for *in vivo* applications even directly during the surgery. This handheld Biopen was also used to study repair of full-thickness chondral defects in a large animal ovine model which showed safety and potential clinical efficacy [223]. This study was important as it was the first *in situ* 3D bioprinting, which can be a key step toward the clinical application of bioprinting technology.

A pure-phase lithium calcium silicate ($L_2C_4S_4$) scaffold was prepared using an extrusion-based precision three-axis positioning printing system by Chen et al. for regeneration of both cartilage and subchondral bone tissues simultaneously as compared to pure β-TCP scaffolds. These 3D printed $L_2C_4S_4$ scaffolds displayed controlled biodegradability and good apatite-mineralization ability [224]. Although this study has not utilized bioprinting, it showed a feasible strategy for osteochondral reconstruction.

39

Recently, Rathan et al. designed the cartilage extracellular matrix (cECM)-functionalized alginate bioinks for bioprinting of cartilaginous tissues using an extrusion-based bioprinter. These bioinks could support MSC post-printing viability and robust chondrogenesis *in vitro.* Bioinks with the highest concentration of cECM showed the highest levels of COL 2 and ACAN (Aggrecan) gene expression. Such bioinks, when loaded with MSCs and TGF-β3, supported robust chondrogenesis, making it suitable for direct "print-and-implant" cartilage repair strategies [225]. This study proposed a novel class of functionalized bioinks that can be used for more general purposes in musculoskeletal regenerative engineering.
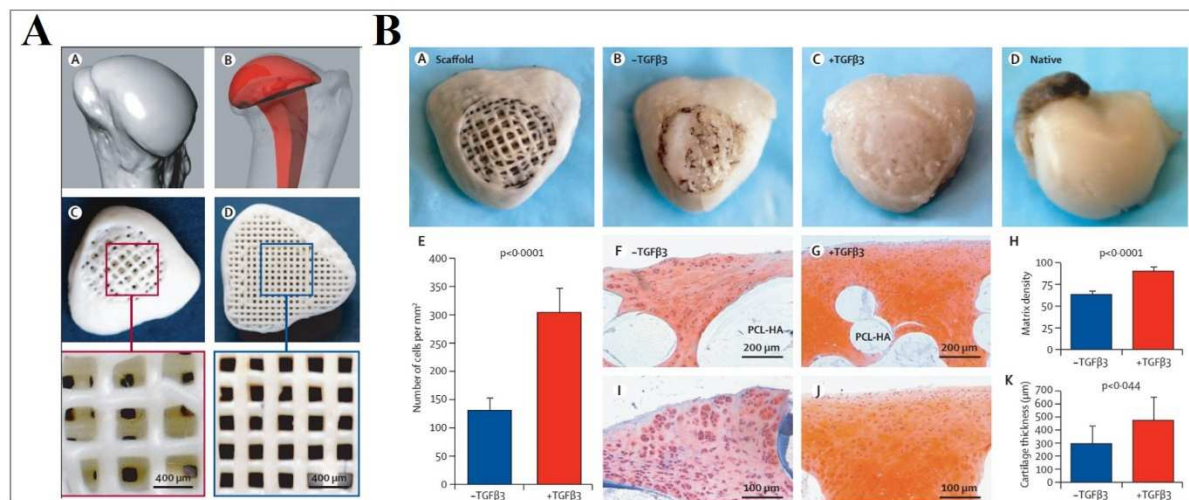
Fig. 5. Design and fabrication of a bioscaffold for articular cartilage regeneration in skeletally mature rabbits. **(A)** Surface morphology of rabbit joint was reconstructed (A) to replace the condylar head with anatomically correct bioscaffold with an intramedullary stem (B). A 200 μm thick shell was designed, along with internal microchannels (200–400 μm diameter) for regeneration of cartilage (C) and bone (D). **(B)** India ink staining of un-implanted bioscaffold (A), TGFβ3-free (B) and TGFβ3-infused (C) bioscaffolds after 4 months of implantation, and native cartilage (D). Number of chondrocytes present in TGFβ3-infused and TGFβ3-free regenerated articular cartilage samples (*n*=8 per group) (E). Safranin O staining of TGFβ3-free (F, I) and TGFβ3-infused (G, J) articular cartilage. Matrix density (H) and cartilage thickness (K) of TGFβ3-infused and TGFβ3-free samples (n=8 per group for both comparisons). TGFβ3=transforming growth factor β3. Adapted with permission from Ref. [220] CC by license.

4.5 Liver

There are established treatments for the management of severe liver disorders, such as liver cirrhosis and hepatocellular carcinoma, but no treatment is completely promising. Liver

transplantation stands as the practical solution for irreversible loss of liver function or liver failure. However, the benefits of transplantation are limited in the setting of surgical complications, health care expenses, donor scarcity, and risk of rejection [226–228]. Nevertheless, producing an artificial liver is challenging. This process is further complicated by the inability to culture primary hepatocytes for many days [229].

Bioprinting was used to develop an *in vitro* 3D microfluidic microanalytic micro-organ device to study the effect of microgravity and space environments on human response to administered drugs and their toxic chemical exposures. The device was entrenched with a micro-scale liver tissue construct (constructed via layered direct cell writing bioprinting) for analyzing the effect of drugs on a printed model in planetary environments [99].

Faulkner-Jones et al. employed valve-based inkjet bioprinting to print human induced pluripotent stem cells (hiPSCs) and human embryonic stem cells (hESCs) that could differentiate into hepatocyte-like cells (HLCs) post-printing. Printed cells showed positive results for nuclear factor 4 alpha (4α) and albumin secretion and were compatible to generate mini livers as drug testing models [230]. This, for the first time, showed that hiPSCs have the potential to be bioprinted without negative effects on biological functions such as viability and pluripotency.

Lee et al. bioprinted primary rat hepatocytes (HCs), HUVECs, and human lung fibroblasts (HLFs) with multiple nozzle-based extrusion-based bioprinting for liver tissue engineering. The 3D constructs were produced by infusing collagen bioink containing cells into the canals of the PCL framework **(Fig. 6)**. The resulting co-culture 3D environment-induced heterotypic interaction among cells, thereby enhancing the survival and functionality of HCs (i.e., albumin secretion and urea synthesis) in the printed liver construct [231]. This study was important as it showed the great potential of 3D bioprinted constructs containing the capillary-like network for functional liver tissue regeneration.

Multiple nozzle extrusion-based 3D bioprinters have also been used by Lei and Wang with ADSCs and primary hepatocytes to fabricate complex organ precursors with branching vascular systems. Based on their findings, they demonstrated that the four-nozzle low-temperature deposition manufacturing technique could be used to generate liver organoids [232]. This combinatorial technique was useful for the fabrication of vascularized constructs

with predefined internal channels. Moreover, it has great potential to be used for other tissues as well as to fabricate complex organs.
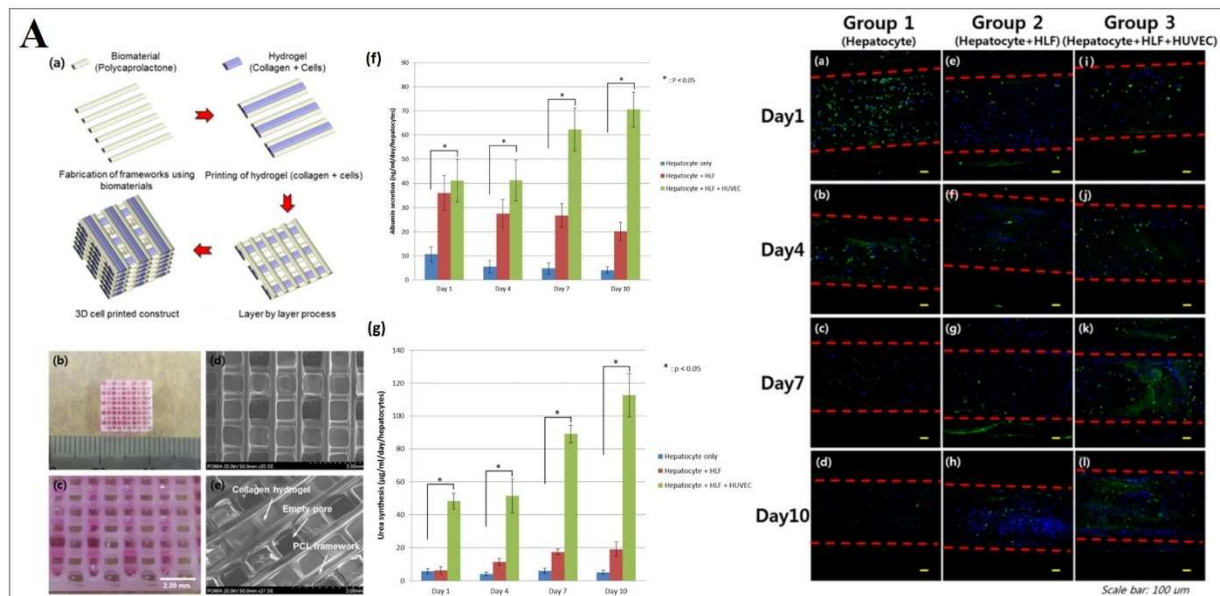
Fig. 6. 3D cell-printed scaffold for the engineering of functional liver tissue. The fabrication process involved to build the liver cell scaffold is depicted in (a). The low and high magnification optical images of the printed scaffold are shown in (b and c), respectively. Low-resolution (d) and high-resolution (e) SEM images of freeze-dried 3D printed scaffold demonstrating infused collagen hydrogels and empty pores within the PCL framework. The functionality of the 3D printed liver construct for albumin secretion (f) and urea synthesis (g) from different cell groups cultured at days 1,4,7 and 10. Confocal microscopy images of stained albumins secreted from hepatocytes in hybrid 3D printed scaffold. Only hepatocytes contained in collagen hydrogel (a-d). Highest albumin intensity on day 1 with subsequent decrease with time. Hepatocyte+ HLFs in collagen hydrogel (e-h). Albumin concentration increased to ~day 4 and then decreased with time. Hepatocytes+ HLFs + HUVECs cultivated together in collagen hydrogel. Increase in albumin concentration until day 10. Green: stained albumins; blue: nuclei; dot line (red): hydrogel area. SEM: scanning electron microscopy; PCL: poly(ε-caprolactone). Adapted with permission from Ref. [231] CC by license.

4.6 Lung

Many patients suffer worldwide from end-stage lung diseases, such as asbestosis (lung tissue scarring and shortness of breath due to inhalation of asbestos fibers), for which lung transplantation is a treatment option for progressive forms of the disease. Unavailability of expert surgeons, donor scarcity, and risk of rejection are concerns associated with lung transplants [233]. Several attempts to regenerate lung tissue *in vitro* using a bioreactor have been made [234–236]. However, the fabrication of *in vitro* 3D alveolar model mimicking native tissue remains unsuccessful.

Horváth et al. presented an *in vitro* human air-blood tissue barrier analog fabrication using a valve-based inkjet bioprinting approach **(Fig. 7)**. Alveolar epithelial type II cells (A549) and endothelial (EA.hy926) cells separated by a thin basement membrane (BM) Matrigel[TM] were deposited LbL. Morphological and structural differences in both cell types occurred depending on the seeding approach followed, i.e., manual vs printing. Manually seeded cells, grew in patches forming multi-layered clusters and a thick ECM layer between the cells, resulting in a lack of cell-cell communication. Contrarily, printed cells could spread uniformly over the membrane surface forming thin mono-layers with a higher resemblance to the air-blood barrier *in vivo*. Notably, the viability of A549 and EA.hy926 mono-cultures or co-cultures were similar with both approaches. Printed cell mono-cultures showed higher tightness and hence, better barrier quality than corresponding manual samples. Nevertheless, printed epithelial cells displayed higher cell viability and barrier quality than printed endothelial cells [158]. The generation of 3D alveolar tissue in this work was the first step in validation of bioprinted lung tissue. This approach can be helpful in fabrication of realistic *in vitro* models for assessments in toxicology and drug screening.
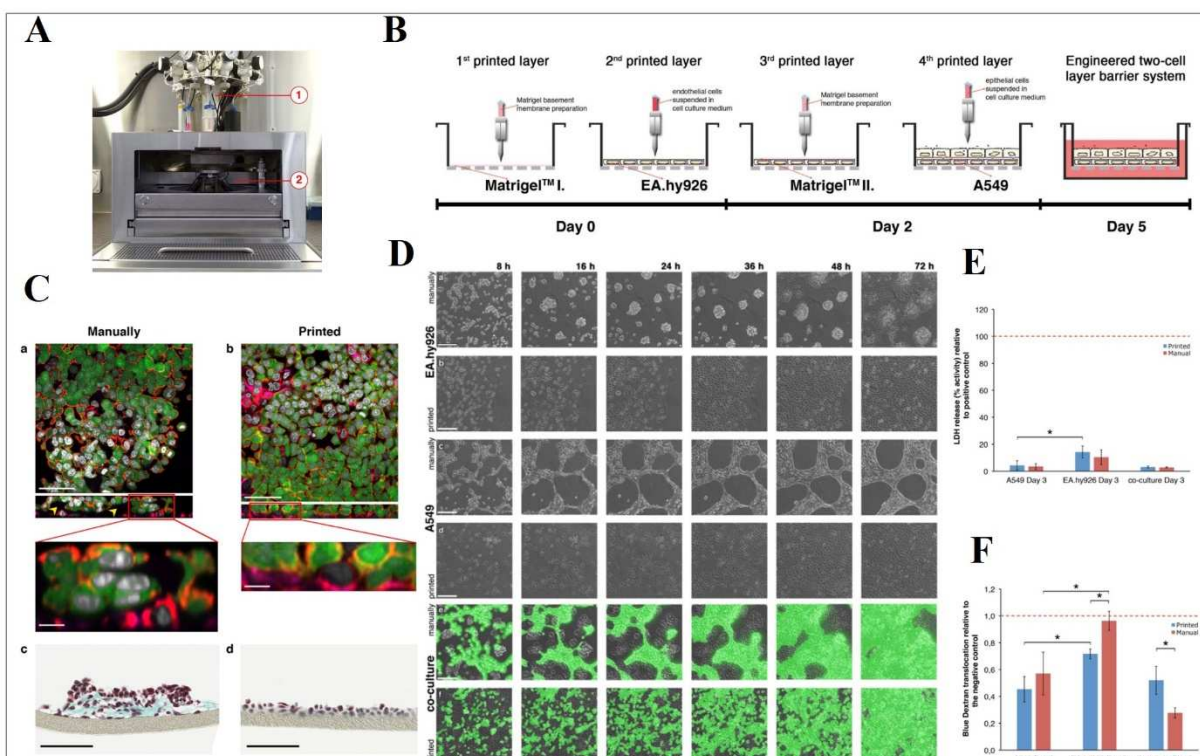
Fig. 7. Biofabrication of the 3D in vitro air-blood tissue barrier and examination of functional-structural relation of the bioprinted constructs. **(A)** Main process unit of bioprinter- BioFactory®, tool changer (1) with multiple print heads and a building platform (2). **(B)** Schematic for the bioprinting of two-cell layer barrier system at predefined times. For the manual co-culture assembly, a similar timeline is followed, however made manually, i.e. by manually pipetting the ECM/cell layers. **(C)** Microscopic characterization of manually seeded and bioprinted co-cultures. F-actin (red) and nuclei (white) cell staining of manually and bioprinted two-cell layers (a, b) after 3 days; visualized by laser scanning microscopy (LSM). A549 cells are represented in green, endothelial cells are viewed in pink after labeling with VE-cadherin. Yellow arrows point to the formation of multilayers and thick Matrigel™ layers with magnified side views. Masson-Goldner trichrome stained manually (c) and bioprinted (d) paraffin-embedded histological cross-sections. Cytoplasm (red), collagen fibers of ECM Matrigel™ (green), nuclei (brown). Scale bars are (a–b) = 50 µm, (a-b close-up) =10 µm and (c–d) =100 µm. **(D)** Phase-contrast micrographs and merged phase-contrast and fluorescence micrographs of EA.hy926 (a, b), A549 (c, d) mono-cultures and co-cultures (e, f). **(E)** Extracellular lactate dehydrogenase (LDH) release (percent increase, measure of cell integrity) relative to positive control; Triton X-100, 24 h (dashed line) 3 days post-printing or manual seeding of cells on Matrigel™. **(F)** Translocation of blue dextran (estimate of barrier quality, i.e. tightness) on 3rd day of mono- and co-culture assembly on printed and manually seeded cultures. Negative control: insert only, w/o cells. All results are expressed as the mean ± standard deviation of n=3 independent experiments (*$p < 0.05$). Adapted with permission from Ref. [158] CC by license.

4.7 Neural

Presently, the domain of 3D bioprinting is important to model neurological diseases *in vitro*, in particular, which lack precise animal models. While the long-term vision of a 3D bioprinter is to engineer and repair neural tissues involved in traumatic brain injuries (TBI) and neurodegenerative diseases.

In the initial studies, Lee et al. demonstrated an artificial neural tissue 3D model by inkjet bioprinting of multiple hydrogel types i.e. collagen hydrogel scaffold with murine neural stem cells (NSCs, C17.2) and embedded vascular endothelial growth factor (VEGF)-releasing fibrin gel. C17.2 cells showed high cell viability of ~ 92% post-printing. When printed within VEGF-fibrin gel, C17.2 cells showed prominent morphological changes, migration, and proliferation in comparison to cells in the control sample (fibrin without VEGF or VEGF

44

directly printed in collagen) [237]. This method has the potential to be used for the evaluation of cellular behavior and application in neural tissue regeneration.

Similarly, Owens et al. reported bioprinting of nerve graft and its successful implantation into the Sprague Dawley rats suffering from sciatic nerve injury. Mouse BMSCs and Schwann cells (SC) were used to fabricate the biocompatible conduit LbL [124]. The cellular cylinders comprised of 90% BMSCs and 10% SCs. This work was the first attempt in bioprinting of a fully cellular nerve graft and developed a proof-of-concept for a novel nerve graft system and its function.

Lozano et al. developed a handheld reactive bathless printing technique (a type of extrusion printing) to 3D print multi-layered brain-like structures (**Fig. 8A**). The bioink composed of RGD peptide modified gellan gum (RGD-GG) hydrogels encapsulating primary cortical neuronal cells representing cortical tissue. The developed bioink could support cell viability ($>70\%$) regardless of the cross-linker used (i.e. DMEM or $CaCl_2$) along with network formation of cells. Cortical neuron cells were found to respond better to RGD-GG hydrogels than to the purified GG hydrogels. This study significantly contributed to fabricate discrete cell-containing layers to develop into a complex, 3D *in vitro* model to investigate neural circuit formation, understanding of TBI and other neural-related applications [149].

Furthermore, Hsieh et al. monitored the implantation of NSCs embedded into polyurethane (PU) hydrogel in zebrafish suffering from traumatic brain injury. They used an extrusion-based bioprinter to fabricate a thermo-responsive PU hydrogel-based scaffold with appropriate stiffness, excellent proliferation, and differentiation. These 3D bioprinted hydrogel constructs could effectively cure the damaged central nervous system (CNS) in zebrafish embryos post-injection [238]. The results of this work showed the potential of this method to save the function of the impaired nervous system in neurodegenerative disease.

Gu et al. reported the formation of novel 3D neural mini-tissue construct by micro-extrusion bioprinting of frontal cortical NSCs supported in a polysaccharide hydrogel of alginate, carboxymethyl chitosan, and agarose. Cells were viable in the construct and could differentiate *in situ* into functional neurons. Such differentiated neurons could form synaptic contacts, networks, and showed a bicuculline-induced increased calcium response [239].

Very recently, Zhang and group developed a conductive hydrogel for biological signal recording and stimulation of living tissues to directly treat patients with various neurological disorders using a laser-assisted bioprinting system. A conductive solution of poly (3,4-ethylenedioxythiophene) (PEDOT): polystyrene sulfonate (PSS) was used to print patterned conductive hydrogel to enhance its electrical conductivity [240]. This work developed a 3D conductive hydrogel structure that has the potential to be used for interfacial bioelectronics with biological stimulation to regulate and induce cell behavior, which is an important aspect in the field of neural tissue regeneration.

A novel filler-free bioink has been designed for micro-extrusion bioprinting of soft neural tissues. *In vitro* studies conducted using 3D printed soft neural tissue revealed HA and Pluronic F-127 bioink as biocompatible bioinks relative to the control alginate hydrogels [241]. These bioinks, developed by Haring et al. can enable 3D bioprinting of soft, free-standing neural tissues for application in disease modeling and also regenerative engineering.

Recently, Ning et al. demonstrated the fabrication of 3D bioprinted Schwann cell (SC)-laden scaffolds from low-viscosity custom-tailored hydrogels of RGD modified alginate, HA and fibrin together with the submerged cross-linking method **(Fig. 8B)**. The hydrogel composition and printing process were optimized to maintain the high viability of SCs (>90%) after printing. Also, the morphologies of SCs and neurite outgrowth could be altered by varying the printing speeds. The results of the work established the feasibility of 3D printing scaffolds with low-viscosity bioinks and favorable for migration of the cells within the scaffolds to support peripheral nerve tissue repair [242].
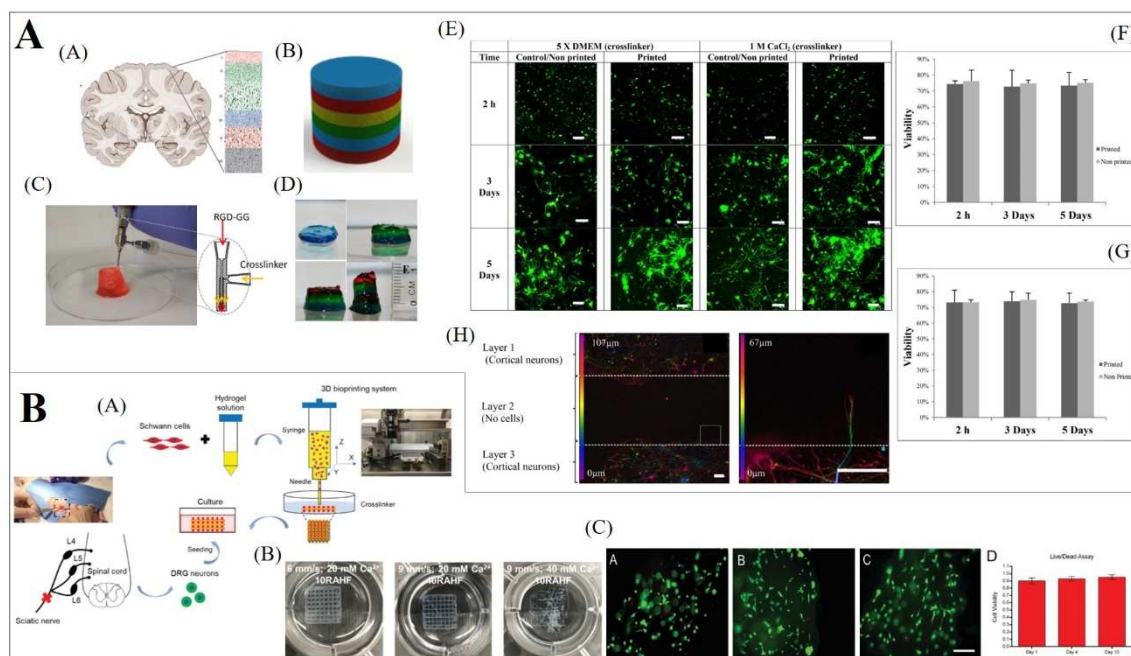
Fig. 8A. Bioprinting of multi-layered brain-like structures. (A) Brain architecture found in the human cortex, (B) the proposed design for ideal free-formed artificial brain-like structures, by (C) handheld-reactive bathless 3D printing process. Grey dotted lines represent schematic of the extrusion tip. (D) Printing process to create a layered construct; each color represents a layer. (E) Viability of cortical neurons encapsulated in 0.5% RGD-GG gels using different cross-linkers. Labeling of cells with Calcein AM (green, live cells) and PI (red, dead cells) 2 h, 3 days and 5 days after the printing process. Scale bars= 100 µm. Quantification of cell viability in (F) 5 X DMEM and (G) 1 M CaCl$_2$ cross-linked gels. (H) Confocal microscopy images of neurons in different layers after 5 days of culture. Scale bars= 100 µm. Adapted with permission from Ref. [149] CC by license. **(B)** Bioprinting of Schwann cell-laden 3D scaffolds. (A) Schematic representing cell derivation and bioink preparation for scaffold bioprinting. (B) Effect of process parameters-bioprinter speed and calcium ion concentration on the stability of scaffold structures. (C) Live/dead estimation of Schwann cells within scaffolds (A-D) at days 1, 4, and 10, respectively. Scale bars= 100 µm. Adapted with permission from Ref. [242] CC by license.

4.8 Pancreas

The ever-increasing number of diabetic patients and the incidence of aggressive diseases such as pancreatic cancer have increased the need for disease-specific treatments such as insulin injections for diabetes and chemotherapy for cancer. Research efforts to differentiate human pluripotent stem cells (hPSCs) to β cells for *in vivo* transplantation therapy for diabetes treatment are ongoing. Millions of glucose-responsive β cells were generated from hPSCs *in vitro* and transplanted into diabetic mice. Shortly after implantation, the cells started secreting insulin in a glucose-regulated manner in mice serum and improved hyperglycemia in diabetic mice [243].

Akkouch et al. investigated the scale-up fabrication of scaffold-free tissue strands by extrusion-based bioprinting with minimum damage to the alginate encapsulating rat dermal fibroblasts (RDFs) and mouse insulinoma beta TC3 (βTC-3) cells. These heterocellular tissue strands demonstrated the potential for pancreatic tissue regeneration after hybrid fabrication. The fabricated tissue strands exhibited negligible contractibility in the longitudinal axis, rapid fusion capability, high viability, and cylindricity, and expressed cell-specific functional markers [244].

Furthermore, Yi et al used extrusion-based 3D printed biodegradable patches of PLGA and PCL to test the controlled release of anticancer drug, Fluorouracil (5-FU), against pancreatic cancer. They were able to suppress pancreatic cancer growth with minimal side effects for >4 weeks following implantation into athymic mice [245]. The result of this work shows the potential of 3D printing techniques for effective and local delivery of drugs with ideal pharmacokinetics.

Very recently, Kim et al. utilized the decellularization process to develop pancreatic tissue-derived ECM (pdECM) bioink from fresh porcine pancreatic tissue (**Fig. 9**). The objective was to provide a tissue-specific microenvironment for islet cells in the 3D constructs fabricated via micro-extrusion based printing. When quantified, 97.60% of residual DNA was removed from pdECM bioink (significant to evade immune rejection response after transplantation). Other ECM components including collagen and GAGs were estimated to be 565% and 86%. Human islets cultured for 5 days in 3D alginate, collagen, pdECM bioinks showed over 60% viability. Secreted insulin levels by islet-laden pdECM bioink were found higher when cultured in the high glucose-containing medium than low glucose medium. Printable bioink composed of pdECM, islets and HUVECs could form 3D constructs using micro extrusion-based printing. The viability of cells in both 3D gels and printed construct was quite similar when cultured post-printing. The construct could enhance pancreatic functions such as elevated regulation of insulin secretion and maturation of insulin-producing cells derived from hiPSCs [246].
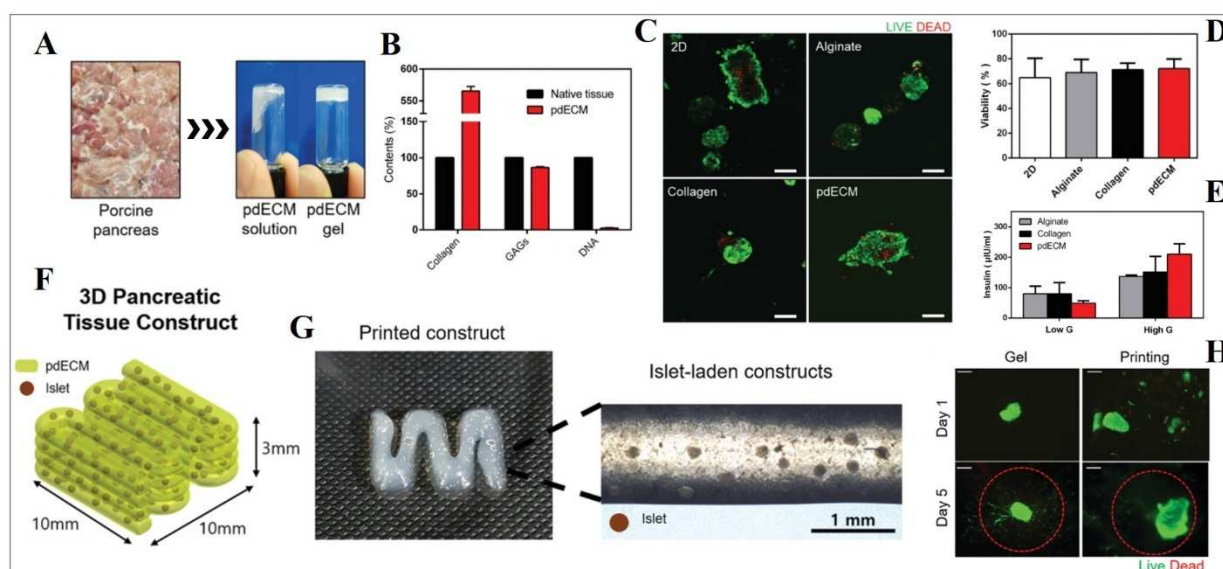
Fig. 9. Construction of 3D pancreatic tissue construct from islet-laden decellularized porcine bioink. **(A)** Decellularization process of porcine pancreas and formation of pancreatic tissue-derived ECM (pdECM) bioink. (B) Biochemical analysis of the pdECM bioink. (C-D) Viability of islet cells in each 3D bioink condition after 5 days of culture. Scale bar=100 µm. (E) Effect of pdECM bioink on the islet function-insulin secretion as a function of glucose concentration. (F) Schematic of 3D pancreatic tissue construct, (G) islet-laden 3D printed construct and (H) it's cell viability over 5 days in culture (green: live; red: dead). Scale bar=100 µm. Adapted with permission from Ref. [246] CC by license.

5. Other application areas of bioprinting

5.1 Cancer research

The ability of bioprinting to mimic the human microenvironment *in vitro* makes it a suitable technology for various applications, such as drug screening and high-throughput assays [247], transplantation and clinical application [9], tissue engineering and regenerative medicine [248] and cancer research [93]. The limitations of conventional 2D tumor models to mimic the actual physiological environment have encouraged the fabrication of 3D cancer models via bioprinting. 3D printed models are beneficial to improve the understanding cancer pathophysiology and metastasis to support the development of advanced cancer therapies [93,249].

Demirci and group reported the use bioprinting for *in vitro* modelling of tumor tissue for cancer research and HTS. Inkjet bioprinting was used to print human ovarian cancer (OVCAR-5) and MRC-5 (normal human fibroblasts cell line) cells on Matrigel™ to form multicellular acini. This advancement in technology aids in the understanding of various unknown regulatory feedback mechanisms between tumor and stromal cells [250]. This approach enables fabrications of physiologically relevant ovarian cancer co-culture models used for better investigation of ovarian cancer biology and clinical therapies. It can also be used for high-throughput screening of drug and treatment responses for reduction of testing cost and provide an alternative for animal testing.

Zhao et al. compared 3D cervical tumor models (fabricated by self-developed extrusion-based 3D printer employing Hela cells and gelatin/fibrinogen/alginate hydrogels) with the conventional 2D planar culture models. Hela cells showed higher proliferation, matrix metalloproteinase (MMP) protein expression, and chemo-resistance in 3D microenvironment contrary to 2D culture. The cell viability achieved was ~90% [251]. This novel 3D bioprinting approach resulted in 3D biological characteristics in the bioprinted tumor models *in vitro* that renders it an important tool for studying 3D tumor biology.

Scaffold-free cellular spheroids are important for tissue engineering, drug screening, and studying tissue pathology; it also bypasses the biocompatibility concerns with scaffold-based models and monolayer cultures. They also mimic the *in vivo* microenvironment of cancer cells well, and thus making them a superior and sought after model system [252]. Ling et al. used a custom-built pressure-assisted value-based inkjet bioprinting system for *in situ* cell seeding to develop cellular spheroids. The spheroids were generated by fabricating concave wells with cell loaded hydrogel arrays. Human breast cancer cells (MCF-7) were seeded *in situ* on gelatin arrays to form cellular spheroids on a chip. The seeded cells displayed high cell viability and were uniformly distributed by the controlled bioprinting system [253].

Breast cancer patients suffer high risk to develop metastatic disease, in which cancer spreads to other organs, and bone may be affected. To study this process *in vitro*, Zhou et al. used a tabletop SLA 3D bioprinter to construct a 3D model of a bone matrix mimetic to analyze the interactions between breast cancer (BrCa) cells and bone stromal cells (fetal osteoblasts, and hBMSCs) **(Fig. 10)**. A series of bone matrices comprising of osteoblasts or MSCs encapsulated in GelMa with nanocrystalline hydroxyapatite (nHA) were developed. When BrCa cells were introduced and co-cultured in osteoblasts and MSCs laden 3D bioprinted matrices **(Fig. 10 A, B)** for 1, 3 and 5 days, their growth was enhanced compared to their mono-cultures. While the proliferation of osteoblasts and MSCs in co-cultures were inhibited by the BrCa cells. In co-culture conditions, BrCa cells presented increased VEGF secretion compared to mono-cultured BrCa cells **(Fig. 10 C).** Moreover, the ALP activity of osteoblasts and MSCs declined substantially in the presence of BrCa cells **(Fig. 10 D)** [254]. The results of this work showed that 3D bioprinting of cell-laden bone matrices can lead to fabrication of constructs that provide an appropriate microenvironment for the cross-talk of multiple cells and therefore a valuable tool for evaluation of breast cancer bone invasion and metastasis.

50

In addition, Vinson and team studied epithelial and adipose cell interactions in breast cancer by fabricating cell-laden hydrogel microbeads into the matrix of differentiated hASCs using LAB. The fabricated 3D construct indeed provided a better understanding of breast cancer invasion into adipose tissue [255]. This platform provided a model that helps to understand the contribution of obesity on MCF-7 and MDA-MB-231 cancer cell invasion at the cellular and tissue level. Also, mammary duct-like structures were fabricated *in vitro* employing sacrificial bioprinting using mammary ductal carcinoma cells in GelMa hydrogel matrix. Such 3D printed structures can additionally be applied to other cancers involving duct-like structures [256].
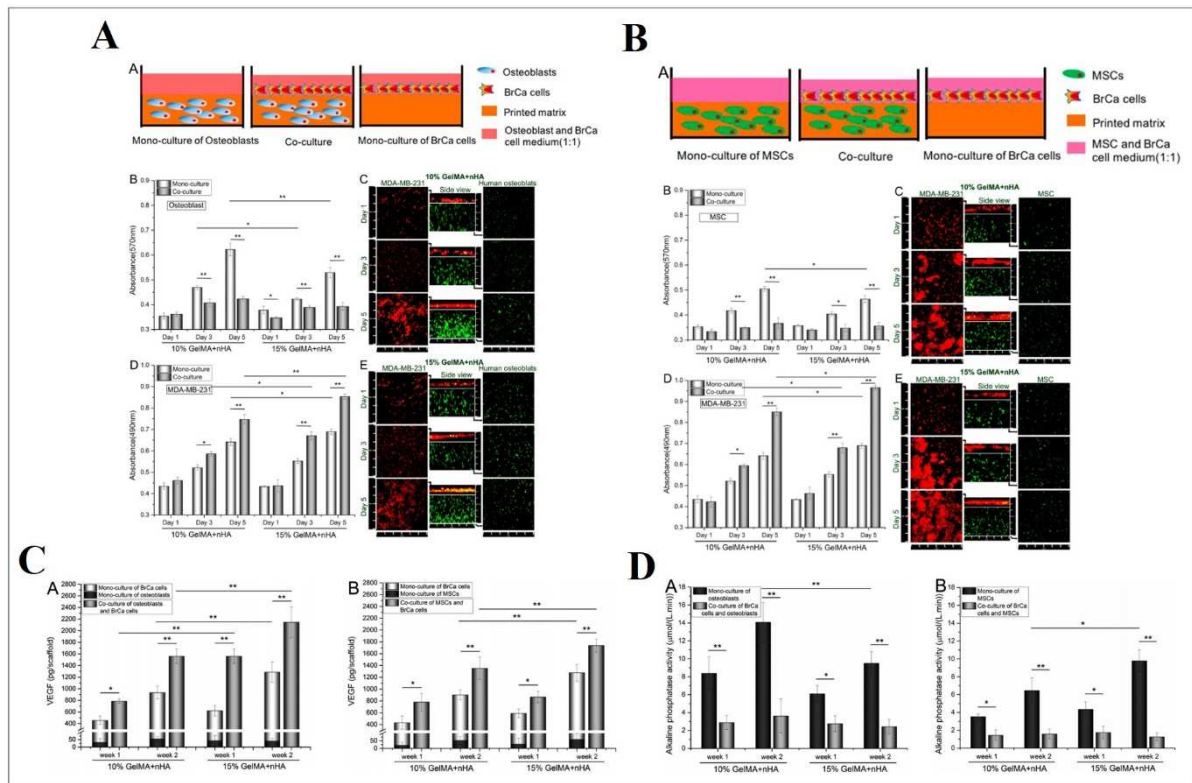
Fig. 10. 3D bioprinted cell-laden bone matrix as a biomimetic model for breast cancer metastasis study. **(A)** Examination of co-cultured osteoblasts and BrCa cells on 3D matrices. (A) Schematic of cells mono- and co-cultured in 3D the bioprinted matrix. Proliferation of (B) osteoblasts and (D) BrCa cells in the 3D bioprinted matrix at 1, 3 and 5 days of culture. (C, E) Representative confocal micrographs of co-cultured cells in the 3D bioprinted matrix. (Middle columns: cross-sectional views) (Osteoblasts (green): stained with Cell Tracker Green CMFDA dye; BrCa cells (red): stained with Orange CMTMR dye). **(B)** Examination of co-cultured MSCs and BrCa cells on 3D matrices. (A) Schematic of cells mono- and co-cultured in 3D the bioprinted matrix. Proliferation of (B) MSCs and (D) BrCa cells in the 3D bioprinted matrix at 1, 3 and 5 days of culture.

(Middle columns: cross-sectional views) (MSCs (green): stained with Cell Tracker Green CMFDA dye; BrCa cells (red): stained with Orange CMTMR dye). **(C)** Quantification of vascular endothelial growth factor (VEGF) levels. VEGF levels of BrCa cells mono- and co-cultured with (A) osteoblasts and (B) MSCs in the 3D bioprinted matrix after 2 weeks. **(D)** Evaluation of alkaline phosphatase activity (ALP). ALP activity of (A) osteoblasts and (B) MSCs mono- and co-cultured with BrCa cells in the 3D bioprinted matrix after 2 weeks (* $p < 0.05$; ** $p < 0.01$). ref. [254]

To demonstrate oral cancer progression, Almela et al. used extrusion-based 3D bioprinting to construct a human alveolar bone mucosal model (ABMM) and the cancerous bone oral mucosal model (CBMM). The 3D scaffold was laden with oral squamous cell carcinoma (OSCC) cell line spheroids to study several stages of oral cancer. It is expected that this strategy will aid in the development of new therapeutic approaches to control OSCC [257].

Ma et al. designed a novel and mechanically robust composite scaffold (Fe-CaSiO$_3$ named as 30CS) exhibiting synergistic effects of photothermal and reactive oxygen species (ROS) tumor therapy. 3D printed 30CS displayed better degradation and *in vivo* bone regeneration capability. Hence, such composite scaffolds are valuable for treating cortical bone cancer and regeneration of cortical bone defects resulting from surgery [258].

5.2 Drug testing, HTS, and Organ-On-A-Chip

The complexity and ethical concerns allied with the testing of drugs on animal and human models have raised demand for the development of specific tissue 3D models ("on-a-chip") *in vitro* or organ-on-a-chip devices. These microfabricated devices can recapitulate the dynamic interactions and aspects of the typical biomechanical and biochemical functions of *in vivo* microenvironments, tissues, and organs within an *in vitro* system. Such systems can be excellent *in vitro* platforms for the evaluation of drug potency and their effects on tissues, delivery testing, and tissue engineering [259].

3D printing applications are being explored to test whether a drug is toxic or effective in complex human organs, such as the liver and heart. The goal is to develop microtissue with the ability to produce the same physiologic responses on a small scale that would be observed in an entire organ, thus eliminating the complex step of animal testing. Also, 3D models would undoubtedly contribute to a better understanding of the mechanisms involved in disease

progression and drug screening [260]. The highly precise control over the microfeatures of the 3D printed constructs, especially in combination with microfabrication technologies, make this technology a perfect tool for creating 3D organ-on-a-chip devices. Additionally, the 3D bioprinting technology enables researchers to incorporate bioinks and celling into these devices to make microchips that can mimic the *in vivo* function and interactions more precisely. It can also be used for better cell culture and more accurate drug screening *in vitro* [99].

Likewise, 3D cancer spheroids have been printed within a tissue-like matrix using an inkjet DOD bioprinter for drug development. Atapattu et al. printed cancer spheroids for glioblastoma, neuroblastoma, and lung cancer with cell viability >95%. The HT drug screening of these spheroids was tested using doxorubicin [261]. A co-culture spheroid model employing non-small cell lung cancer (NSCLC) cells, PDX and lung cancer-associated fibroblasts (CAFs) have also been developed via an extrusion-based 3D bioprinting in sodium alginate/gelatin scaffold for HT drug screening [262]. This model has the potential to be used as a platform for high throuput drug screening. Furthermore, the use of human liver ECM bioink to print hepatic tissue to gain insight into the biology of liver diseases and drug screening is under investigation. Such cell-instructive bioinks are prospective for making artificial liver transplants [263].

Highlighting the importance of 3D printing in pharmaceutics, Sun et al. developed a template for fabricating customizable tablets with a desirable drug release profile [264]. However, this process is limited by its complexity, unavailability of material, and time constraints. To overcome this, Xu and colleagues employed extrusion-based 3D printing (FDM) to fabricate a shell with an external round shape and internal tetrahedron shape for designing a tablet with a convex drug release profile. The medicine encapsulated in the tetrahedron cavity inside the shell is gradually exposed to a buffer solution after the dissolution of the shell. The convex drug release profile serves a special purpose, such as for patients with hypertension whose peak blood pressures occur in the early morning hours. This drug release profile would allow patients to take their medications at night and the blood concentration would reach its maximum in the morning [265].

Chang et al. developed an automated syringe-based, multi-nozzle, direct cell writing process which is a specific type of extrusion-based bioprinting for biofabrication of 3D liver-cells

contained constructs [60,87,99,247]. They combined this process with micro-patterning techniques to create a liver-on-a-chip device containing bioprinted liver cells that are encapsulated in a hydrogel, as mentioned in section 4.5, liver bioprinting. Briefly, they fabricated a PDMS substrate containing a tissue chamber, using microfabrication methods such as photolithography and soft-lithography. Then they bioprinted the HepG2 liver cells encapsulated alginate hydrogels within the tissue chamber. Lastly, cover glass with required perfusion channels was applied to the device to enclose the cells [99]. This model was used for drug metabolism studies and provided the foundation for similar strategies in 3D bioprinting technology for direct fabrication of organ-on-a-chip devices, and living cells and tissues for screening the efficacy and toxicity of agents of interests *in vitro*.

Bhise et al. also developed a liver-on-a-chip platform using hepatic spheroids bioprinted with direct cell writing into a microfluidic bioreactor chip. Briefly, small spheroids were made out of HepG2/C3A human hepatocarcinoma cells using the microwell technique. Then the spheroids were encapsulated in GelMA and bioprinted with a modified version of commercially available NovoGen Bioprinter (Organovo, USA) [266]. This platform is an important step in the organ-on-a-chip field that facilitates the fabrication of *in vitro* testing devices for the evaluation of multiple drugs and cells efficiently and can be beneficial in the detection of some drug-induced liver injuries that are difficult to predict.

Homan et al. reported a bioprinting process for the fabrication of a kidney-on-a-chip device that mimics human renal proximal tubules *in vitro*. They combined bioprinting, 3D cell culture, and organ-on-a-chip methods to make a platform for the fabrication of 3D proximal tubules on a chip with a convoluted shape and capable of being perfused. The 3D proximal tubules constructs were fabricated using a custom-designed extrusion-based four-head 3D bioprinter. Briefly, ECM solution, composed of fibrinogen and gelatin was created and then mixed with thrombin and immediately casted on base of the chip and then allowed to dry and make a flat surface. In the next step the sacrificial ink was printed on the ECM surface according to the convoluted shape of the tubule, while its ends were connected to the inlet and outlet metal hollow perfusion pins. Then the top layer of ECM formed a cast similar to the surface and next the chip was covered with a glass slide. Finally, the sacrificial ink was flushed out of the chip resulted in an open tube that mimics proximal tubules [267]. This kidney-on-a-chip model can test and explain the mechanism of drug-induced tubule damages

and is a new approach for fabrication of organ-on-a-chip devices with more accurate recapitulation of *in vivo* microenvironments *in vitro*.

Moreover, Zhang et al. developed a 3D bioprinting based hybrid technology to produce endothelialized human myocardium as part of a heart-on-a-chip device with potential for drug screening, regenerative medicine, and disease modeling. Briefly, they used a modified extrusion-based bioprinter for 3D bioprinting of HUVEC encapsulated alginate-GelMA hydrogel as the bioink. HUVEC on microfabricated alginate-GelMA hydrogel and the formation of aligned myocardium seeded with CMs in a 3D endothelial bed and microfluidic perfusion bioreactor for cardiovascular toxicity evaluation [199]. This endothelialized-myocardium-on-a-chip model, in combination with a microfluidic perfusion bioreactor, can act as a platform for cardiovascular drug screening. This work showed that a combination of 3D bioprinting, microfluidics and stem cells for fabrication of organ-on-a-chip devices can provide innovative technology for the development of a new generation of *in vitro* human organ models for use in drug screening.

One of the other techniques that are used for the fabrication of organ-on-a-chip platforms is microcontact printing [259]. Although microcontact printing cannot be categorized in any of conventional bioprinting technologies, as it is more similar to 2D patterning rather than 3D printing, it can be considered a bioprinter despite printing only one layer (patterning). It can print/pattern bioactive contained inks and consequently pattern cells on a substrate to be used in organ-on-a-chip devices. Basically, microcontact printing is an expansion of replica molding, one of the soft-lithography techniques. Once the PDMS membrane is fabricated by replica molding, an elastomeric PDMS stamp will be created using that membrane and then coated with one layer of proteins. Then a substrate will be stamped with this protein-coated stamp resulting in areas of interest covered with proteins. These areas of protein can be patterned and controlled by changing the design of the PDMS stamp and therefore changing the pattern of cells on the substrate since the cells grow only in the areas containing the proteins [268].

6. Clinical translation in 3D bioprinting

3D bioprinting technology has made progressive strides towards clinical translation; despite this, numerous challenges must be overcome before clinical application. Several works

foreshadow promising technologies, but few are optimized for human use. Accordingly, the previously mentioned work of Albanna and colleagues in establishing a proof-of-concept skin bioprinter and Dvir and associates' work in bioprinting cardiac patches derived from patients' cells are notable advancements not quite ready for clinical utilization. Furthermore, Kang and colleagues demonstrated the fabrication of human-sized mandible bone, ear-shaped cartilage, and skeletal muscle using an integrated tissue-organ printer (ITOP), the results are encouraging for future clinical application. They conclude that ITOP has the potential to fabricate various types of vascularized tissues [269]. Such progress is encouraging considering that an essential challenge in clinical translation is the fabrication of vascularized tissues and organs. With the establishment of the *in situ* 3D bioprinting technology, BioPen, there is an indication that the field is making headway. Nevertheless, there is no large-scale clinical translation for 3D bioprinting. Furthermore, bioprinting of solid human organs for transplant is not yet feasible as current progress is limited to pre-clinical research [270].

There are currently no clinical trials using bioprinted cell-laden bone or cartilage constructs [271]. There are, however, cases where cell-free 3D printed technologies are utilized, with the majority of clinical trials within the fields of orthopedic surgery, maxillofacial surgery, and dentistry. Such fields have established clinical trials to assess the safety and efficacy of fabricated surgical templates, orthotic devices, implants for bone defects, and dentures [272]. Some advantages of 3D printed constructs in surgery include improved anticipation of anatomic variations, accurate guides and templates, increased time efficiency during surgical procedures, and improved aesthetic results.

Acellular 3D printed constructs have been implanted into patients. Zopf and associates reported the fabrication of a bioresorbable tracheal splint obtained via laser-based 3D printing to treat the life-threatening condition of tracheomalacia in an infant, a condition that causes an excessive collapse of the airway during breathing. The Food and Drug Administration (FDA) approved the intervention for an emergency-use exemption, exemplifying the dire need for the intervention. The infant experienced a significant improvement in respiratory symptoms, and subsequent imaging demonstrated an open airway [273].

Furthermore, 3D printing is useful for anatomical visualization during preoperative planning, especially in the case of complex anatomy. More specifically, Zein and associates printed 3D synthetic liver models with complex networks of vascular and biliary structures similar to the

native livers of six patients, including donors and recipients involved in living donor liver transplantation (LDLT). The study aimed to generate highly accurate models to facilitate surgical planning by preoperatively identifying the vascular and biliary anatomy to minimize operative complications [274]. Overall, the field still requires ongoing research before 3D printed devices can be used as therapeutic devices in standard clinical practice [275]. In addition, the field must overcome numerous challenges before the implementation of large-scale 3D bioprinting technologies.

6.1 Challenges and limitations in clinical translation

There are unique challenges ahead in the use of 3D bioprinting technologies for clinical translation. Specifically, there are limitations of bioinks as they must possess unique characteristics for optimization in clinical use. Such properties include insolubility *in vivo* and in culture, structural stability, a degradation rate congruent with the regeneration of tissue, promotion of cell growth, and nontoxic properties. Bioinks must also integrate with cells and permit vascularization [270]. As previously addressed, bioinks are also affected by the bioprinting modality used, as the process may impact cell viability. Currently, bioinks are limited in meeting all of these requirements and an ideal bioink has not been established.

There are even further limitations in realizing the ambitious goal of *in situ* bioprinting [276] in which living tissues are directly printed into the defect site in the operating room. Challenges include maintaining a sterile surgical field while incorporating a printer that integrates well with the operative process. In addition, there are ethical considerations as the process requires a multi-disciplinary approach that discloses sensitive medical information to the practitioner, engineer, and others. Furthermore, this process must also meet regulatory standards for clinical use and should be affordable [270].

7. Future perspective and concluding remarks

The innovation of bioprinting technology has the potential to revolutionize the medical sciences arena to create scaffolds for tissue and organ transplantation, drug screening, and regenerative medicine. The field has even moved forward with the commercialization of bioprinting technologies [277]. Despite great advancement, designing suitable bioinks and complex tissue fabrication remains challenging. Maintaining the viability of cells

encapsulated in bioinks and ensuring their protection from damage encountered during the printing process calls for novel bioink formulations, new cell sources, and advanced printing technologies. Therefore, standardization and quality-control methods will need to be established.

This review provides an overview of current progress in 3D bioprinting technology for tissue/organ engineering, in addition to the printing process parameters and recommended bioinks. We placed special emphasis on the application of 3D bioprinting for cancer research, drug testing, high throughput screening, and fabrication of organ-on-a-chip devices.

Bioprinting is moving beyond 3D towards the emergence of 4D. Conceptually, 4D printing employs 'smart' 3D constructs which can be programmed to alter their shape and function in response to external stimuli such as heat, ultraviolet light, current, pressure, and other energy sources [278,279]. Interestingly, support-free bioprinting for the fabrication of functional tissue has recently garnered attention. Researchers have used freshly printed human placenta to study the nutrient transport from mother to fetus. This method enables the study of various life-threatening conditions that can potentially arise in either mother or child during pregnancy and delivery. Despite the current success, considerable research is still required for the fabrication of compatible tissue grafts and full organ transplantation. Overall, we believe that in the near future 3D bioprinting will achieve new heights by patient-driven precision medicine and complex-tissue fabrication.

Declarations

Ethics approval and consent to participate- not applicable

Consent for Publication- not applicable

Availability of data and material- not applicable

Competing interests- The authors declare that they have no competing interests.

Funding- Not applicable

Author contributions- All authors read and approved the final manuscript

Acknowledgements- not applicable

59

References

[1]   X. Tang, L. Daneshmandi, G. Awale, L.S. Nair, C.T. Laurencin, Skeletal muscle regenerative engineering, Regen. Eng. Transl. Med. 5 (2019) 233–251. doi:10.1007/s40883-019-00102-9.

[2]   S. V Murphy, A. Atala, 3D bioprinting of tissues and organs, Nat. Biotechnol. 32 (2014) 773–785. doi:10.1038/nbt.2958.

[3]   C. Mandrycky, Z. Wang, K. Kim, D. Kim, 3D bioprinting for engineering complex tissues, 34 (2017) 422–434. doi:10.1016/j.biotechadv.2015.12.011.3d.

[4]   A. Arslan-Yildiz, R. El Assal, P. Chen, S. Guven, F. Inci, U. Demirci, Towards artificial tissue models: past, present, and future of 3D bioprinting, Biofabrication. 8 (2016) 014103. doi:10.1088/1758-5090/8/1/014103.

[5]   J. Malda, J. Visser, F.P. Melchels, T. Jüngst, W.E. Hennink, W.J.A. Dhert, J. Groll, D.W. Hutmacher, 25th Anniversary article: Engineering hydrogels for biofabrication, Adv. Mater. 25 (2013) 5011–5028. doi:10.1002/adma.201302042.

[6]   S. Tasoglu, U. Demirci, Bioprinting for stem cell research, Trends Biotechnol. 31

(2013) 10–19. doi:10.1016/j.tibtech.2012.10.005.

[7]   B. Derby, Printing and prototyping of tissues and scaffolds, Science. 338 (2012) 921–926. doi:10.1126/science.1226340.

[8]   F. Marga, K. Jakab, C. Khatiwala, B. Shepherd, S. Dorfman, B. Hubbard, S. Colbert, F. Gabor, Toward engineering functional organ modules by additive manufacturing, Biofabrication. 4 (2012). doi:10.1088/1758-5082/4/2/022001.

[9]   I.T. Ozbolat, Bioprinting scale-up tissue and organ constructs for transplantation, Trends Biotechnol. 33 (2015) 395–400. doi:10.1016/j.tibtech.2015.04.005.

[10]   F. Guillemot, V. Mironov, M. Nakamura, Bioprinting is coming of age: Report from the international conference on bioprinting and biofabrication in bordeaux (3B'09), Biofabrication. 2 (2010). doi:10.1088/1758-5082/2/1/010201.

[11]   V. Kériquel, M. Ali, J.-C. Fricain, A. Fontaine, B. Guillotin, M. Rémy, J. Amédée-Vilamitjana, R. Bareille, S. Catros, F. Guillemot, Laser-assisted bioprinting to deal with tissue complexity in regenerative medicine, MRS Bull. 36 (2011) 1015–1019. doi:10.1557/mrs.2011.272.

[12]   S. Khalil, W. Sun, Bioprinting endothelial cells with alginate for 3D tissue constructs, J. Biomech. Eng. 131 (2010) 111002. doi:10.1115/1.3128729.

[13]   A.B. Dababneh, I.T. Ozbolat, Bioprinting Technology: A current state-of-the-art review, J. Manuf. Sci. Eng. 136 (2014) 061016. doi:10.1115/1.4028512.

[14]   A. Atala, F.K. Kasper, A.G. Mikos, Engineering complex tissues, Sci. Transl. Med. 4 (2012) 160rv12-160rv12. doi:10.1126/scitranslmed.3004890.

[15]   F.P.W. Melchels, W.J.A. Dhert, D.W. Hutmacher, J. Malda, Development and characterisation of a new bioink for additive tissue manufacturing, J. Mater. Chem. B. 2 (2014) 2282–2289. doi:10.1039/c3tb21280g.

[16]   I.T. Ozbolat, Yin Yu, Bioprinting toward organ fabrication: Challenges and future trends, IEEE Trans. Biomed. Eng. 60 (2013) 691–699. doi:10.1109/tbme.2013.2243912.

[17]   L.G. Griffith, M.A. Swartz, Capturing complex 3D tissue physiology in vitro, Nat. Rev. Mol. Cell Biol. 7 (2006) 211–224. doi:10.1038/nrm1858.

[18] J. Li, M. Chen, X. Fan, H. Zhou, Recent advances in bioprinting techniques: approaches, applications and future prospects., J. Transl. Med. 14 (2016) 271. doi:10.1186/s12967-016-1028-0.

[19] S. Knowlton, S. Anand, T. Shah, S. Tasoglu, Bioprinting for neural tissue engineering, Trends Neurosci. 41 (2018) 31–46. doi:10.1016/j.tins.2017.11.001.

[20] F.P.W. Melchels, M.A.N. Domingos, T.J. Klein, J. Malda, P.J. Bartolo, D.W. Hutmacher, Additive manufacturing of tissues and organs, Prog. Polym. Sci. 37 (2012) 1079–1104. doi:10.1016/j.progpolymsci.2011.11.007.

[21] S. Wüst, R. Müller, S. Hofmann, S. Wüst, R. Müller, S. Hofmann, Controlled Positioning of cells in biomaterials—Approaches towards 3D tissue printing, J. Funct. Biomater. 2 (2011) 119–154. doi:10.3390/jfb2030119.

[22] T. Billiet, M. Vandenhaute, J. Schelfhout, S. Van Vlierberghe, P. Dubruel, A review of trends and limitations in hydrogel-rapid prototyping for tissue engineering, Biomaterials. 33 (2012) 6020–6041. doi:10.1016/j.biomaterials.2012.04.050.

[23] N. Shanks, R. Greek, J. Greek, Are animal models predictive for humans?, Philos. Ethics, Humanit. Med. 4 (2009) 2. doi:10.1186/1747-5341-4-2.

[24] W. Peng, P. Datta, B. Ayan, V. Ozbolat, D. Sosnoski, I.T. Ozbolat, 3D bioprinting for drug discovery and development in pharmaceutics, Acta Biomater. 57 (2017) 26–46. doi:10.1016/j.actbio.2017.05.025.

[25] C. Xu, W. Chai, Y. Huang, R.R. Markwald, Scaffold-free inkjet printing of three-dimensional zigzag cellular tubes, Biotechnol. Bioeng. 109 (2012) 3152–3160. doi:10.1002/bit.24591.

[26] T. Lu, Y. Li, T. Chen, Techniques for fabrication and construction of three-dimensional scaffolds for tissue engineering., Int. J. Nanomedicine. 8 (2013) 337–50. doi:10.2147/ijn.s38635.

[27] A.N. Leberfinger, D.J. Ravnic, A. Dhawan, I.T. Ozbolat, Concise Review: Bioprinting of stem cells for transplantable tissue fabrication, Stem Cells Transl. Med. 6 (2017) 1940–1948. doi:10.1002/sctm.17-0148.

[28] M. Varkey, D.O. Visscher, P.P.M. van Zuijlen, A. Atala, J.J. Yoo, Skin bioprinting: the future of burn wound reconstruction?, Burn. Trauma. 7 (2019) 1–12.

doi:10.1186/s41038-019-0142-7.

[29]   R.E. Saunders, B. Derby, Inkjet printing biomaterials for tissue engineering: bioprinting, Int. Mater. Rev. 59 (2014) 430–448. doi:10.1179/1743280414y.0000000040.

[30]   T. Boland, T. Xu, B. Damon, X. Cui, Application of inkjet printing to tissue engineering, (2006) 910–917. doi:10.1002/biot.200600081.

[31]   B. Derby, Inkjet printing of functional and structural materials: Fluid property requirements, feature stability, and resolution, Annu. Rev. Mater. Res. 40 (2010) 395–414. doi:10.1146/annurev-matsci-070909-104502.

[32]   C.-H. Choi, L.-Y. Lin, C.-C. Cheng, C. Chang, Printed oxide thin film transistors: A mini review, ECS J. Solid State Sci. Technol. 4 (2015) P3044–P3051. doi:10.1149/2.0071504jss.

[33]   P.L. Hue, Progress and trends in ink-jet printing technology, J. Imaging Sci. Technol. 42 (1998) 49–62.

[34]   Print quality optimization for a color ink-jet printer by using a larger nozzle for the black ink only, (1994). https://patents.google.com/patent/US5521622 (accessed March 22, 2019).

[35]   Method and apparatus for reducing the size of drops ejected from a thermal ink jet printhead, (1994). https://patents.google.com/patent/US5673069 (accessed March 22, 2019).

[36]   Ink drop volume variance compensation for inkjet printing, (1997). https://patents.google.com/patent/US6042211A/en (accessed March 22, 2019).

[37]   Q. Gao, Y. He, J. zhong Fu, A. Liu, L. Ma, Coaxial nozzle-assisted 3D bioprinting with built-in microchannels for nutrients delivery, Biomaterials. 61 (2015) 203–215. doi:10.1016/j.biomaterials.2015.05.031.

[38]   T. Xu, J. Jin, C. Gregory, J.J. Hickman, T. Boland, Inkjet printing of viable mammalian cells, Biomaterials. 26 (2005) 93–99. doi:10.1016/j.biomaterials.2004.04.011.

[39]   X. Cui, D. Dean, Z.M. Ruggeri, T. Boland, Cell damage evaluation of thermal inkjet

printed chinese hamster ovary cells, Biotechnol. Bioeng. 106 (2010) 963–969. doi:10.1002/bit.22762.

[40] X. Cui, T. Boland, Human microvasculature fabrication using thermal inkjet printing technology, Biomaterials. 30 (2009) 6221–6227. doi:10.1016/j.biomaterials.2009.07.056.

[41] G. Gao, T. Yonezawa, K. Hubbell, G. Dai, X. Cui, Inkjet-bioprinted acrylated peptides and PEG hydrogel with human mesenchymal stem cells promote robust bone and cartilage formation with minimal printhead clogging, Biotechnol. J. 10 (2015) 1568–1577. doi:10.1002/biot.201400635.

[42] P. Ihalainen, A. Määttänen, N. Sandler, Printing technologies for biomolecule and cell-based applications, Int. J. Pharm. 494 (2015) 585–592. doi:10.1016/j.ijpharm.2015.02.033.

[43] R.E. Saunders, J.E. Gough, B. Derby, Delivery of human fibroblast cells by piezoelectric drop-on-demand inkjet printing, Biomaterials. 29 (2008) 193–203. doi:10.1016/j.biomaterials.2007.09.032.

[44] R. Saunders, J. Gough, B. Derby, Ink Jet printing of mammalian primary cells for tissue engineering applications, MRS Proc. 845 (2004) AA2.8. doi:10.1557/proc-845-aa2.8.

[45] R. Saunders, L. Bosworth, J. Gough, B. Derby, N. Reis, Selective cell delivery for 3D tissue culture and engineering, Eur Cells Mater. 2004;784. (2004). https://www.escholar.manchester.ac.uk/uk-ac-man-scw:194798 (accessed March 25, 2019).

[46] C.B. Arnold, P. Serra, A. Piqué, Laser direct-write techniques for printing of complex materials, MRS Bull. 32 (2007) 23–32. doi:10.1557/mrs2007.11.

[47] J. Bohandy, B.F. Kim, F.J. Adrian, Metal deposition from a supported metal film using an excimer laser, J. Appl. Phys. 60 (1986) 1538–1539. doi:10.1063/1.337287.

[48] D.B. Chrisey, Materials processing: The power of direct writing, Science. 289 (2000) 879–881. doi:10.1126/science.289.5481.879.

[49] M. Colina, P. Serra, J.M. Fernández-Pradas, L. Sevilla, J.L. Morenza, DNA deposition through laser induced forward transfer, Biosens. Bioelectron. 20 (2005) 1638–1642.

doi:10.1016/j.bios.2004.08.047.

[50] V. Dinca, E. Kasotakis, J. Catherine, A. Mourka, A. Ranella, A. Ovsianikov, B.N. Chichkov, M. Farsari, A. Mitraki, C. Fotakis, Directed three-dimensional patterning of self-assembled peptide fibrils, Nano Lett. 8 (2008) 538–543. doi:10.1021/nl072798r.

[51] J.A. Barron, P. Wu, H.D. Ladouceur, B.R. Ringeisen, Biological laser printing: A novel technique for creating heterogeneous 3-dimensional cell patterns, Biomed. Microdevices. 6 (2004) 139–147. doi:10.1023/b:bmmd.0000031751.67267.9f.

[52] V. Keriquel, H. Oliveira, M. Rémy, S. Ziane, B. Rousseau, S. Rey, S. Catros, J. Amédée, In situ printing of mesenchymal stromal cells , by laser-assisted bioprinting , for in vivo bone regeneration applications, (2017) 1–10. doi:10.1038/s41598-017-01914-x.

[53] F. Guillemot, A. Souquet, S. Catros, B. Guillotin, Laser-assisted cell printing: principle, physical parameters versus cell fate and perspectives in tissue engineering, Nanomedicine. 5 (2010) 507–515. doi:10.2217/nnm.10.14.

[54] B.R. Ringeisen, C.M. Othon, J.A. Barron, D. Young, B.J. Spargo, Jet-based methods to print living cells, Biotechnol. J. 1 (2006) 930–948. doi:10.1002/biot.200600058.

[55] S. Catros, B. Guillotin, M. Bačáková, J.-C. Fricain, F. Guillemot, Effect of laser energy, substrate film thickness and bioink viscosity on viability of endothelial cells printed by laser-assisted bioprinting, Appl. Surf. Sci. 257 (2011) 5142–5147. doi:10.1016/j.apsusc.2010.11.049.

[56] P. Calvert, Inkjet printing for materials and devices, (2001). doi:10.1021/cm0101632.

[57] V. Mironov, Printing technology to produce living tissue, Expert Opin. Biol. Ther. 3 (2003) 701–704. doi:10.1517/14712598.3.5.701.

[58] R.F. Pereira, P.J. Bártolo, 3D bioprinting of photocrosslinkable hydrogel constructs, J. Appl. Polym. Sci. 132 (2015) n/a-n/a. doi:10.1002/app.42458.

[59] S. Wüst, M.E. Godla, R. Müller, S. Hofmann, Tunable hydrogel composite with two-step processing in combination with innovative hardware upgrade for cell-based three-dimensional bioprinting, Acta Biomater. 10 (2014) 630–640. doi:10.1016/j.actbio.2013.10.016.

[60] R. Chang, J. Nam, W. Sun, Effects of dispensing pressure and nozzle diameter on cell survival from solid freeform fabrication–based direct cell writing, Tissue Eng. Part A. 14 (2008) 41–48. doi:10.1089/ten.a.2007.0004.

[61] N.-T. Nguyen, J. St. John, H. Kamble, M. Barton, R.K. Vadivelu, A. Munaz, Three-dimensional printing of biological matters, J. Sci. Adv. Mater. Devices. 1 (2016) 1–17. doi:10.1016/j.jsamd.2016.04.001.

[62] U. Jammalamadaka, K. Tappa, Recent advances in biomaterials for 3D printing and tissue engineering, J. Funct. Biomater. 9 (2018). doi:10.3390/jfb9010022.

[63] J. Malda, M.W. Pot, W. Schuurman, P.R. van Weeren, V. Khristov, W.J.A. Dhert, Bioprinting of hybrid tissue constructs with tailorable mechanical properties, Biofabrication. 3 (2011) 021001. doi:10.1088/1758-5082/3/2/021001.

[64] H.N. Chia, B.M. Wu, Recent advances in 3D printing of biomaterials, J. Biol. Eng. 9 (2015) 1–14. doi:10.1186/s13036-015-0001-4.

[65] Z. Xie, P. Li, J.P. Lata, Z. Mao, Y. Chen, J. Liu, L. Ren, F. Guo, M. Dao, S. Suresh, J. Yang, T.J. Huang, Three-dimensional manipulation of single cells using surface acoustic waves, Proc. Natl. Acad. Sci. 113 (2016) 1522–1527. doi:10.1073/pnas.1524813113.

[66] Q. Gu, J. Hao, Y.J. Lu, L. Wang, G.G. Wallace, Q. Zhou, Three-dimensional bio-printing, Sci. China Life Sci. 58 (2015) 411–419. doi:10.1007/s11427-015-4850-3.

[67] U. Demirci, Acoustic picoliter droplets for emerging applications in semiconductor industry and biotechnology, J. Microelectromechanical Syst. 15 (2006) 957–966. doi:10.1109/jmems.2006.878879.

[68] U. Demirci, G. Montesano, Single cell epitaxy by acoustic picolitre droplets, Lab Chip. 7 (2007) 1139–1145. doi:10.1039/b704965j.

[69] P. Zorlutuna, R. Bashir, H. Kong, V. Chan, J.H. Jeong, Three-dimensional photopatterning of hydrogels using stereolithography for long-term cell encapsulation, Lab Chip. 10 (2010) 2062. doi:10.1039/c004285d.

[70] G. Mapili, Y. Lu, S. Chen, K. Roy, Laser-layered microfabrication of spatially patterned functionalized tissue-engineering scaffolds, J. Biomed. Mater. Res. - Part B Appl. Biomater. 75 (2005) 414–424. doi:10.1002/jbm.b.30325.

[71]   K.C. Hribar, P. Soman, J. Warner, P. Chung, S. Chen, Light-assisted direct-write of 3D functional biomaterials, Lab Chip. 14 (2014) 268–275. doi:10.1039/c3lc50634g.

[72]   V.B. Morris, S. Nimbalkar, M. Younesi, P. McClellan, O. Akkus, Mechanical properties, cytocompatibility and manufacturability of chitosan:PEGDA hybrid-gel scaffolds by stereolithography, Ann. Biomed. Eng. 45 (2017) 286–296. doi:10.1007/s10439-016-1643-1.

[73]   R. Gauvin, Y.-C. Chen, J.W. Lee, P. Soman, P. Zorlutuna, J.W. Nichol, H. Bae, S. Chen, A. Khademhosseini, Microfabrication of complex porous tissue engineering scaffolds using 3D projection stereolithography, Biomaterials. 33 (2012) 3824–3834. doi:10.1016/j.biomaterials.2012.01.048.

[74]   B. Parker, S. Ghosh, R. Abdulla, Z. Wang, K. Kim, R. Samanipour, A simple and high-resolution stereolithography-based 3D bioprinting system using visible light crosslinkable bioinks, Biofabrication. 7 (2015) 045009. doi:10.1088/1758-5090/7/4/045009.

[75]   S.-J. Lee, M. Nowicki, B. Harris, L.G. Zhang, Fabrication of a highly aligned neural scaffold via a table top stereolithography 3D printing and electrospinning , Tissue Eng. Part A. 23 (2016) 491–502. doi:10.1089/ten.tea.2016.0353.

[76]   W.L. Haisler, D.M. Timm, J.A. Gage, H. Tseng, T.C. Killian, G.R. Souza, Three-dimensional cell culturing by magnetic levitation, Nat. Protoc. 8 (2013) 1940–1949. doi:10.1038/nprot.2013.125.

[77]   H. Tseng, J.A. Gage, R.M. Raphael, R.H. Moore, T.C. Killian, K.J. Grande-Allen, G.R. Souza, Assembly of a three-dimensional multitype bronchiole coculture model using magnetic levitation, Tissue Eng. - Part C Methods. 19 (2013) 665–675. doi:10.1089/ten.tec.2012.0157.

[78]   H. Tseng, L.R. Balaoing, B. Grigoryan, R.M. Raphael, T.C. Killian, G.R. Souza, K.J. Grande-Allen, A three-dimensional co-culture model of the aortic valve using magnetic levitation, Acta Biomater. 10 (2014) 173–182. doi:10.1016/j.actbio.2013.09.003.

[79]   J.M. Lee, S.L. Sing, M. Zhou, W.Y. Yeong, 3D bioprinting processes: A perspective on classification and terminology, Int. J. Bioprinting. 4 (2018) 0–10.

67

doi:10.18063/ijb.v4i2.151.

[80]   A.R. Abdel Fattah, E. Meleca, S. Mishriki, A. Lelic, F. Geng, R.P. Sahu, S. Ghosh, I.K. Puri, In situ 3D label-free contactless bioprinting of cells through diamagnetophoresis, ACS Biomater. Sci. Eng. 2 (2016) 2133–2138. doi:10.1021/acsbiomaterials.6b00614.

[81]   B.R. Whatley, X. Li, N. Zhang, X. Wen, Magnetic-directed patterning of cell spheroids, J. Biomed. Mater. Res. - Part A. 102 (2014) 1537–1547. doi:10.1002/jbm.a.34797.

[82]   H. Tseng, J.A. Gage, T. Shen, W.L. Haisler, S.K. Neeley, S. Shiao, J. Chen, P.K. Desai, A. Liao, C. Hebel, R.M. Raphael, J.L. Becker, G.R. Souza, A spheroid toxicity assay using magnetic 3D bioprinting and real-time mobile device-based imaging, Sci. Rep. 5 (2015) 1–11. doi:10.1038/srep13987.

[83]   G.R. Souza, H. Tseng, J.A. Gage, A. Mani, P. Desai, F. Leonard, A. Liao, M. Longo, J.S. Refuerzo, B. Godin, Magnetically bioprinted human myometrial 3D cell rings as a model for uterine contractility, Int. J. Mol. Sci. 18 (2017). doi:10.3390/ijms18040683.

[84]   S. Hou, H. Tiriac, B.P. Sridharan, L. Scampavia, F. Madoux, J. Seldin, G.R. Souza, D. Watson, D. Tuveson, T.P. Spicer, Advanced development of primary pancreatic organoid tumor models for high-throughput phenotypic drug screening, SLAS Discov. 23 (2018) 574–584. doi:10.1177/2472555218766842.

[85]   P. Baillargeon, J. Shumate, S. Hou, V. Fernandez-Vega, N. Marques, G. Souza, J. Seldin, T.P. Spicer, L. Scampavia, Automating a magnetic 3D spheroid model technology for high-throughput screening, SLAS Technol. (2019). doi:10.1177/2472630319854337.

[86]   M. Cornelissen, T. De Schryver, E. Gevaert, T. Billiet, P. Dubruel, The 3D printing of gelatin methacrylamide cell-laden tissue-engineered constructs with high cell viability, Biomaterials. 35 (2013) 49–62. doi:10.1016/j.biomaterials.2013.09.078.

[87]   S. Ji, M. Guvendiren, Recent advances in bioink design for 3D bioprinting of tissues and organs, Front. Bioeng. Biotechnol. 5 (2017) 1–8. doi:10.3389/fbioe.2017.00023.

[88]   F. Pati, J. Jang, J.W. Lee, D.W. Cho, Extrusion bioprinting, 2015. doi:10.1016/b978-0-12-800972-7.00007-4.

[89]   M. Burke, B.M. Carter, A.W. Perriman, Bioprinting: uncovering the utility layer-by-
       layer, J. 3D Print. Med. 1 (2017) 165–179. doi:10.2217/3dp-2017-0006.

[90]   H. Gudapati, M. Dey, I. Ozbolat, A comprehensive review on droplet-based
       bioprinting: Past, present and future, Biomaterials. 102 (2016) 20–42.
       doi:10.1016/j.biomaterials.2016.06.012.

[91]   B. Guillotin, A. Souquet, S. Catros, M. Duocastella, B. Pippenger, S. Bellance, R.
       Bareille, M. Rémy, L. Bordenave, J. Amédée j, F. Guillemot, Laser assisted
       bioprinting of engineered tissue with high cell density and microscale organization,
       Biomaterials. 31 (2010) 7250–7256. doi:10.1016/j.biomaterials.2010.05.055.

[92]   A. Ovsianikov, S. Lin, K. Hölzl, L. Tytgat, S. Van Vlierberghe, L. Gu, Bioink
       properties before, during and after 3D bioprinting, Biofabrication. 8 (2016) 032002.
       doi:10.1088/1758-5090/8/3/032002.

[93]   I.T. Ozbolat, W. Peng, V. Ozbolat, Application areas of 3D bioprinting, Drug Discov.
       Today. 21 (2016) 1257–1271. doi:10.1016/j.drudis.2016.04.006.

[94]   L. Ouyang, R. Yao, Y. Zhao, W. Sun, Effect of bioink properties on printability and
       cell viability for 3D bioplotting of embryonic stem cells, Biofabrication. 8 (2016) 1–
       12. doi:10.1088/1758-5090/8/3/035020.

[95]   P.S. Gungor-Ozkerim, I. Inci, Y.S. Zhang, A. Khademhosseini, M.R. Dokmeci,
       Bioinks for 3D bioprinting: An overview, Biomater. Sci. 6 (2018) 915–946.
       doi:10.1039/c7bm00765e.

[96]   J.K. Carrow, P. Kerativitayanan, M.K. Jaiswal, G. Lokhande, A.K. Gaharwar, Chapter
       13 – Polymers for bioprinting, Essentials 3D Biofabrication Transl. (2015) 229–248.
       doi:10.1016/b978-0-12-800972-7.00013-x.

[97]   J. Groll, J.A. Burdick, D.-W. Cho, B. Derby, M. Gelinsky, S.C. Heilshorn, T. Jüngst, J.
       Malda, V.A. Mironov, K. Nakayama, A. Ovsianikov, W. Sun, S. Takeuchi, J.J. Yoo,
       T.B.F. Woodfield, A definition of bioinks and their distinction from biomaterial inks,
       Biofabrication. 11 (2018) 013001. doi:10.1088/1758-5090/aaec52.

[98]   D. Williams, P. Thayer, H. Martinez, E. Gatenholm, A. Khademhosseini, A
       perspective on the physical, mechanical and biological specifications of bioinks and
       the development of functional tissues in 3D bioprinting, Bioprinting. 9 (2018) 19–36.

doi:10.1016/j.bprint.2018.02.003.

[99] R. Chang, K. Emami, H. Wu, W. Sun, Biofabrication of a three-dimensional liver micro-organ as an in vitro drug metabolism model, Biofabrication. 2 (2010). doi:10.1088/1758-5082/2/4/045004.

[100] A. Blaeser, A. Korsten, S. Neuss, H. Fischer, D.F. Duarte Campos, J. Jäkel, M. Vogt, The stiffness and structure of three-dimensional printed hydrogels direct the differentiation of mesenchymal stromal cells toward adipogenic and osteogenic lineages, Tissue Eng. Part A. 21 (2014) 740–756. doi:10.1089/ten.tea.2014.0231.

[101] A. Ewald, M. Schweinlin, K. Schacht, T. Jüngst, T. Scheibel, J. Groll, Biofabrication of cell-loaded 3D spider silk constructs, Angew. Chemie Int. Ed. 54 (2015) 2816–2820. doi:10.1002/anie.201409846.

[102] L. Pescosolido, W. Schuurman, J. Malda, P. Matricardi, F. Alhaique, T. Coviello, P.R. Van Weeren, W.J.A. Dhert, W.E. Hennink, T. Vermonden, Hyaluronic acid and dextran-based semi-IPN hydrogels as biomaterials for bioprinting, Biomacromolecules. 12 (2011) 1831–1838. doi:10.1021/bm200178w.

[103] T.A. Busbee, J.A. Lewis, D.B. Kolesky, R.L. Truby, A.S. Gladman, K.A. Homan, 3D bioprinting of vascularized, heterogeneous cell-laden tissue constructs, Adv. Mater. 26 (2014) 3124–3130. doi:10.1002/adma.201305506.

[104] A. Atala, J.J. Yoo, W. Zhao, D. Dice, K.W. Binder, T. Xu, M.Z. Albanna, Hybrid printing of mechanically and biologically improved constructs for cartilage tissue engineering applications, Biofabrication. 5 (2012) 015001. doi:10.1088/1758-5082/5/1/015001.

[105] D.F. Duarte Campos, B. Theek, A. Blaeser, H. Fischer, S. Neuss, W. Jahnen-Dechent, M. Weber, Biofabrication under fluorocarbon: A novel freeform fabrication technique to generate high aspect ratio tissue-engineered constructs, Biores. Open Access. 2 (2013) 374–384. doi:10.1089/biores.2013.0031.

[106] R. Levato, J. Visser, J.A. Planell, E. Engel, J. Malda, M.A. Mateos-Timoneda, Biofabrication of tissue constructs by 3D bioprinting of cell-laden microcarriers, Biofabrication. 6 (2014). doi:10.1088/1758-5082/6/3/035020.

[107] G.D. Prestwich, A. Skardal, J. Zhang, L. McCoard, S. Oottamasathien, Dynamically

crosslinked gold nanoparticle-hyaluronan hydrogels, Adv. Mater. 22 (2010) 4736–4740. doi:10.1002/adma.201001436.

[108] F. Pati, J.-W. Rhie, D.-W. Cho, J. Jang, H.H. Han, D.-H. Ha, Biomimetic 3D tissue printing for soft tissue regeneration, Biomaterials. 62 (2015) 164–175. doi:10.1016/j.biomaterials.2015.05.043.

[109] A. Souquet, J.C. Fricain, M. Rémy, B. Guillotin, M. Faucon, J. Amédée, F. Guillemot, S. Catros, J. Lopez, R. Bareille, B. Pippenger, S. Bellance, P. Chabassier, High-throughput laser printing of cells and biomaterials for tissue engineering, Acta Biomater. 6 (2009) 2494–2500. doi:10.1016/j.actbio.2009.09.029.

[110] N. Paxton, W. Smolan, T. Böck, F. Melchels, J. Groll, T. Jungst, Proposal to assess printability of bioinks for extrusion-based bioprinting and evaluation of rheological properties governing bioprintability, Biofabrication. 9 (2017) 044107. doi:10.1088/1758-5090/aa8dd8.

[111] V.H.M. Mouser, A. Abbadessa, R. Levato, W.E. Hennink, T. Vermonden, D. Gawlitta, J. Malda, Development of a thermosensitive HAMA-containing bio-ink for the fabrication of composite cartilage repair constructs, Biofabrication. 9 (2017) 015026. doi:10.1088/1758-5090/aa6265.

[112] W.L. Ng, W.Y. Yeong, M.W. Naing, Polyvinylpyrrolidone-based bio-ink improves cell viability and homogeneity during drop-on-demand printing, Materials (Basel). 10 (2017). doi:10.3390/ma10020190.

[113] M. Müller, J. Becher, M. Schnabelrauch, M. Zenobi-Wong, Nanostructured pluronic hydrogels as bioinks for 3D bioprinting, Biofabrication. 7 (2015) 35006. doi:10.1088/1758-5090/7/3/035006.

[114] S. Stichler, T. Böck, N. Paxton, S. Bertlein, R. Levato, V. Schill, W. Smolan, J. Malda, J. Teßmar, T. Blunk, J. Groll, Double printing of hyaluronic acid/poly(glycidol) hybrid hydrogels with poly(ϵ-caprolactone) for MSC chondrogenesis, Biofabrication. 9 (2017) 0–23. doi:10.1088/1758-5090/aa8cb7.

[115] M. Sadat-Shojai, M.T. Khorasani, A. Jamshidi, A new strategy for fabrication of bone scaffolds using electrospun nano-HAp/PHB fibers and protein hydrogels, Chem. Eng. J. 289 (2016) 38–47. doi:10.1016/j.cej.2015.12.079.

71

[116] N.E. Fedorovich, E. Kuipers, D. Gawlitta, W.J.A. Dhert, J. Alblas, Scaffold porosity and oxygenation of printed hydrogel constructs affect functionality of embedded osteogenic progenitors, Tissue Eng. Part A. 17 (2011) 2473–2486. doi:10.1089/ten.tea.2011.0001.

[117] R. Goldshmid, D. Seliktar, Hydrogel modulus affects proliferation rate and pluripotency of human mesenchymal stem cells grown in three-dimensional culture, ACS Biomater. Sci. Eng. 3 (2017) 3433–3446. doi:10.1021/acsbiomaterials.7b00266.

[118] A. Banerjee, M. Arha, S. Choudhary, R.S. Ashton, S.R. Bhatia, D. V. Schaffer, R.S. Kane, The influence of hydrogel modulus on the proliferation and differentiation of encapsulated neural stem cells, Biomaterials. 30 (2009) 4695–4699. doi:10.1016/j.biomaterials.2009.05.050.

[119] B. Duan, L.A. Hockaday, K.H. Kang, J.T. Butcher, 3D Bioprinting of heterogeneous aortic valve conduits with alginate/gelatin hydrogels, J. Biomed. Mater. Res. - Part A. 101 A (2013) 1255–1264. doi:10.1002/jbm.a.34420.

[120] D.F. Duarte Campos, A. Blaeser, M. Weber, J. Jäkel, S. Neuss, W. Jahnen-Dechent, H. Fischer, Three-dimensional printing of stem cell-laden hydrogels submerged in a hydrophobic high-density fluid, Biofabrication. 5 (2013). doi:10.1088/1758-5082/5/1/015003.

[121] S. Michael, H. Sorg, C.T. Peck, L. Koch, A. Deiwick, B. Chichkov, P.M. Vogt, K. Reimers, Tissue engineered skin substitutes created by laser-assisted bioprinting form skin-like structures in the dorsal skin fold chamber in mice, PLoS One. 8 (2013). doi:10.1371/journal.pone.0057741.

[122] T. Zhang, K.C. Yan, L. Ouyang, W. Sun, Mechanical characterization of bioprinted in vitro soft tissue models, Biofabrication. 5 (2013). doi:10.1088/1758-5082/5/4/045010.

[123] B. Peters, W.J.A. Dhert, J. Malda, T.J. Burger, J. Visser, J. Boomstra, F.P.W. Melchels, Biofabrication of multi-material anatomically shaped tissue constructs, Biofabrication. 5 (2013) 035007. doi:10.1088/1758-5082/5/3/035007.

[124] C.M. Owens, F. Marga, G. Forgacs, C.M. Heesch, Biofabrication and testing of a fully cellular nerve graft, Biofabrication. 5 (2013). doi:10.1088/1758-5082/5/4/045007.

[125] Y. Zhao, Y. Li, S. Mao, W. Sun, R. Yao, The influence of printing parameters on cell

survival rate and printability in microextrusion-based 3D cell printing technology, Biofabrication. 7 (2015) 045002. doi:10.1088/1758-5090/7/4/045002.

[126] K.H. Kang, L.A. Hockaday, J.T. Butcher, Quantitative optimization of solid freeform deposition of aqueous hydrogels, Biofabrication. 5 (2013) 035001. doi:10.1088/1758-5082/5/3/035001.

[127] E.K. Cushnie, B.D. Ulery, S.J. Nelson, M. Deng, S. Sethuraman, S.B. Doty, K.W.H. Lo, Y.M. Khan, C.T. Laurencin, Simple signaling molecules for inductive bone regenerative engineering, PLoS One. 9 (2014) e101627. doi:10.1371/journal.pone.0101627.

[128] L. Gasperini, D. Maniglio, A. Motta, C. Migliaresi, An electrohydrodynamic bioprinter for alginate hydrogels containing living cells, Tissue Eng. Part C Methods. 21 (2015) 123–132. doi:10.1089/ten.tec.2014.0149.

[129] H. Gudapati, J. Yan, Y. Huang, D.B. Chrisey, Alginate gelation-induced cell death during laser-assisted cell printing, Biofabrication. 6 (2014). doi:10.1088/1758-5082/6/3/035022.

[130] Y. Zhang, Y. Yu, H. Chen, I.T. Ozbolat, Characterization of printable cellular micro-fluidic channels for tissue engineering, Biofabrication. 5 (2013). doi:10.1088/1758-5082/5/2/025004.

[131] Y. Zhang, Y. Yu, A. Akkouch, A. Dababneh, F. Dolati, I.T. Ozbolat, In vitro study of directly bioprinted perfusable vasculature conduits, Biomater. Sci. 3 (2015) 134–143. doi:10.1039/c4bm00234b.

[132] D.M. Kingsley, A.D. Dias, D.B. Chrisey, D.T. Corr, Single-step laser-based fabrication and patterning of cell-encapsulated alginate microbeads, Biofabrication. 5 (2013). doi:10.1088/1758-5082/5/4/045006.

[133] M. Marcolongo, W. Sun, M. Gandhi, S. Khalil, K.C. Yan, K. Barbee, K. Nair, Characterization of cell viability during bioprinting processes, Biotechnol. J. 4 (2009) 1168–1177. doi:10.1002/biot.200900004.

[134] S.K. Williams, J.S. Touroo, K.H. Church, J.B. Hoying, Encapsulation of adipose stromal vascular fraction cells in alginate hydrogel spheroids using a direct-write three-dimensional printing system, Biores. Open Access. 2 (2013) 448–454.

doi:10.1089/biores.2013.0046.

[135] C. Xu, M. Zhang, Y. Huang, A. Ogale, J. Fu, R.R. Markwald, Study of droplet formation process during drop-on-demand inkjetting of living cell-laden bioink, Langmuir. 30 (2014) 9130–9138. doi:10.1021/la501430x.

[136] R.R. Markwald, R.P. Visconti, Y. Tan, S. Pollard, H. Yao, T.C. Trusk, Y. Mei, M.J. Yost, J. Rodriguez, D.J. Richards, J. Jia, Engineering alginate as bioink for bioprinting, Acta Biomater. 10 (2014) 4323–4331. doi:10.1016/j.actbio.2014.06.034.

[137] J.P. Trasatti, S.-S. Yoo, G. Singh, X. Xu, V. Lee, T.N. Tran, G. Dai, C. Bjornsson, P. Karande, Design and fabrication of human skin by three-dimensional bioprinting, Tissue Eng. Part C Methods. 20 (2013) 473–484. doi:10.1089/ten.tec.2013.0335.

[138] A. Deiwick, V. Coger, A. Schambach, M. Gruene, S. Schlie, D. Zychlinski, B. Chichkov, K. Reimers, P.M. Vogt, L. Koch, S. Michael, Skin tissue generation by laser cell printing, Biotechnol. Bioeng. 109 (2012) 1855–1863. doi:10.1002/bit.24455.

[139] S. Moon, S.K. Hasan, Y.S. Song, F. Xu, H.O. Keles, F. Manzur, S. Mikkilineni, J.W. Hong, J. Nagatomi, E. Haeggstrom, A. Khademhosseini, U. Demirci, Layer by layer three-dimensional tissue epitaxy by cell-laden hydrogel droplets., Tissue Eng. Part C. Methods. 16 (2010) 157–66. doi:10.1089/ten.tec.2009.0179.

[140] H.J. Lee, Y.B. Kim, S.H. Ahn, J.S. Lee, C.H. Jang, H. Yoon, W. Chun, G.H. Kim, A new approach for fabricating collagen/ecm-based bioinks using preosteoblasts and human adipose stem cells, Adv. Healthc. Mater. 4 (2015) 1359–1368. doi:10.1002/adhm.201500193.

[141] S. Das, F. Pati, Y.J. Choi, G. Rijal, J.H. Shim, S.W. Kim, A.R. Ray, D.W. Cho, S. Ghosh, Bioprintable, cell-laden silk fibroin-gelatin hydrogel supporting multilineage differentiation of stem cells for fabrication of three-dimensional tissue constructs, Acta Biomater. 11 (2015) 233–246. doi:10.1016/j.actbio.2014.09.023.

[142] R. Levato, W.R. Webb, I.A. Otto, A. Mensinga, Y. Zhang, M. van Rijen, R. van Weeren, I.M. Khan, J. Malda, The bio in the ink: cartilage regeneration with bioprintable hydrogels and articular cartilage-derived progenitor cells, Acta Biomater. 61 (2017) 41–53. doi:10.1016/j.actbio.2017.08.005.

[143] A.C. Daly, S.E. Critchley, E.M. Rencsok, D.J. Kelly, A comparison of different

bioinks for 3D bioprinting of fibrocartilage and hyaline cartilage, Biofabrication. 8 (2016) 1–10. doi:10.1088/1758-5090/8/4/045002.

[144] Q. Feng, R. Steffen, B. Diehl-Seifert, H.C. Schröder, M. Neufurth, X. Wang, W.E.G. Müller, T. Ziebart, S. Wang, Engineering a morphogenetically active hydrogel for bioprinting of bioartificial tissue derived from human osteoblast-like SaOS-2 cells, Biomaterials. 35 (2014) 8810–8819. doi:10.1016/j.biomaterials.2014.07.002.

[145] M.R. Dokmeci, W.A. Araujo, N.S. Bhise, N.E. Vrana, A.M. Ghaemmaghami, P. Zorlutuna, V. Manoharan, L.E. Bertassoni, J.C. Cardoso, A. Khademhosseini, A.L. Cristino, Direct-write bioprinting of cell-laden methacrylated gelatin hydrogels, Biofabrication. 6 (2014) 024105. doi:10.1088/1758-5082/6/2/024105.

[146] M. Nakamura, S. Iwanaga, C. Henmi, K. Arai, Y. Nishiyama, Biomatrices and biomaterials for future developments of bioprinting and biofabrication, Biofabrication. 2 (2010). doi:10.1088/1758-5082/2/1/014110.

[147] S. Jockenhoevel, A. Deiwick, M. Wilhelmi, S. Schlie, M. Gruene, A. Haverich, L. Koch, S. Diamantouros, C. Hess, B. Chichkov, M. Pflaum, Laser printing of three-dimensional multicellular arrays for studies of cell–cell and cell–environment interactions, Tissue Eng. Part C Methods. 17 (2011) 973–982. doi:10.1089/ten.tec.2011.0185.

[148] F. Xu, B.P. Sridharan, N.G. Durmus, S.Q. Wang, A.S. Yavuz, U.A. Gurkan, U. Demirci, Living bacterial sacrificial porogens to engineer decellularized porous scaffolds, PLoS One. 6 (2011). doi:10.1371/journal.pone.0019344.

[149] R. Gorkin, M. in het Panhuis, M. Romero-Ortega, G.G. Wallace, E.M. Stewart, B.C. Thompson, L. Stevens, R. Lozano, K.J. Gilmore, 3D printing of layered brain-like structures using peptide modified gellan gum substrates, Biomaterials. 67 (2015) 264–273. doi:10.1016/j.biomaterials.2015.07.022.

[150] J.Y. Park, J.C. Choi, J.H. Shim, J.S. Lee, H. Park, S.W. Kim, J. Doh, D.W. Cho, A comparative study on collagen type I and hyaluronic acid dependent cell behavior for osteochondral tissue bioprinting, Biofabrication. 6 (2014). doi:10.1088/1758-5082/6/3/035004.

[151] M. Kesti, M. Müller, J. Becher, M. Schnabelrauch, M. D'Este, D. Eglin, M. Zenobi-

Wong, A versatile bioink for three-dimensional printing of cellular scaffolds based on thermally and photo-triggered tandem gelation, Acta Biomater. 11 (2015) 162–172. doi:10.1016/j.actbio.2014.09.033.

[152] G.D. Prestwich, A. Skardal, L. McCoard, S. Oottamasathien, J. Zhang, X. Xu, Photocrosslinkable hyaluronan-gelatin hydrogels for two-step bioprinting, Tissue Eng. Part A. 16 (2010) 2675–2685. doi:10.1089/ten.tea.2009.0798.

[153] P.A. Levett, D.W. Hutmacher, J. Malda, M.W. Pot, W. Schuurman, T.J. Klein, F.P.W. Melchels, P.R. van Weeren, W.J.A. Dhert, Gelatin-methacrylamide hydrogels as potential biomaterials for fabrication of tissue-engineered cartilage constructs, Macromol. Biosci. 13 (2013) 551–561. doi:10.1002/mabi.201200471.

[154] B. Duan, E. Kapetanovic, L.A. Hockaday, J.T. Butcher, Three-dimensional printed trileaflet valve conduits using biological hydrogels and human valve interstitial cells, Acta Biomater. 10 (2014) 1836–1846. doi:10.1016/j.actbio.2013.12.005.

[155] F. Pati, J. Jang, D.H. Ha, S. Won Kim, J.W. Rhie, J.H. Shim, D.H. Kim, D.W. Cho, Printing three-dimensional tissue analogues with decellularized extracellular matrix bioink, Nat. Commun. 5 (2014) 1–11. doi:10.1038/ncomms4935.

[156] A. Skardal, M. Devarasetty, H.W. Kang, I. Mead, C. Bishop, T. Shupe, S.J. Lee, J. Jackson, J. Yoo, S. Soker, A. Atala, A hydrogel bioink toolkit for mimicking native tissue biochemical and mechanical properties in bioprinted tissue constructs, Acta Biomater. 25 (2015) 24–34. doi:10.1016/j.actbio.2015.07.030.

[157] M.T. Poldervaart, H. Gremmels, K. Van Deventer, J.O. Fledderus, F.C. Öner, M.C. Verhaar, W.J.A. Dhert, J. Alblas, Prolonged presence of VEGF promotes vascularization in 3D bioprinted scaffolds with defined architecture, J. Control. Release. 184 (2014) 58–66. doi:10.1016/j.jconrel.2014.04.007.

[158] L. Horvath, Y. Umehara, C. Jud, F. Blank, A. Petri-Fink, B. Rothen-Rutishauser, Engineering an in vitro air-blood barrier by 3D bioprinting, Sci. Rep. 5 (2015). doi:10.1038/srep07974.

[159] J. van der Stok, F.C. Öner, W.J.A. Dhert, H. Weinans, H. Wang, M.T. Poldervaart, J. Alblas, S.C.G. Leeuwenburgh, Sustained release of BMP-2 in bioprinted alginate for osteogenicity in mice and rats, PLoS One. 8 (2013) e72610.

doi:10.1371/journal.pone.0072610.

[160] G. Gao, A.F. Schilling, T. Yonezawa, J. Wang, G. Dai, X. Cui, Bioactive nanoparticles stimulate bone tissue formation in bioprinted three-dimensional scaffold and human mesenchymal stem cells, Biotechnol. J. 9 (2014) 1304–1311. doi:10.1002/biot.201400305.

[161] S. Wüst, M.E. Godla, R. Müller, S. Hofmann, Tunable hydrogel composite with two-step processing in combination with innovative hardware upgrade for cell-based three-dimensional bioprinting, Acta Biomater. 10 (2014) 630–640. doi:10.1016/j.actbio.2013.10.016.

[162] S. Catros, B. Desbat, B. Pippenger, E. Lebraud, J. Amédée, F. Guillemot, M. Remy, B. Guillotin, R. Bareille, J.-C. Fricain, Laser-assisted bioprinting for creating on-demand patterns of human osteoprogenitor cells and nano-hydroxyapatite, Biofabrication. 3 (2011) 025001. doi:10.1088/1758-5082/3/2/025001.

[163] P.G. Campbell, G.E. DeCesare, J. Huard, E.L. Lensie, A. Usas, L.E. Weiss, G.M. Cooper, E.D. Miller, M.R. Bykowski, J.E. Losee, Inkjet-based biopatterning of bone morphogenetic protein-2 to spatially control calvarial bone formation, Tissue Eng. Part A. 16 (2009) 1749–1759. doi:10.1089/ten.tea.2009.0650.

[164] L. Walker, G. Fisher, L. Weiss, J. Phillippi, E. Miller, P. Campbell, Inkjet printing of growth factor concentration gradients and combinatorial arrays immobilized on biologically-relevant substrates, Comb. Chem. High Throughput Screen. 12 (2009) 604–618. doi:10.2174/138620709788681907.

[165] K. Dubbin, A. Tabet, S.C. Heilshorn, Quantitative criteria to benchmark new and existing bio-inks for cell compatibility, Biofabrication. 9 (2017) 044102. doi:10.1088/1758-5090/aa869f.

[166] A.L. Rutz, K.E. Hyland, A.E. Jakus, W.R. Burghardt, R.N. Shah, A multimaterial bioink method for 3D printing tunable, cell-compatible hydrogels, Adv. Mater. 27 (2015) 1607–1614. doi:10.1002/adma.201405076.

[167] S. Hong, D. Sycks, H.F. a. Chan, S. Lin, G.P. Lopez, F. Guilak, K.W. Leong, X. Zhao, 3D printing: 3D printing of highly stretchable and tough hydrogels into complex, cellularized structures, Adv. Mater. 27 (2015) 4034. doi:10.1002/adma.201570182.

[168] A. Skardal, J. Zhang, G.D. Prestwich, Bioprinting vessel-like constructs using hyaluronan hydrogels crosslinked with tetrahedral polyethylene glycol tetracrylates, Biomaterials. 31 (2010) 6173–6181. doi:10.1016/j.biomaterials.2010.04.045.

[169] S. Xin, D. Chimene, J.E. Garza, A.K. Gaharwar, D.L. Alge, Clickable PEG hydrogel microspheres as building blocks for 3D bioprinting, Biomater. Sci. 7 (2019) 1179–1187. doi:10.1039/c8bm01286e.

[170] J. Kundu, J.-H. Shim, J. Jang, S.-W. Kim, D.-W. Cho, An additive manufacturing-based PCL-alginate-chondrocyte bioprinted scaffold for cartilage tissue engineering, J. Tissue Eng. Regen. Med. 9 (2015) 1286–1297. doi:10.1002/term.1682.

[171] P. Liu, H. Shen, Y. Zhi, J. Si, J. Shi, L. Guo, S.G. Shen, 3D bioprinting and in vitro study of bilayered membranous construct with human cells-laden alginate/gelatin composite hydrogels, Colloids Surfaces B Biointerfaces. 181 (2019) 1026–1034. doi:10.1016/j.colsurfb.2019.06.069.

[172] S. Freeman, R. Ramos, P. Alexis Chando, L. Zhou, K. Reeser, S. Jin, P. Soman, K. Ye, A bioink blend for rotary 3D bioprinting tissue engineered small-diameter vascular constructs, Acta Biomater. (2019) 1–13. doi:10.1016/j.actbio.2019.06.052.

[173] X. Li, Y. Wang, Z. Wang, Y. Qi, L. Li, P. Zhang, X. Chen, Y. Huang, Composite PLA/PEG/nHA/Dexamethasone scaffold prepared by 3D printing for bone regeneration, Macromol. Biosci. 18 (2018) 1–11. doi:10.1002/mabi.201800068.

[174] Y. Wu, Z.Y. (William) Lin, A.C. Wenger, K.C. Tam, X. (Shirley) Tang, 3D bioprinting of liver-mimetic construct with alginate/cellulose nanocrystal hybrid bioink, Bioprinting. 9 (2018) 1–6. doi:10.1016/j.bprint.2017.12.001.

[175] Z.M. Jessop, A. Al-Sabah, N. Gao, S. Kyle, B. Thomas, N. Badiei, K. Hawkins, I.S. Whitaker, Printability of pulp derived crystal, fibril and blend nanocellulose-alginate bioinks for extrusion 3D bioprinting, Biofabrication. 11 (2019) 045006. doi:10.1088/1758-5090/ab0631.

[176] N. Law, B. Doney, H. Glover, Y. Qin, Z.M. Aman, T.B. Sercombe, L.J. Liew, R.J. Dilley, B.J. Doyle, Characterisation of hyaluronic acid methylcellulose hydrogels for 3D bioprinting, J. Mech. Behav. Biomed. Mater. 77 (2018) 389–399. doi:10.1016/j.jmbbm.2017.09.031.

[177] H. Kwak, S. Shin, H. Lee, J. Hyun, Formation of a keratin layer with silk fibroin-polyethylene glycol composite hydrogel fabricated by digital light processing 3D printing, J. Ind. Eng. Chem. 72 (2019) 232–240. doi:10.1016/j.jiec.2018.12.023.

[178] S. Chen, Y. Shi, Y. Luo, J. Ma, Layer-by-layer coated porous 3D printed hydroxyapatite composite scaffolds for controlled drug delivery, Colloids Surfaces B Biointerfaces. 179 (2019) 121–127. doi:10.1016/j.colsurfb.2019.03.063.

[179] G. Cidonio, C.R. Alcala-Orozco, K.S. Lim, M. Glinka, I. Mutreja, Y.-H. Kim, J.I. Dawson, T.B.F. Woodfield, R.O.C. Oreffo, Osteogenic and angiogenic tissue formation in high fidelity nanocomposite laponite-gelatin bioinks, Biofabrication. 11 (2019) 035027. doi:10.1088/1758-5090/ab19fd.

[180] B. Raphael, T. Khalil, V.L. Workman, A. Smith, C.P. Brown, C. Streuli, A. Saiani, M. Domingos, 3D cell bioprinting of self-assembling peptide-based hydrogels, Mater. Lett. 190 (2017) 103–106. doi:10.1016/j.matlet.2016.12.127.

[181] J. Li, R. Xing, S. Bai, X. Yan, Recent advances of self-assembling peptide-based hydrogels for biomedical applications, Soft Matter. 15 (2019) 1704–1715. doi:10.1039/c8sm02573h.

[182] C. Cofiño, S. Perez☐Amodio, C.E. Semino, E. Engel, M.A. Mateos☐Timoneda, Development of a self☐assembled peptide/methylcellulose☐based bioink for 3D bioprinting, Macromol. Mater. Eng. 1900353 (2019) 1900353. doi:10.1002/mame.201900353.

[183] A. K Das, Printable self-assembled peptide bio-inks: Promising future applications in nanomedicine, Arch. Nanomedicine Open Access J. 1 (2018). doi:10.32474/anoaj.2018.01.000113.

[184] J. Chen, X. Zou, Self-assemble peptide biomaterials and their biomedical applications, Bioact. Mater. 4 (2019) 120–131. doi:10.1016/j.bioactmat.2019.01.002.

[185] M. Ni, S. Zhuo, Applications of self-assembling ultrashort peptides in bionanotechnology, RSC Adv. 9 (2019) 844–852. doi:10.1039/c8ra07533f.

[186] Y. Loo, A. Lakshmanan, M. Ni, L.L. Toh, S. Wang, C.A.E. Hauser, Peptide bioink: self-assembling nanofibrous scaffolds for three-dimensional organotypic cultures, Nano Lett. 15 (2015) 6919–6925. doi:10.1021/acs.nanolett.5b02859.

[187] W. Arab, S. Rauf, O. Al-Harbi, C.A.E. Hauser, Novel ultrashort self-assembling peptide bioinks for 3D culture of muscle myoblast cells, Int. J. Bioprinting. 4 (2018) 1–13. doi:10.18063/ijb.v4i2.129.

[188] Preparation and applications of RGD conjugated polysaccharide bioinks with or without fibrin for 3D bioprinting of human skin with novel printing head for use as model for testing cosmetics and for transplantation, (2017). https://patents.google.com/patent/wo2017210663a1/en (accessed September 19, 2019).

[189] N. Cubo, M. Garcia, J.F. del Cañizo, D. Velasco, J.L. Jorcano, 3D bioprinting of functional human skin: production and *in vivo* analysis, Biofabrication. 9 (2016) 015006. doi:10.1088/1758-5090/9/1/015006.

[190] S. Vijayavenkataraman, W.F. Lu, J.Y.H. Fuh, 3D bioprinting of skin: A state-of-the-art review on modelling, materials, and processes, Biofabrication. 8 (2016). doi:10.1088/1758-5090/8/3/032001.

[191] J.-H. Lee, V.K. Lee, K. Edminster, J.-K. Park, J.C. Debasitis, W. Lee, K. Fischer, S.-S. Yoo, Multi-layered culture of human skin fibroblasts and keratinocytes through three-dimensional freeform fabrication, Biomaterials. 30 (2008) 1587–1595. doi:10.1016/j.biomaterials.2008.12.009.

[192] R. Gaebel, H. Sorg, K. Reimers, P.M. Vogt, S. Schlie, M. Gruene, G. Steinhoff, B. Polchow, S. Stoelting, L. Koch, N. Ma, B. Chichkov, S. Kuhn, Laser printing of skin cells and human stem cells, Tissue Eng. Part C Methods. 16 (2009) 847–854. doi:10.1089/ten.tec.2009.0397.

[193] W.L. Ng, W.Y. Yeong, M.W. Naing, Polyelectrolyte gelatin-chitosan hydrogel optimized for 3D bioprinting in skin tissue engineering, Int. J. Bioprinting. 2 (2016). doi:10.18063/ijb.2016.01.009.

[194] B.S. Kim, J.-S. Lee, G. Gao, D.-W. Cho, Direct 3D cell-printing of human skin with functional transwell system, Biofabrication. 9 (2017) 025034. doi:10.1088/1758-5090/aa71c8.

[195] Q. Wang, S. Xiong, H. Sun, H. Ouyang, B.C. Heng, P. Lu, V. Bunpetch, X. Zhang, Y. Wu, S. Zhang, A gelatin-sulfonated silk composite scaffold based on 3D printing technology enhances skin regeneration by stimulating epidermal growth and dermal

neovascularization, Sci. Rep. 7 (2017) 1–12. doi:10.1038/s41598-017-04149-y.

[196] Y. Shi, T.L. Xing, H.B. Zhang, R.X. Yin, S.M. Yang, J. Wei, W.J. Zhang, Tyrosinase-doped bioink for 3D bioprinting of living skin constructs, Biomed. Mater. 13 (2018) 035008. doi:10.1088/1748-605x/aaa5b6.

[197] M. Albanna, K.W. Binder, S. V. Murphy, J. Kim, S.A. Qasem, W. Zhao, J. Tan, I.B. El-Amin, D.D. Dice, J. Marco, J. Green, T. Xu, A. Skardal, J.H. Holmes, J.D. Jackson, A. Atala, J.J. Yoo, In situ bioprinting of autologous skin cells accelerates wound healing of extensive excisional full-thickness wounds, Sci. Rep. 9 (2019) 1–15. doi:10.1038/s41598-018-38366-w.

[198] S.H. Choi, H. Kim, H.-J. Park, M.N. Park, P.-J. Kim, S.J. Na, S.-W. Kim, S.-M. Kwon, D.-W. Cho, S.W. Kim, J.Y. Park, J. Jang, H.J. Kim, S.H. Park, 3D printed complex tissue construct using stem cell-laden decellularized extracellular matrix bioinks for cardiac repair, Biomaterials. 112 (2016) 264–274. doi:10.1016/j.biomaterials.2016.10.026.

[199] Y.S. Zhang, A. Arneri, S. Bersini, S.R. Shin, K. Zhu, Z. Goli-Malekabadi, J. Aleman, C. Colosi, F. Busignani, V. Dell'Erba, C. Bishop, T. Shupe, D. Demarchi, M. Moretti, M. Rasponi, M.R. Dokmeci, A. Atala, A. Khademhosseini, Bioprinting 3D microfibrous scaffolds for engineering endothelialized myocardium and heart-on-a-chip, Biomaterials. 110 (2016) 45–59. doi:10.1016/j.biomaterials.2016.09.003.

[200] T. Boland, M. Aho, M. Zile, T. Xu, C. Baicu, Fabrication and characterization of bio-engineered cardiac pseudo tissues, Biofabrication. 1 (2009) 035001. doi:10.1088/1758-5082/1/3/035001.

[201] J. Liu, W. Wang, G. Steinhoff, R. Gaebel, A. Toelk, N. Ma, F. Wang, P. Mark, W. Li, M. Gruene, L. Koch, J. Guan, B. Chichkov, C. Klopsch, Patterning human stem cells and endothelial cells with laser printing for cardiac regeneration, Biomaterials. 32 (2011) 9218–9230. doi:10.1016/j.biomaterials.2011.08.071.

[202] R. Gaetani, P.A. Doevendans, C.H.G. Metz, J. Alblas, E. Messina, A. Giacomello, J.P.G. Sluijter, Cardiac tissue engineering using tissue printing technology and human cardiac progenitor cells, Biomaterials. 33 (2012) 1782–1790. doi:10.1016/j.biomaterials.2011.11.003.

[203] F. Maiullari, M. Costantini, M. Milan, V. Pace, M. Chirivì, S. Maiullari, A. Rainer, D. Baci, H.E.S. Marei, D. Seliktar, C. Gargioli, C. Bearzi, R. Rizzi, A multi-cellular 3D bioprinting approach for vascularized heart tissue engineering based on HUVECs and iPSC-derived cardiomyocytes, Sci. Rep. 8 (2018) 1–15. doi:10.1038/s41598-018-31848-x.

[204] N. Noor, A. Shapira, R. Edri, I. Gal, L. Wertheim, T. Dvir, 3D printing of personalized thick and perfusable cardiac patches and hearts, Adv. Sci. 1900344 (2019) 1900344. doi:10.1002/advs.201900344.

[205] S.K. Nandi, B.B. Mandal, Y.P. Singh, B.K. Bhunia, J.C. Moses, Hierarchically structured seamless silk scaffolds for osteochondral interface tissue engineering, J. Mater. Chem. B. 6 (2018) 5671–5688. doi:10.1039/c8tb01344f.

[206] J. Li, L. He, C. Zhou, Y. Zhou, Y. Bai, F.Y. Lee, J.J. Mao, 3D printing for regenerative medicine: From bench to bedside, MRS Bull. 40 (2015) 145–154. doi:10.1557/mrs.2015.5.

[207] J.W. Lee, K.S. Kang, S.H. Lee, J.Y. Kim, B.K. Lee, D.W. Cho, Bone regeneration using a microstereolithography-produced customized poly(propylene fumarate)/diethyl fumarate photopolymer 3D scaffold incorporating BMP-2 loaded PLGA microspheres, Biomaterials. 32 (2011) 744–752. doi:10.1016/j.biomaterials.2010.09.035.

[208] S. Tarafder, V.K. Balla, N.M. Davies, A. Bandyopadhyay, S. Bose, Microwave-sintered 3D printed tricalcium phosphate scaffolds for bone tissue engineering, J. Tissue Eng. Regen. Med. 7 (2013) 631–641. doi:10.1002/term.555.

[209] S. Tarafder, N.M. Davies, A. Bandyopadhyay, S. Bose, 3D printed tricalcium phosphate bone tissue engineering scaffolds: Effect of SrO and MgO doping on in vivo osteogenesis in a rat distal femoral defect model, Biomater. Sci. 1 (2013) 1250–1259. doi:10.1039/c3bm60132c.

[210] G. Fielding, S. Bose, SiO2and ZnO dopants in three-dimensionally printed tricalcium phosphate bone tissue engineering scaffolds enhance osteogenesis and angiogenesis in vivo, Acta Biomater. 9 (2013) 9137–9148. doi:10.1016/j.actbio.2013.07.009.

[211] J. Jensen, J.H.D. Rölfing, D.Q. Svend Le, A.A. Kristiansen, J.V. Nygaard, L.B. Hokland, M. Bendtsen, M. Kassem, H. Lysdahl, C.E. Bünger, Surface-modified

functionalized polycaprolactone scaffolds for bone repair: *In vitro* and *in vivo* experiments, J. Biomed. Mater. Res. Part A. 102 (2014) 2993–3003. doi:10.1002/jbm.a.34970.

[212] J.P. Temple, D.L. Hutton, B.P. Hung, P.Y. Huri, C.A. Cook, R. Kondragunta, X. Jia, W.L. Grayson, Engineering anatomically shaped vascularized bone grafts with hASCs and 3D-printed PCL scaffolds, J. Biomed. Mater. Res. - Part A. 102 (2014) 4317–4325. doi:10.1002/jbm.a.35107.

[213] J.P. Kelly, H.A. Awad, D. Olvera, O.A. Graeve, J.A. Inzana, S.L. Kates, E.M. Schwarz, S.M. Fuller, 3D printing of composite calcium phosphate and collagen scaffolds for bone regeneration, Biomaterials. 35 (2014) 4026–4034. doi:10.1016/j.biomaterials.2014.01.064.

[214] K. Al-Abedalla, E. Lopez-Cabarcos, D.C. Bassett, M.H. Alkhraisat, J.E. Barralet, U. Gbureck, J. Torres, F. Tamimi, Osseointegration of dental implants in 3D-printed synthetic onlay grafts customized according to bone metabolic activity in recipient site, Biomaterials. 35 (2014) 5436–5445. doi:10.1016/j.biomaterials.2014.03.050.

[215] B. Byambaa, N. Annabi, K. Yue, G. Trujillo-de Santiago, M.M. Alvarez, W. Jia, M. Kazemzadeh-Narbat, S.R. Shin, A. Tamayol, A. Khademhosseini, Bioprinted osteogenic and vasculogenic patterns for engineering 3D bone tissue, Adv. Healthc. Mater. 6 (2017) 1–15. doi:10.1002/adhm.201700015.

[216] A novel technique for tissue engineering periosteum using three- dimensional bioprinting presenter : Brandon Alba , BA Co-Authors : Pooja Swami , MS ; Neil Affiliation : Donald and Barbara Zucker School of Medicine at Hofstra / Northwell , Harnessing Mech, (2018) 2018. doi:10.1016/j.actbio.2014.06.034.a.

[217] M. Ojansivu, A. Rashad, A.E. Ahlinder, J. Massera, A. Mishra, K. Syverud, A. Finne-Wistrand, S. Miettinen, K. Mustafa, Wood-based nanocellulose and bioactive glass modified gelatin-alginate bioinks for 3D bioprinting of bone cells, Biofabrication. (2019). doi:10.1088/1758-5090/ab0692.

[218] C. Sharma, S. Gautam, A.K. Dinda, N.C. Mishra, Cartilage tissue engineering: Current scenario and challenges, Adv. Mater. Lett. 2 (2011) 90–99. doi:10.5185/amlett.2011.1211.

[219] C.H. Lee, N.W. Marion, S. Hollister, J.J. Mao, Tissue formation and vascularization in anatomically shaped human joint condyle ectopically in vivo , Tissue Eng. Part A. 15 (2009) 3923–3930. doi:10.1089/ten.tea.2008.0653.

[220] J.J. Mao, C.H. Lee, H. Yao, A. Mendelson, J.L. Cook, E.K. Moioli, Regeneration of the articular surface of the rabbit synovial joint by cell homing: a proof of concept study, Lancet. 376 (2010) 440–448. doi:10.1016/s0140-6736(10)60668-x.

[221] C.D. O'Connell, C. Di Bella, F. Thompson, C. Augustine, S. Beirne, R. Cornock, C.J. Richards, J. Chung, S. Gambhir, Z. Yue, J. Bourke, B. Zhang, A. Taylor, A. Quigley, R. Kapsa, P. Choong, G.G. Wallace, Development of the biopen: A handheld device for surgical printing of adipose stem cells at a chondral wound site, Biofabrication. 8 (2016) 0. doi:10.1088/1758-5090/8/1/015019.

[222] S. Duchi, C. Onofrillo, C.D. O'Connell, R. Blanchard, C. Augustine, A.F. Quigley, R.M.I. Kapsa, P. Pivonka, G. Wallace, C. Di Bella, P.F.M. Choong, Handheld co-axial bioprinting: Application to in situ surgical cartilage repair, Sci. Rep. 7 (2017) 1–12. doi:10.1038/s41598-017-05699-x.

[223] C. Di Bella, S. Duchi, C.D. O'Connell, R. Blanchard, C. Augustine, Z. Yue, F. Thompson, C. Richards, S. Beirne, C. Onofrillo, S.H. Bauquier, S.D. Ryan, P. Pivonka, G.G. Wallace, P.F. Choong, *In situ* handheld three-dimensional bioprinting for cartilage regeneration, J. Tissue Eng. Regen. Med. 12 (2018) 611–621. doi:10.1002/term.2476.

[224] J. Li, L. Wang, Q. Yao, C. Deng, C. Wu, L. Chen, J. Chang, 3D printing of a lithium-calcium-silicate crystal bioscaffold with dual bioactivities for osteochondral interface reconstruction, Elsevier Ltd, 2018. doi:10.1016/j.biomaterials.2018.04.005.

[225] S. Rathan, L. Dejob, R. Schipani, B. Haffner, M.E. Möbius, D.J. Kelly, Fiber reinforced cartilage ECM functionalized bioinks for functional cartilage tissue engineering, Adv. Healthc. Mater. 1801501 (2019) 1–11. doi:10.1002/adhm.201801501.

[226] S.J. Yu, A concise review of updated guidelines regarding the management of hepatocellular carcinoma around the world: 2010-2016., Clin. Mol. Hepatol. 22 (2016) 7–17. doi:10.3350/cmh.2016.22.1.7.

[227] I. V. Kholodenko, K.N. Yarygin, Cellular mechanisms of liver regeneration and cell-based therapies of liver diseases, Biomed Res. Int. 2017 (2017) 1–17. doi:10.1155/2017/8910821.

[228] A. Tayyeb, F. Azam, R. Nisar, R. Nawaz, U. Qaisar, G. Ali, Regenerative medicine in liver cirrhosis: Promises and pitfalls, in: liver cirrhosis - updat. curr. challenges, InTech, 2017. doi:10.5772/intechopen.68729.

[229] Y. Kim, K. Kang, J. Jeong, S.S. Paik, J.S. Kim, S.A. Park, W.D. Kim, J. Park, D. Choi, Three-dimensional (3D) printing of mouse primary hepatocytes to generate 3D hepatic structure, Ann. Surg. Treat. Res. 92 (2017) 67–72. doi:10.4174/astr.2017.92.2.67.

[230] W. Shu, A. Courtney, C. Fyfe, D.-J. Cornelissen, A. Faulkner-Jones, J. Gardner, J. King, Bioprinting of human pluripotent stem cells and their directed differentiation into hepatocyte-like cells for the generation of mini-livers in 3D, Biofabrication. 7 (2015) 044102. doi:10.1088/1758-5090/7/4/044102.

[231] J.W. Lee, Y.J. Choi, W.J. Yong, F. Pati, J.H. Shim, K.S. Kang, I.H. Kang, J. Park, D.W. Cho, Development of a 3D cell printed construct considering angiogenesis for liver tissue engineering, Biofabrication. 8 (2016) 15007. doi:10.1088/1758-5090/8/1/015007.

[232] M. Lei, X. Wang, Biodegradable polymers and stem cells for bioprinting, Molecules. 21 (2016) 539. doi:10.3390/molecules21050539.

[233] 3D printed lungs – The future of treating asbestos illnesses? | Mesothelioma.net, (2019). https://mesothelioma.net/3d-printed-lungs-future-treating-asbestos-illnesses/ (accessed April 2, 2019).

[234] A. Mammoto, D. Huh, B.D. Matthews, D.E. Ingber, H.Y. Hsin, M. Montoya-Zavala, Reconstituting organ-level lung functions on a chip, Science (80-.). 328 (2010) 1662–1668. doi:10.1126/science.1188302.

[235] H.C. Ott, B. Clippinger, C. Conrad, C. Schuetz, I. Pomerantseva, L. Ikonomou, D. Kotton, J.P. Vacanti, Regeneration and orthotopic transplantation of a bioartificial lung, Nat. Med. 16 (2010) 927–933. doi:10.1038/nm.2193.

[236] E.J. Lee, Z.W. Zhuang, T.H. Petersen, L. Zhao, K. Gavrilov, E. Herzog, E.A. Calle, T. Yi, M.B. Raredon, L. Gui, C. Breuer, L.E. Niklason, Tissue-engineered lungs for in

vivo implantation, Science. 329 (2010) 538–541. doi:10.1126/science.1189345.

[237] Y.B. Lee, S. Polio, W. Lee, G. Dai, L. Menon, R.S. Carroll, S.S. Yoo, Bio-printing of collagen and VEGF-releasing fibrin gel scaffolds for neural stem cell culture, Exp. Neurol. 223 (2010) 645–652. doi:10.1016/j.expneurol.2010.02.014.

[238] F.Y. Hsieh, H.H. Lin, S. hui Hsu, 3D bioprinting of neural stem cell-laden thermoresponsive biodegradable polyurethane hydrogel and potential in central nervous system repair, Biomaterials. 71 (2015) 48–57. doi:10.1016/j.biomaterials.2015.08.028.

[239] Q. Gu, E. Tomaskovic-Crook, R. Lozano, Y. Chen, R.M. Kapsa, Q. Zhou, G.G. Wallace, J.M. Crook, Functional 3D neural mini-tissues from printed gel-based bioink and human neural stem cells, Adv. Healthc. Mater. 5 (2016) 1429–1438. doi:10.1002/adhm.201600095.

[240] D.N. Heo, S.-J. Lee, R. Timsina, X. Qiu, N.J. Castro, L.G. Zhang, Development of 3D printable conductive hydrogel with crystallized PEDOT:PSS for neural tissue engineering, Mater. Sci. Eng. C. 99 (2019) 582–590. doi:10.1016/j.msec.2019.02.008.

[241] A.P. Haring, E.G. Thompson, Y. Tong, S. Laheri, E. Cesewski, H. Sontheimer, B.N. Johnson, Process- and bio-inspired hydrogels for 3D bioprinting of soft free-standing neural and glial tissues, Biofabrication. 11 (2019) 025009. doi:10.1088/1758-5090/ab02c9.

[242] L. Ning, N. Zhu, F. Mohabatpour, M.D. Sarker, D.J. Schreyer, X. Chen, Bioprinting schwann cell-laden scaffolds from low-viscosity hydrogel compositions, J. Mater. Chem. B. 7 (2019) 4538–4551. doi:10.1039/c9tb00669a.

[243] F.W. Pagliuca, J.R. Millman, M. Gu, M. Segel, A. Van Dervort, J.H. Ryu, Q.P. Peterson, D. Greiner, D.A. Melton, Resource generation of functional human pancreatic β cells in vitro, (2014). doi:10.1016/j.cell.2014.09.040.

[244] A. Akkouch, Y. Yu, I.T. Ozbolat, Microfabrication of scaffold-free tissue strands for three-dimensional tissue engineering, Biofabrication. 7 (2015) 031002. doi:10.1088/1758-5090/7/3/031002.

[245] H. Yi, Y. Choi, K. Shin, J. Min, R. Gupta, M. Nyeo, I. Kyong, C. Mi, S. Cheol, D. Cho, A 3D-printed local drug delivery patch for pancreatic cancer growth suppression,

J. Control. Release. 238 (2016) 231–241. doi:10.1016/j.jconrel.2016.06.015.

[246] J. Kim, I.K. Shim, D.G. Hwang, Y.N. Lee, M. Kim, H. Kim, S. Kim, S. Lee, S.C. Kim, D. Cho, J. Jang, 3D cell printing of islet-laden pancreatic tissue-derived extracellular matrix bioink constructs for enhancing pancreatic functions, (2019). doi:10.1039/c8tb02787k.

[247] J.E. Snyder, Q. Hamid, C. Wang, R. Chang, K. Emami, H. Wu, W. Sun, Bioprinting cell-laden matrigel for radioprotection study of liver by pro-drug conversion in a dual-tissue microfluidic chip, Biofabrication. 3 (2011) 034112. doi:10.1088/1758-5082/3/3/034112.

[248] K. Jakab, C. Norotte, F. Marga, K. Murphy, G. Vunjak-Novakovic, G. Forgacs, Tissue engineering by self-assembly and bio-printing of living cells, Biofabrication. 2 (2010) 022001. doi:10.1088/1758-5082/2/2/022001.

[249] A. Sachdev, R. Raj, I. Matai, 3D printing for in vitro and in vivo disease models, Elsevier, 2019. doi:10.1016/b978-0-12-815890-6.00007-4.

[250] T. Hasan, U. Demirci, I. Rizvi, F. Xu, S. Moon, J. Celli, A three-dimensional in vitro ovarian cancer coculture model using a high-throughput cell patterning platform, Biotechnol. J. 6 (2011) 204–212. doi:10.1002/biot.201000340.

[251] T. Zhang, S. Cheng, K. Zhang, L. Ouyang, R. Yao, Y. Zhao, H. Ding, W. Sun, Three-dimensional printing of hela cells for cervical tumor model in vitro , Biofabrication. 6 (2014) 035001. doi:10.1088/1758-5082/6/3/035001.

[252] P.R. Baraniak, T.C. McDevitt, Scaffold-free culture of mesenchymal stem cell spheroids in suspension preserves multilineage potential, Cell Tissue Res. 347 (2012) 701–711. doi:10.1007/s00441-011-1215-5.

[253] Y. Ma, F. Xu, G. Huang, J. Liu, K. Ling, T. Lu, X. Zhang, Bioprinting-based high-throughput fabrication of three-dimensional MCF-7 human breast cancer cellular spheroids, Engineering. 1 (2015) 269–274. doi:10.15302/j-eng-2015062.

[254] X. Zhou, W. Zhu, M. Nowicki, S. Miao, H. Cui, B. Holmes, R.I. Glazer, L.G. Zhang, 3D bioprinting a cell-laden bone matrix for breast cancer metastasis study, ACS Appl. Mater. Interfaces. 8 (2016) 30017–30026. doi:10.1021/acsami.6b10673.

[255] B.T. Vinson, T.B. Phamduy, J. Shipman, B. Riggs, A.L. Strong, S.C. Sklare, W.L.

Murfee, M.E. Burow, B.A. Bunnell, Y. Huang, D.B. Chrisey, Laser direct-write based fabrication of a spatially-defined, biomimetic construct as a potential model for breast cancer cell invasion into adipose tissue, Biofabrication. 9 (2017). doi:10.1088/1758-5090/aa6bad.

[256] Y.S. Zhang, M. Duchamp, L.W. Ellisen, M. Moses, A. Khademhosseini, Abstract 4828: Recapitulating mammary ductal carcinoma microenvironment *in vitro* using sacrificial bioprinting, in: Tumor Biol., American Association for Cancer Research, 2017: pp. 4828–4828. doi:10.1158/1538-7445.am2017-4828.

[257] T. Almela, S. Al-Sahaf, I.M. Brook, K. Khoshroo, M. Rasoulianboroujeni, F. Fahimipour, M. Tahriri, E. Dashtimoghadam, R. Bolt, L. Tayebi, K. Moharamzadeh, 3D printed tissue engineered model for bone invasion of oral cancer, Tissue Cell. 52 (2018) 71–77. doi:10.1016/j.tice.2018.03.009.

[258] H. Ma, T. Li, Z. Huan, M. Zhang, Z. Yang, J. Wang, J. Chang, C. Wu, 3D printing of high-strength bioscaffolds for the synergistic treatment of bone cancer, NPG Asia Mater. 10 (2018) 31–44. doi:10.1038/s41427-018-0015-8.

[259] Z. Wang, R. Samanipour, K. Kim, Organ-on-a-chip platforms for drug screening and tissue engineering, in: 2016: pp. 209–233. doi:10.1007/978-3-319-21813-7_10.

[260] J. Vanderburgh, J.A. Sterling, S.A. Guelcher, 3D printing of tissue engineered constructs for in vitro modeling of disease progression and drug screening, Ann. Biomed. Eng. 45 (2017) 164–179. doi:10.1007/s10439-016-1640-4.

[261] L. Atapattu, R. Utama, A. O'Mahony, C. Fife, J. Baek, T. Allard, K. O'Mahony, J. Ribeiro, K. Gaus, J. Gooding, M. Kavallaris, Abstract 5022: Precision medicine: High-throughput 3D bioprinting of embedded multicellular cancer spheroids, Cancer Res. 78 (2018) 5022–5022. doi:10.1158/1538-7445.am2018-5022.

[262] A. Mondal, A. Gebeyehu, R. Subramanian, A. Rishi, M. Singh, Abstract 5018: Bioprinted (3D) co-cultured spheroids with NSCLC PDX cells and cancer associated fibroblasts (CAFs) using alginate/gelatin hydrogel, in: Tumor Biol., American Association for Cancer Research, 2018: pp. 5018–5018. doi:10.1158/1538-7445.am2018-5018.

[263] D. Ortmann, L. Vallier, K. Zacharis, B. Wesley, R. Tomaz, A novel differentiation

system to produce hepatocytes for disease modelling and drug screening, J. Hepatol. 68 (2018) S55. doi:10.1016/s0168-8278(18)30330-1.

[264] Y. Sun, S. Soh, Printing tablets with fully customizable release profiles for personalized medicine, Adv. Mater. 27 (2015) 7847–7853. doi:10.1002/adma.201504122.

[265] J. Zhao, X. Xu, M. Wang, L. Wang, A new model of a 3D-printed shell with convex drug release profile, Dissolution Technol. 25 (2018) 24–28. doi:10.14227/dt250118p24.

[266] N.S. Bhise, V. Manoharan, S. Massa, A. Tamayol, M. Ghaderi, M. Miscuglio, Q. Lang, Y. Shrike Zhang, S.R. Shin, G. Calzone, N. Annabi, T.D. Shupe, C.E. Bishop, A. Atala, M.R. Dokmeci, A. Khademhosseini, A liver-on-a-chip platform with bioprinted hepatic spheroids, Biofabrication. 8 (2016) 014101. doi:10.1088/1758-5090/8/1/014101.

[267] K.A. Homan, D.B. Kolesky, M.A. Skylar-Scott, J. Herrmann, H. Obuobi, A. Moisan, J.A. Lewis, Bioprinting of 3D convoluted renal proximal tubules on perfusable chips, Sci. Rep. 6 (2016) 34845. doi:10.1038/srep34845.

[268] John L. Tan, and Joe Tien, C.S. Chen, Microcontact printing of proteins on mixed self-assembled monolayers, 18 (2001) 519-523. doi:10.1021/la011351+.

[269] H.-W. Kang, S.J. Lee, I.K. Ko, C. Kengla, J.J. Yoo, A. Atala, A 3D bioprinting system to produce human-scale tissue constructs with structural integrity, Nat. Biotechnol. 34 (2016) 312–319. doi:10.1038/nbt.3413.

[270] D.J. Ravnic, A.N. Leberfinger, S. V Koduru, M. Hospodiuk, K.K. Moncal, P. Datta, M. Dey, E. Rizk, I.T. Ozbolat, Transplantation of bioprinted tissues and organs: Technical and clinical challenges and future perspectives., Ann. Surg. 266 (2017) 48–58. doi:10.1097/sla.0000000000002141.

[271] S. Loai, B. R. Kingston, Z. Wang, D. N. Philpott, M. Tao, H-L. M. Cheng, Clinical perspectives on 3D bioprinting paradigms for regenerative medicine, Regen. Med. Front. (2019). doi:10.20900/rmf20190004.

[272] J. Witowski, M. Sitkowski, T. Zuzak, J. Coles-Black, J. Chuen, P. Major, M. Pdziwiatr, From ideas to long-term studies: 3D printing clinical trials review, Int. J.

Comput. Assist. Radiol. Surg. 13 (2018) 1473–1478. doi:10.1007/s11548-018-1793-8.

[273] D.A. Zopf, S.J. Hollister, M.E. Nelson, R.G. Ohye, G.E. Green, Bioresorbable airway splint created with a three-dimensional printer, N. Engl. J. Med. 368 (2013) 2043–2045. doi:10.1056/nejmc1206319.

[274] N.N. Zein, I.A. Hanouneh, P.D. Bishop, M. Samaan, B. Eghtesad, C. Quintini, C. Miller, L. Yerian, R. Klatte, Three-dimensional print of a liver for preoperative planning in living donor liver transplantation, Liver Transplant. 19 (2013) 1304–1310. doi:10.1002/lt.23729.

[275] L.E. Diment, M.S. Thompson, J.H.M. Bergmann, Clinical efficacy and effectiveness of 3D printing: a systematic review., BMJ Open. 7 (2017) e016891. doi:10.1136/bmjopen-2017-016891.

[276] P.G. Campbell, L.E. Weiss, Tissue engineering with the aid of inkjet printers, Expert Opin. Biol. Ther. 7 (2007) 1123–1127. doi:10.1517/14712598.7.8.1123.

[277] Y.M. Balakhovsky, A.Y. Ostrovskiy, Y.D. Khesuani, Emerging business models toward commercialization of bioprinting technology, in: 3D Print. Biofabrication, Springer International Publishing, Cham, 2017: pp. 1–22. doi:10.1007/978-3-319-40498-1_25-1.

[278] S. Miao, N. Castro, M. Nowicki, L. Xia, H. Cui, X. Zhou, W. Zhu, S. Lee, K. Sarkar, G. Vozzi, Y. Tabata, J. Fisher, L.G. Zhang, 4D printing of polymeric materials for tissue and organ regeneration, Mater. Today. 20 (2017) 577–591. doi:10.1016/j.mattod.2017.06.005.

[279] Z. Zhang, K.G. Demir, G.X. Gu, Developments in 4D-printing: a review on current smart materials, technologies, and applications, Int. J. Smart Nano Mater. 10 (2019) 205–224. doi:10.1080/19475411.2019.1591541.